Doctoral Dissertation

STUDIES ON THE MICRO-PHASE SEPARATION IN MIXED CARRAGEENAN GELS USING PARTICLE TRACKING

September 2019

Graduate School of Marine Science and Technology
Tokyo University of Marine Science and Technology
Doctoral Course of Applied Marine Biosciences

LESTER CANQUE GEONZON

I would like to dedicate this thesis to my loving wife, son and daughter . . .

Acknowledgements

This milestone will never be possible without the help and presence of the following persons:

First and foremost, I am very grateful and indebt to my supervisor, Prof. Shingo Matsukawa who created this opportunity and patiently supported my research throughout my PhD studies. Without your guidance and support, this thesis would never be possible. By his continuous support and trust, it is a real luxury to grow and be trained in Prof. Matsukawa's lab.

I am thankful to the Ministry of Education, Culture, Sport, Science and Technology for the scholarship and funding throughout my research. This opened the opportunity for me and my family to live and experience life in Japan.

I would also like to thank Prof. Toru Suzuki and the Refrigeration laboratory, for their kindness in allowing us to use the microscope and for the fruitful discussion about the results of fluorescence microscopy.

I am very grateful to the committee members for their time and consideration: Prof. Toru Suzuki, Prof. Tomoaki Hagiwara, Prof. Mika Fukuoka. Your kindness and consideration has made the last stage of my dissertation relatively stress free.

To Doc. Mel Bacabac, thank you for introducing me to the world of microscopic rheology and most importantly, introducing me to Prof. Matsukawa. This opened all the opportunities for me.

To the members of Bussei Laboratory, thank you for making my time in the laboratory pleasurable despite all the pressures. Special mention to Moriya-san, Yoshida-san and Fukuda-san,

your invaluable help made my life both in the laboratory and outside the laboratory stress free. You helped me and my family with all the necessary information to survive in Japan.
To my Filipino colleagues: Amos, Stephen and Faith, for the discussion and random chats.
To Te Vivian, Uncle Ruel, Keiji and Kervin, your unconditional help and presence really helped us to survive in Japan. We are very grateful and indebted to.
To my family in the Philippines, Papa, Mama, brother, sister, and my-in laws, thank you for your support. To my papa and mama, you have brought me into this world and have given me your unending support. I cant thank you enough.

Finally, to my family, my wife Christel Mae, my son Vince Dwayne, and my daughter Vanechka Leicy, your presence and in all possible ways you inspire me. To my wife, you always keep the balance when the other side of the equation in my life seems lost.

And to the God above, this will never possible if not in your will.

Table of contents

List of figures

Chapter 1

Introduction

1.1 General introduction

Food products ranging from liquid, semi-solid to solids often utilize polymers/biopolymers as food hydrocolloids to control the texture for meeting the specific sensory preference of targeted consumers. In food industry, different food hydrocolloids i.e., agar, carrageenan and gellan gum were traditionally recognized as rheology modifier (gelling, thickening and stabilizing agent). The functionality of food polymers in various applications depends largely on their rheological properties. Polysaccharide mixtures or blends have gained widespread applications in foods due to greater controllability of the physical property and texture enhancement of the final product (Zheng, 2018).

However, complication may arise after mixing these ingredients under certain conditions of concentration, pH and ionic strength due to the components may redistribute themselves to attain a certain favorable thermodynamic state. Depending on the net charge, molecular weight, pH, etc., the interactions between ingredients can be either associative or segregative. Hence, the optimum structure of food products may be engineered by proper mixing of food polymers and process the formula with dedicated parameters and procedures. Therefore, to

maximize the potential use of these polysaccharides, characterization of gel properties is needed, and the gelation mechanism must be clarified at different length scale of observations for mixture solutions of polysaccharide such as carrageenan.

1.2 Objective

In the present study, the gelation mechanism and network structure of pure carrageenans and its mixtures (KC:IC and KC:LC) were investigated macroscopically using rheometer and microscopically using particle tracking. The main objective of this study is to clarify and elucidate the gelation mechanism and network structure of pure carrageenans (KC and IC) as well as mixture of KC:IC and KC:LC in the microscopic point of view. Concurrently, the phase separation phenomenon on the mixture of KC:IC and KC:LC were elucidated and discussed in greater detail. The previous studies on carrageenans are overviewed and methodologies used in this research were discussed most importantly the particle tracking.

The present work was outlined as follows:

I. Develop an algorithm with improved accuracy for determining centroid coordinates and particle identification for the particle tracking.

II. Elucidate the network structure and gelation mechanism of pure KC and IC gels using the particle tracking technique.

III. Microscopic investigation on the gelation mechanism and phase separation of mixed KC:IC gels.

IV. Studies on the phase separation of mixed KC and LC gels were also carried out.

1.3 Carrageenans

Carrageenans belong to the family of polyelectrolyte biopolymers. Carrageenan is a generic name of a water-soluble biopolymer, linear sulfated polysaccharide consisting of repeating disaccharide units of 1,3 linked β-D-galactopyranose (G) and a 1,4 linked 3,6-anhydro-α-D-galactopyranose (AG), commonly extracted from red seaweeds of the Rhodophycea family (Necas and Bartosikova, 2013). The *Eucheuma spp.* and *Kappaphycus spp.* seaweeds are the main raw materials used for extraction of the carrageenan. The carrageenans are classified into various types using the Greek letter such as λ (lambda), κ (kappa), ι (iota), ν (nu), μ (mu) and θ (theta) based on the difference in the number and position of sulfate groups within the disaccharide repeat structure.

1.3.1 Types of carrageenans

The most industrially utilized carrageenans are the κ- (KC), ι- (IC) and λ- (LC) carrageenan which differs in the amount of sulfate groups: one (G4S-DA) for KC, two (G4S-DA2S) for IC, and three (G2S-D2S,6S) for LC (Usov, 1992; van de Velde, 2008). Among the three types, KC and IC exhibited gelling properties influenced by temperature and presence of cations (K^+, Ca^{2+}), while LC is a non-gelling type carrageenan. They are widely used in the food industry as rheology modifiers (gelling, thickening and stabilizing agents); and for pigment dispersion in cosmetics and pharmaceutical formulations. The most important gelling carrageenans are κ-carrageenan (KC) and ι-carrageenan (IC) thanks to their gelling ability. KC and IC differ in the degree of sulfation, with KC carrying one sulfate group at O-4 of the G residue, while IC carries an additional one sulfate group at O-2 of the AG residue. Meanwhile, LC is a non-gelling type carrageenan.

As shown in Figure 2.1, KC and IC only differ by the presence of an additional sulfate group at the second carbon of the 1,4 linked galactose unit for the latter. LC has the highest

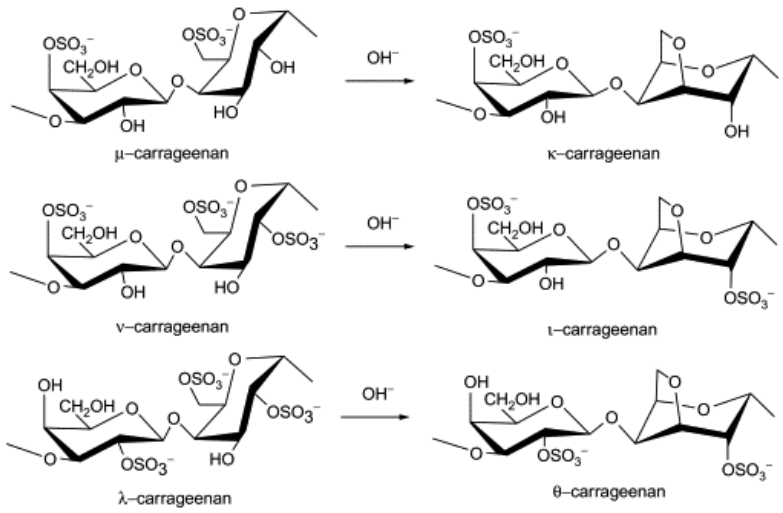

Fig. 1.1 Schematic representation of chemical structures of carrageenans.

sulfate content and no 3,6-AG. Higher levels of sulfate lead to lower solubility temperature and lower gel strength. Besides the three major carrageenan types, two other types, μ and ν carrageenan (Fig. 2.1), are often encountered in commercial carrageenan samples, which are the biochemical precursors of KC and IC, respectively. The difference in the degree of sulfation leads to a distinct differences in the gel structure and property of these two carrageenans.

1.3.2 Gelation mechanism

A very important property of many polysaccharides is the ability to form gels. The gelling ability of carrageenan gives a very important information for the vital functions of carrageenananans in food industry. Gelation ability of carrageenans is a complex process that depends on type of carrageenan, polymer concentration, temperature and type and amount of counter ions. Some cations such as K^+, Ca^{2+}, etc. are found to induce conformational changes effectively.

The gelation mechanism of different carrageenans have been the focus of many research over the past decades using different techniques wherein different models of gel formation have been proposed (Figure 1.2). The gelling process in carrageenan solutions is generally accepted as a model involving a coil-to-helix transition followed by aggregation of double helices to form a space-spanning network (Rochas and Rinaudo, 1980; Takemasa, Chiba, and Date, 2001) as shown in Figure 2.2.

The conformation changes of carrageenan chains in aqueous solution is believed to involve random coil to a helix transition below a critical temperature, T_c, followed by the aggregation of helices to form a spanning network. For KC, the gelation is generally considered to involve extensive aggregation of double-helices that results to a stiff network and a strong and brittle gel (Rochas and Rinaudo, 1980; Takemasa, Chiba, and Date, 2001). KC gels also exhibit thermal hysteresis between formation and melting observed in rheological and micro DSC measuremetns, which is usually attributed to the disaggregation of the helix aggregates.

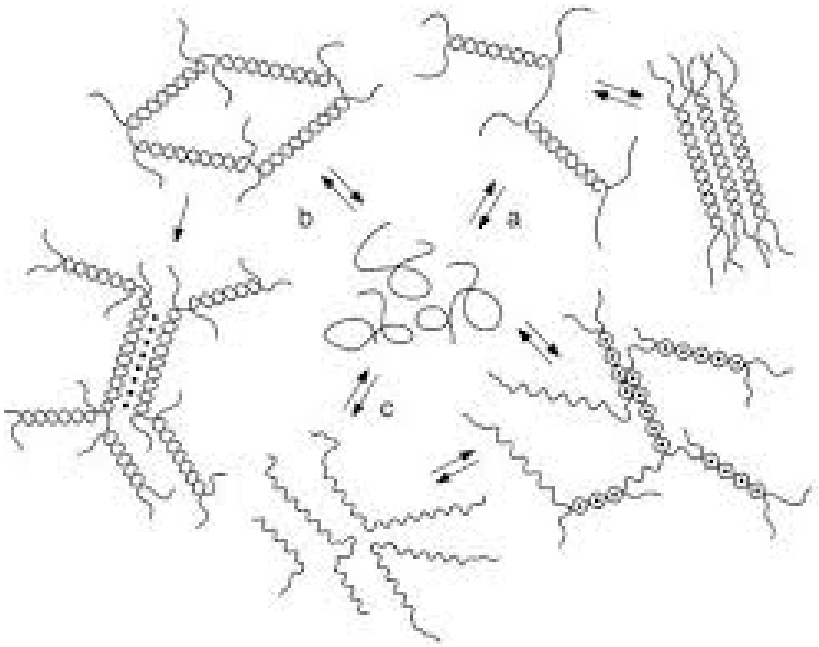

Fig. 1.2 Model of gel formation: a) double-helical model, b) domain model and c) nested, single-helix model. Adapted from (Tuvikene, Truus, Kollist, Volobujeva, Mellikov, and Pehk, 2007) with permission from Springer Nature.

Conversely, as for IC, the gels are soft and do not show thermal hysteresis indicating that very limited or no inter-helical aggregation takes place. In addition, IC gels are typically clear and much weaker than KC gels. However, the order of steps and type of conformational transition has not been fully established yet and requires further investigations.

The difference in gelation mechanism of different carrageenans was attributed to the difference in the chemical structure. KC undergo extensive aggregation that results to the formation of hard and brittle gels while IC forms a soft and weak gel. Later, more researchers focus their attention on the properties of mixed carrageenan gels. The mixed KC/IC gels provide greater control on the physical property of the carrageenan gels. Picullel et.al. investigated (Piculell, Nilsson, and Muhrbeck, 1992) the effect of small amounts of KC impurity to IC using rheological measurements and concluded that separate networks of KC and IC were formed. Furthermore, Parker et.al. (Parker, Brigand, Miniou, Trespoey, and Vallée, 1993) studied the mixture more extensively using rheological measurements confirming the independent gelation steps of the individual KC and IC components.

1.3.3 Mixture of carrageenans

Due to greater demand in the development of food products, biopolymer mixtures were utilized to enhance the texture quality, stability and gelling ability of the final product to meet the specific preference of the consumer. However, as mentioned in Section 1.1, interactions between compatible and incompatible ingredients (segregative or associative) might yields to an undesired texture. For instance, mixtures of KC and IC have been studied extensively over the past decades which concluded two possibilities, either it formed a phase separated

network structure or interpenetrated network structure.

Rheological and dynamic scanning calorimetry (DSC) studies showed a two-step gelation process at temperatures that were equal to the coil– helix temperature (T_c) of the individual carrageenan solutions (Du, Brenner, Xie, Liu, Wang, and Matsukawa, 2016; Du, Brenner, Xie, and Matsukawa, 2016). This implies that the coil-helix transition of carrageenan chains is not influenced by the presence of other type. In addition, the results suggested that the network structure of each type are microphase separated. Brenner et al discussed in details of whether the mixture formed an interpenetrated or micro-phase separated network based on the rheological measurements and theoretical model. It was concluded that the results were compatible with formation of bicontinuous microphase separated networks. However, these studies provided information on gel bulk properties, where the microscopic properties, such as micro-viscosity, are averaged.

Some studies attempted to visualize the gel structure using various imaging techniques: scanning electron microscopy (SEM) (Thrimawithana et al., 2010), transmission electron microscopy (TEM) (Amici et al., 2002), and confocal laser scanning microscopy (CLSM) (Heilig et al., 2009). While the methods provide direct information on the gel microstructure, it might lead to formation of artifacts (Aguilera and Stanley, 1999) caused by extensive drying (for SEM), staining (for TEM) or fluorophore labelling (for CSLM), thus obscuring the actual gel structure and gelation mechanism. Therefore, no decisive evidence has been reported for the phase separated network structure of KC-rich ad IC-rich domains.

Recently, diffusion of probe polymers using pulse field gradient nuclear magnetic resonance (NMR) was performed to elucidate underlying network structure of the mixed carrageenan gels (Hu, Du, and Matsukawa, 2016). These studies indicated coarse network

structures were formed with thick aggregates in KC gels, while fine network structures were formed in IC gels. However, NMR diffusion measurements of probe polymers are not adequate to elucidate the network structure because of the long diffusion of the probe polymer (ca. 10 nm) during the diffusion time (10ms) which averages out the structure of micro phase separation.

1.4 Rheology

Rheology in general is the observation of flow properties of different kinds of media. Macrorheology is a technique that measures the viscoelasticity of materials ("solid-like" or "fluid-like") using mechanical rheometer (i.e. cone-plate, Couette, etc.). The materials' properties are quantified in terms of elastic moduli for solid materials and viscous moduli for liquids. They are calculated from the ratio of stress to strain for elastic moduli and stress to strain rate for viscous moduli, respectively. Traditionally, these measurements have been performed on several of millilters of samples in a mechanical rheometer by applying small amplitude oscillatory shear strain $\gamma(t) = \gamma_0 sin(\omega t)$ where γ_0 and ω are the amplitude and frequency of oscillation, respectively. In addition, commercial rheometers probe frequencies up to hundreds of Hz due to inertial effects.

Rheology measurements provided valuable insights into the structural rearrangements and mechanical response of the materials, particularly, the soft materials and complex fluids, such as colloidal suspensions, emulsions and polymer networks. However, the conventional mechanical technique are not always well-suited for those systems. Morever, conventional rheometers provide an average measurements on the physical property of the materials, and do not allow for microscopic measurements especially for inhomogeneous materials. To address the existing issue, microrheology technique was developed wherein the micron-size probe particles are embedded in the solutions to locally deform the sample either by Brownian

motion or with and external forces.

1.5 Microrheology

Instead of using macroscopically applied and detected stress and strain to extract a material's moduli, microrheology is a technique that determines the local mechanical properties of a complex fluid, namely the ability to store and dissipate energy. In addition, microrheology can be performed *in situ* in an environment that cannot be reached by a macrorheology experiment. There are two classes of microrheology techniques: those involving external forces or active manipulation of the probe particles and those relying on the passive motion of probe particles due to Brownian motion.

1.5.1 Active Microrheology

Active microrheology involves the active manipulation of the probe particles by the externals forces using magnetic fields, electric fields and micromechanical forces. This is analogous to the conventional rheological measurements in which an external stress is applied to the sample and the resulting strain is measured. However, the measurements are at microscopic scale and probe the local viscoelastic property of the materials. In addition, active microrheology allows the application of large stresses to stiff and hard materials in order to obtain detectable strains.

One of the most common active microrheology technique manipulates the probe particles using optical tweezers (Ashkin, Dziedzic, Bjorkholm, and Chu, 1986) shown in Figure 2.3. The experimental design is typically based on an inverted microscope with a high numerical aperture oil-immersion objective lens. The microscope allows for simultaneous imaging of the sample and allows placement of the particles within the sample. The laser beam is used to

steer the particles with an external optical stain. Also, the advantage is that the motion of the particle is not purely random, and the response is observed at the frequency of the excitation.

In order to apply a known force to the material, the trap constant must be measured in which variety of methods can be used. As shown in Figure 2.3, the trap constant is approximated by Hooke's law with an effective spring constant k_{OT}. By moving the trap with respect to the position of the probe particles, stress can be applied locally and the resulting particle displacement can be determined wherein the corresponding strain can be recorded. Finally, the rheological information can be obtained.

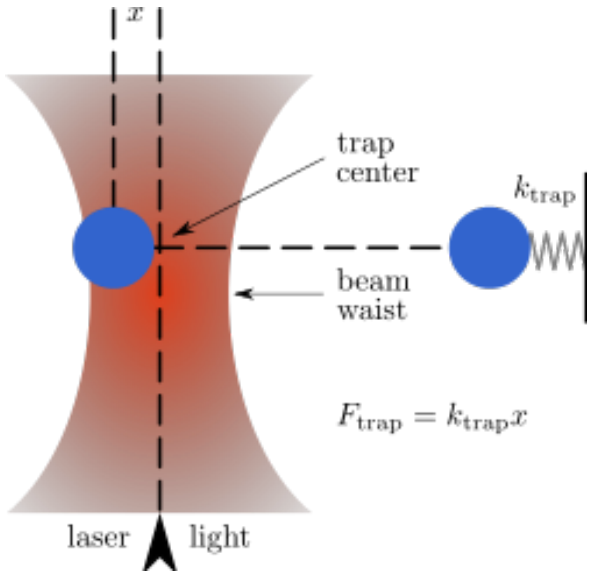

Fig. 1.3 Schematic representation of optical trapping.

1.5.2 Passive Microrheology

Another class of microrheology is the passive microrheology technique wherein it takes advantage of the unperturbed thermal (excited by broadband thermal energy (i.e k_BT)) and nonthermal fluctuations (if present) of a probe particle embedded in the medium. Unlike the active microrheology technique, passive microrheology relies on the thermal energy k_BT of the embedded probe particles to obtain the viscoelastic properties of its host medium using

the time series position, *r(t)* of the probe particle.

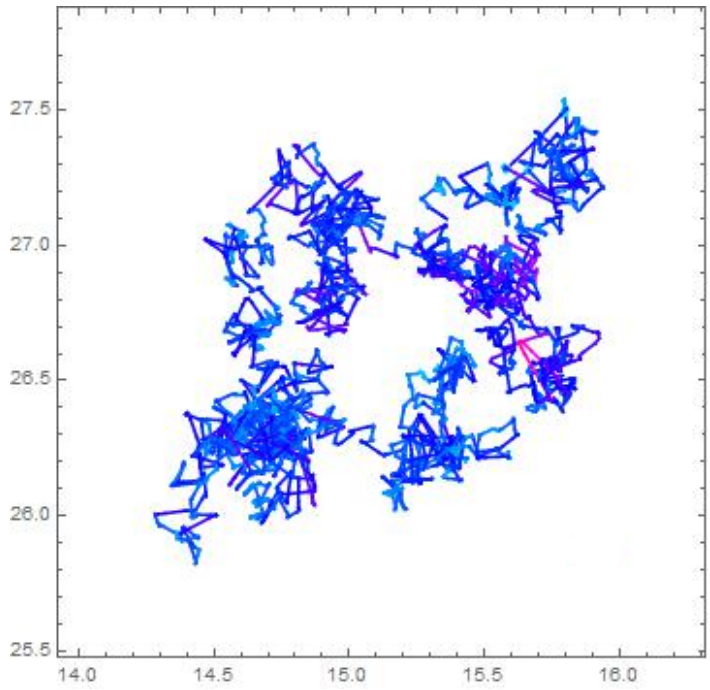

Fig. 1.4 Trajectory of a single particle in gel.

Passive particle tracking is a noninvasive technique performed by monitoring the thermally driven random motion of the probe particle as shown in Figure 1.4. The random motion of particles provides information on the microscopic viscoelasticity of fluids (Mason, Ganesan, van Zanten, Wirtz, and Kuo, 1997; Waigh, 2005). In this approach, probe particles are driven purely by Brownian forces, i.e., thermal energy. The Brownian motion of the individual probe particles can be used to extract the physical properties of the host sample, based on signatures of the corresponding mean square displacement (MSD) (Mason, Ganesan, van Zanten, Wirtz, and Kuo, 1997) quantified using the following equation:

$$msd(\tau) = \frac{1}{N - \frac{\tau}{\triangle t}} \sum_{i=1}^{N-\frac{\tau}{\triangle t}} [r(i\triangle t + \tau) - r(i\triangle t)]^2 \tag{1.1}$$

where $\triangle$t is the interval time for each frame, that is the inverse of the frame rate, and r($\triangle$t) is

the position of the centroids of each tracked particle. Using particle tracking, the microscopic physical properties of the sample can be probed without affecting the developing network structure (Caggioni, Spicer, Blair, Lindberg, and Weitz, 2007; Moschakis, 2013). While bulk rheology provides information on the overall mechanical response of the material, it is important to understand the origin of this response.

Chapter 2

Accuracy improvement of centroid coordinates and particle identification in particle tracking technique

In this chapter, we have applied an algorithm to improve the accuracy of particle identification and centroid coordinates for each particle image in particle tracking technique. The algorithm introduced two techniques; 1) cutting off by each threshold at the peak in the pixel intensity distribution for each image of local area around the particle, and 2) calculation of the centroid based on pixel intensities in the original image of the particle instead of binarized data. The former properly cuts the noise in the background for each particle which has large variety in level particle by particle due to fluctuating illuminations and out-of-focus particles in the image, and the latter avoids the loss of accuracy by the commonly used binarization. We have demonstrated that the algorithm significantly improves the accuracy in determination of centroid coordinates and the correctness in particle identification. We have also validated the advantage of the algorithm in accuracy by applying the algorithm to a sequence of confocal microscopy images of diffusing particles in a polysaccharide solution. This algorithm will

be significantly useful in particle tracking technique for biological systems, especially for fluorescence microscopy observations with considerable obstructive stray fluorescent signals.

Based on: Lester C. Geonzon, Shingo Matsukawa. Accuracy improvement of centroid coordinates and particle identification in particle tracking technique. Journal of Biorheology, 33(1), 2-7, 2019

2.1 Introduction

Particle tracking has been used in numerous applications to study the mechanical and rheological properties of microscopic environments in polymer gels like Carbopol gels (Oppong et al., 2006), in biological systems such as intercellular region of live cells (Tseng et al., 2002, 2004), and actin solutions and bundles (Apgar et al., 2000) and in food gels, such as gelatin (Shabaniverki and Juárez, 2017), β-glucan solutions (Moschakis et al., 2012), carrageenan systems (Du, Brenner, Xie, and Matsukawa, 2016; Du, Lu, Geonzon, Xie, and Matsukawa, 2016) and emulsion systems (Cheng et al., 2017; Moschakis et al., 2006) providing valuable information on the microstructure and local physical property of the media. The thermal fluctuation of added probe particles gives information of the microenvironment rheology, that is, the local rheological parameters in the spatial range of the particle size (Mason et al., 1997; Waigh, 2005).

Several methods have been developed to track probe particles for the micro-rheological studies in different media. The commonly used algorithm to track particles utilizes the binarization at a threshold for the whole image of each frame, and then, the binarized image data are used to calculate the center of mass or the weighted centroid (Kreizer et al., 2010). Because of its simplicity and fast processing, this method is widely used in image processing routines and particle tracking algorithm. However, the simplification by the binarization

loses details of the image and leads to an inaccurate calculation of the centroid for each particle. Further, improper determination of the threshold can cause significant error in the centroid calculation especially for images with large noise, undesirable images of fluctuating illuminations and out-of-focus particles. There are some approaches to calculate the centroid without using the binarization, accordingly a cut off is obtained at a certain percentage from the maximum intensity and applied to all the particles in the frame (Cheezum et al., 2001; Crocker and Grier, 1996; Fish and Scrimgeour, 2015; Furst and Squires, 2017). Meanwhile no use of the threshold resulted in unsatisfactory accuracy due to the background pixel intensity with the noise Cheezum et al. (2001). Since particle tracking technique can contribute valuable insights in the micro-rheology, the improvement of accuracy in the calculation is extremely important.

In this study, we have applied an algorithm to improve the accuracy of centroid coordinates and particle identification in particle tracking technique. The algorithm introduced a cut-off threshold for each image of local area around the particle, and a calculation of the centroid based on the pixel intensity instead of binarized data. The former is expected to properly cut the noise in the background for each particle, and the latter avoids the loss of accuracy from the binarization. Improvements of the accuracy of centroid coordinates and the correctness in particle identification have been examined. The advantage of the algorithm has been validated by applying the algorithm to a sequence of confocal microscopy images of diffusing particles in a polysaccharide solution.

2.2 Materials and Methods

2.2.1 Particle tracking algorithm

Particle tracking algorithm was implemented in Mathematica 10 (Wolfram Research, Inc., Champaign, IL). Fig. 2.1 shows the flowchart of the particle tracking algorithm. The main steps of the algorithm included: Step 1) selection of candidate particles and determination of the initial centroids, Step 2) calculation of the weighted centroid coordinate of each candidate particle and Step 3) link the centroids in a series of frames into trajectories for each particles. In Step 1, the candidate particles were determined in each frame and the initial centroid coordinates for each particles were obtained. In Step 2, the local image of each particle was extracted, which may suffer from spiky noise due to background variations of in and out of focus particles and uneven illumination. The median filter was applied to the local image which removes spiky noise without affecting the particle image and Gaussian filter was applied to reduce the noise (Ahmed et al., 2015). Cutting off by a threshold was performed to each local image to remove the effect of the background in the calculation of the weighted centroid. The weighted centroid coordinate was determined based on the pixel intensities of the particle. In Step 3, the particle was connected to the particle with the closest coordinate in the subsequent frame from the first to the end of the series of frames to obtain particle trajectory.

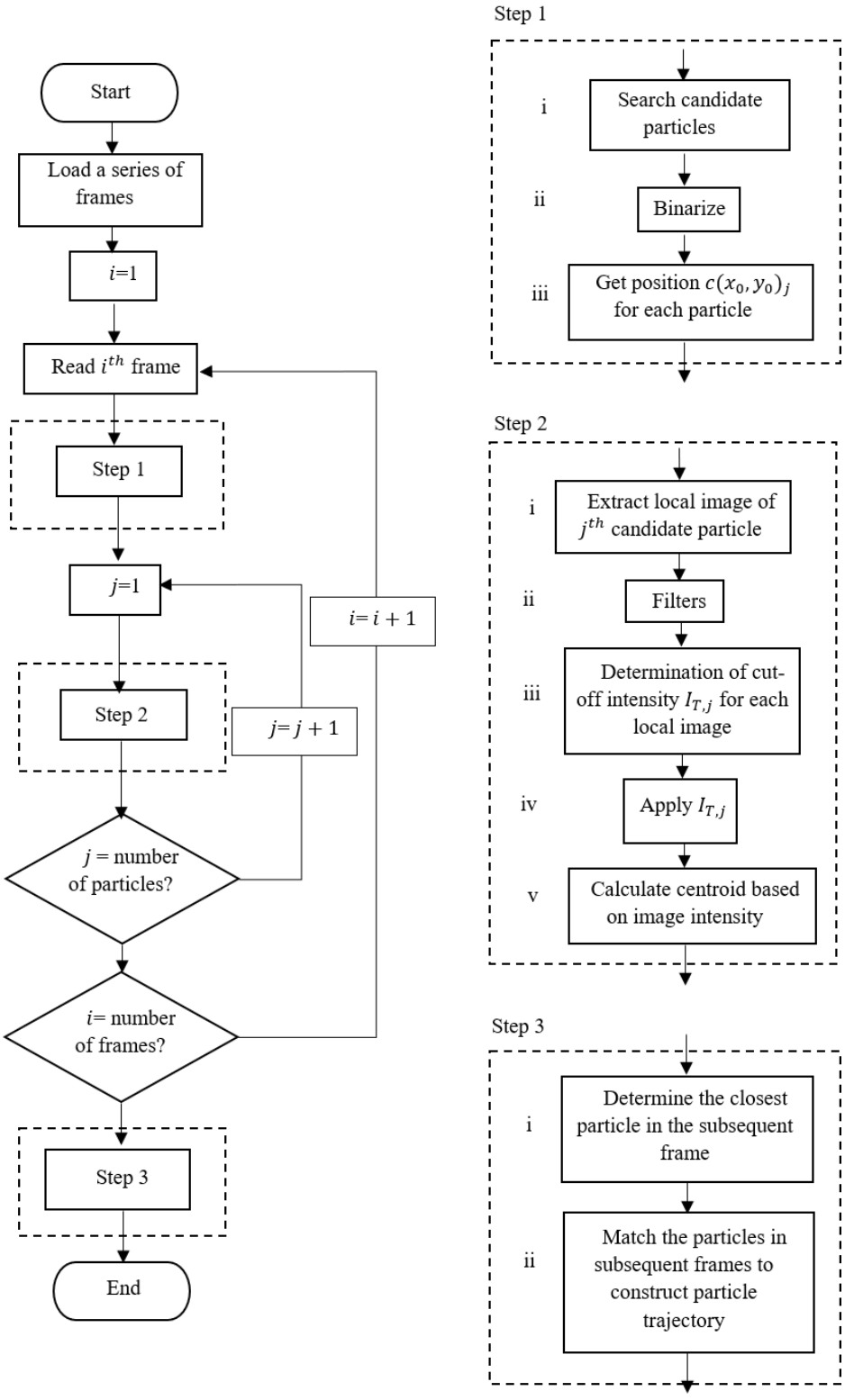

Fig. 2.1 Flowchart of the particle tracking algorithm.

2.2.2 Experimental details

Carrageenan samples were purchased from Tokyo Chemical Industry Co., Ltd. (Tokyo, Japan). All carrageenan samples were dialyzed against NaCl solution and subsequently against deionized water, to obtain Na^+ type carrageenan solutions. The samples for particle tracking experiments were prepared by diluting the dialyzed stock solution and KCl solution with deionized water separately, followed by heating at 70°C for 30 min under vigorous stirring. The prepared solutions were mixed to obtain a total carrageenan concentration of 1.5% w/w and KCl concentration of 10 mM and then heated at 90°C for 20 min. Subsequently, fluorescent labeled probe particles (0.1 μm, Green, Thermo Scientific) were added at a total solid concentration of $\sim$0.01% (w/v). The sample solution was stirred and heated at 90°C for another 5 min to assure homogeneous dispersion of probe particles. The hot sample solution containing probe particles was placed in a custom-built sample chamber of a glass bottom dish (Matsunami Glass Inc., Ltd.) equipped with a temperature sensor for temperature monitoring and sealed with a cover glass and a silicone glue.

Particle tracking experiments were performed on a BZ-9000 microscope (Keyence), equipped with a PlanFlour 100$\times$ NA 1.30 oil-immersion objective lens (Nikon). Movies of the diffusing fluorescent labeled particles were recorded using a built-in 2/3 inch, 1.5 megapixel, 12-bit, monochrome cooled CCD camera (Keyence) at a frame rate of 7.5 frames per second. The video recording of diffusing probe particles was deconstructed into a series of frames using Virtualdub software wherein each frame has approximately 30-50 particles.

2.3 Results and Discussion

The performance of the method was evaluated using a series of time lapse microscope frames. The approach was to determine the centroid coordinate of each particle based on the pixel intensities with proper cutting off method of the background intensity.

2.3.1 Calculation of weighted centroid coordinate

The series of frames were processed to track each probe particles by the particle tracking algorithm shown in Fig. 2.1. In Step 1-i, the candidate particles were determined by template-matching where a particle image was selected as a template and was used to find particles in each frame which have similar images with the template (Lewis, 1995). In Step 1-ii, the image of frame in Step 1-i was binarized to determine the candidate particles from the noisy background. In Step 1-iii, the initial centroid coordinate of the binarized image of the jth particle, $c(x_0, y_0)_j$ was calculated using a built-in function in Mathematica.

In Step 2-i, the local image of the jth particle, $L_{org,j}$, was clipped out from the raw frame as a square with the center of $c(x_0, y_0)_j$ and a side of d_s pixels as shown in Fig. 2.2a. The d_s was set as the search diameter larger than the particle diameter and smaller than the average distance between particles. In microscopy experiments, the $L_{org,j}$ suffers from a considerable imperfection including nonuniform contrast, random noise, and geometric distortion. In Step 2-ii, therefore, each $L_{org,j}$ was treated by the 2-dimensional median filter and Gaussian filter. The former replaces each pixel intensity with the median value of the neighboring pixels and is effective to remove spiky noise without blurring the detail of particle image (Fish and Scrimgeour, 2015) and the later suppresses the random noise of the local image. As seen in Fig. 2.2b, the smoothed local image, $L_{sm,j}$, showed a great improvement in the signal to noise ratio without affecting the details of the particle image.

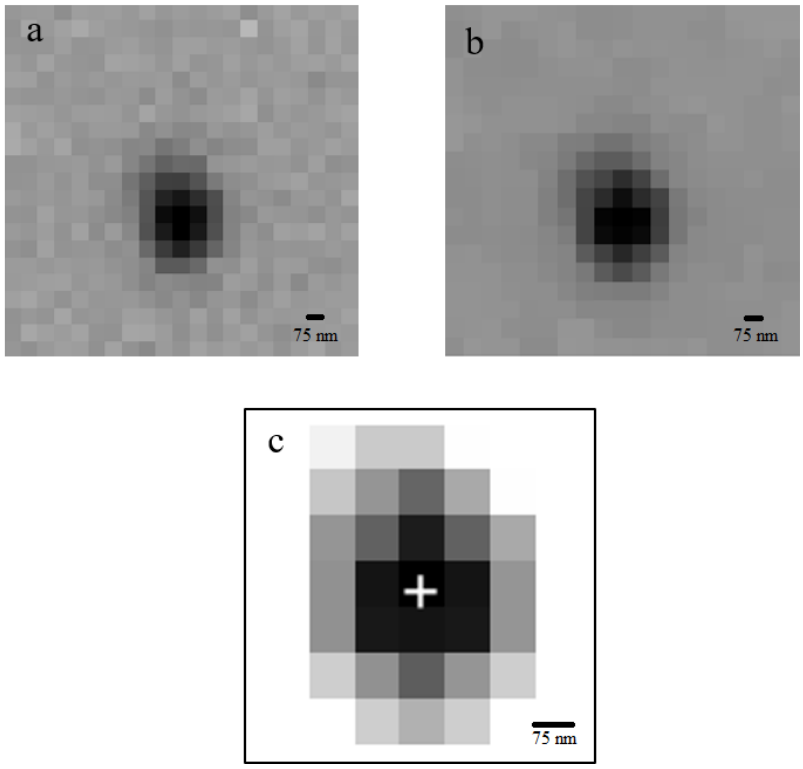

Fig. 2.2 Local images of a candidate particle i a 21×21-array of pixel intensities (d_s=21). a) $L_{org,j}$ b) $L_{sm,j}$ c) Zoomed image of $L_{cut,j}$ with the centroid coordinate (white cross).

The inclusion of the background intensities in the calculations of the weighted centroid coordinate leads to a larger bias and causes undesired inaccuracy (Cheezum et al., 2001). Image thresholding was carried out for each $L_{sm,j}$ to decouple the effect of the background by application of cut off intensity, I_T. In the previous works (Crocker and Grier, 1996; Fish and Scrimgeour, 2015; Furst and Squires, 2017), the I_T was set at a certain percentage of the maximum pixel intensity in the frame e.g. 30%-60%, which only include portion of the whole particle image. In our method, the cut off intensity for each $L_{sm,j}$, $I_{T,j}$, was calculated independently. In Step 2-iii, pixel intensities were ranked in ascending order as shown in Fig. 2.3, and $I_{T,j}$ was calculated from the peak in the second derivative of the ranking. The peak indicates the steepest change in the frequency of pixel intensity in the $L_{sm,j}$. This method extracts the whole intensity profile of the particle. In Step 2-iv, the cut off $I_{T,j}$ was applied to each $L_{sm,j}$ to obtain the local image, $L_{cut,j}$ using Eq. 1,

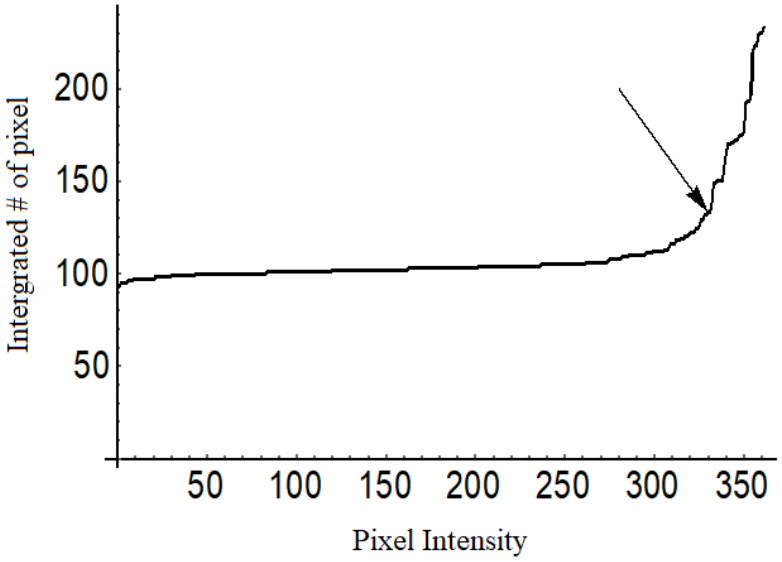

Fig. 2.3 Pixel intensity as a function of pixel index. The arrow indicates the steepest change in the frequency of pixel intensity

$$L_{cut,j}(m,n) = \begin{cases} I_{sm,j}(m,n) & \text{if } I_{sm,j}(m,n) > I_{T,j} \\ 0 & \text{otherwise} \end{cases} \tag{2.1}$$

where $I_{sm,j}(m,n)$ is the pixel intensity in the $L_{sm,j}$ indexed by integer m=1,...,d_s as the pixel row index and n=1,...,d_s as the pixel column index and $I_{cut,j}(m,n)$ is the pixel intensity of the $L_{cut,j}$. In Eq. 2.1, pixel intensity greater than the $I_{T,j}$ are unaltered while pixel intensity lower than the $I_{T,j}$ are set to zero.

It is expected that the intensity weighted centroid could provide sub pixel resolution for the particle tracking (Crocker and Grier, 1996; Fish and Scrimgeour, 2015; Furst and Squires, 2017). In Step 2-v, the weighted centroid coordinates of the $L_{cut,j}$, $C_{w,j}$, was calculated by

$$C_{w,j} = c(x_0,y_0)_j + \sum_{m=1}^{d_s}\sum_{n=1}^{d_s}\left(c(m,n)\times I_{cut,j}(m,n)\right) / \sum_{m=1}^{d_s}\sum_{n=1}^{d_s}\left(I_{cut,j}(m,n)\right) \tag{2.2}$$

where $c(m,n)$ is the integer coordinate of $I_{cut,j}(m,n)$. The $C_{w,j}$ is marked by white cross in Fig. 3.2c. The result on the calculation of the $C_{w,j}$ showed efficacy on the determination of the centroid of particle.

2.3.2 Improvement of accuracy in weighted centroid coordinate for a geometrically distorted $L_{org,j}$

Fig. 2.4a shows the surface plot of $L_{org,j}$ with geometric distortions and asymmetry. The geometric distortions of particles are usually caused by the optical aberrations in the microscope optics, uneven illumination and digitization of frames. High $I_{T,j}$ (upper plane) and low $I_{T,j}$ (lower plane) are also indicated. Fig. 2.4b shows the $L_{org,j}$ with the outlines of cut off images using low $I_{T,j}$ (thin) and high $I_{T,j}$ (thick), which are corresponding to lower and higher planes in Fig. 2.4a, respectively.

The binarized images of the particle after cutting off with the low and high $I_{T,j}$ are shown in Fig. 2.4c. The centroid coordinates from the binarized images with the low $I_{T,j}$ and high $I_{T,j}$ are indicated by white cross and "$\times$", respectively. A large difference between the centroid coordinates was observed. This indicates that a small change in $I_{T,j}$ can cause a large shift on the centroid coordinate. The change in $I_{T,j}$ comes from the randomly flickering noise in the background. As a consequence, the calculations for the particle movements, such as the mean square displacement, are affected by the flickering noise which frequently appears in the fluorescence microscopy observation.

On the other hand, the weighted centroid calculation is expected to improve the accuracy. Fig. 2.4d shows the $L_{cut,j}$ of the particle using the low and high $I_{T,j}$ with the weighted centroid coordinates $C_{w,j}$ calculated by Eq. 2.2 indicated by white cross and "$\times$", respectively. The results of the centroid calculation with different $I_{T,j}$ did not show a significant difference

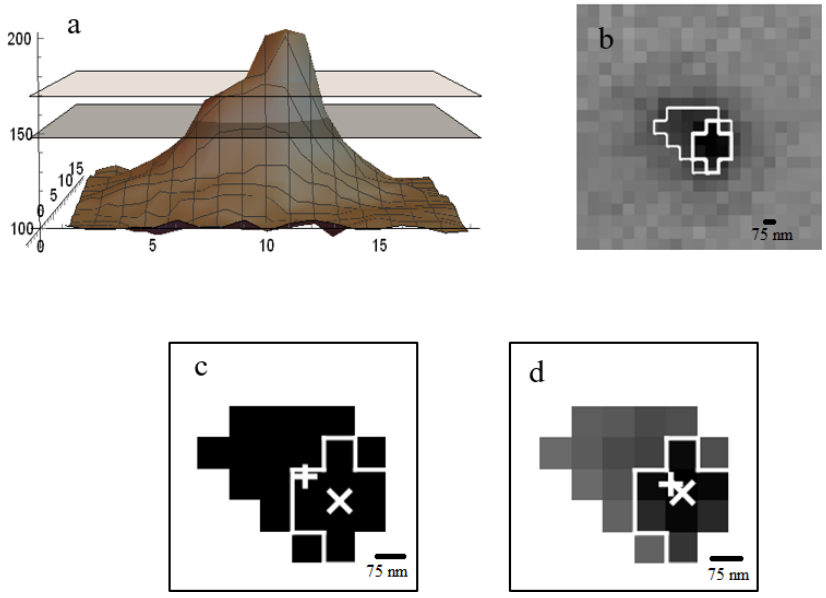

Fig. 2.4 $L_{org,j}$ with geometric distortion in a 21×21 array of pixel intensities (d_s=21). a) Surface plot of $L_{org,j}$. The planes indicate the levels of applied $I_{T,j}$ of high level (upper plane) and low level (lower plane). b) $L_{org,j}$ with outlines of cut off images using a low $I_{T,j}$ (thin) and using a high $I_{T,j}$ (thick) c) Zoomed binarized image of the particle after cut off with centroid coordinate using the low $I_{T,j}$ (white cross) and high $I_{T,j}$ (white "×") Zoomed image of $L_{cut,j}$ with $C_{w,j}$ using the low $I_{T,j}$ (white cross) and high $I_{T,j}$ (white "×"). The outlines in Fig. c and d indicates the particle image with high $I_{T,j}$.

in the centroid coordinate. This indicates that the centroid is not significantly affected by the level of the applied $I_{T,j}$. In the calculation of the weighted centroid coordinate using the image intensity of the particle, each pixel intensity has a different value which mitigate the change of $I_{T,j}$ by fluctuating noise level. Additionally, the distribution of the values of pixel intensity provides the information on the actual centroid coordinate of the particle. Finally, the algorithm showed improved accuracy on the determination of centroid coordinate even for geometrically distorted particles.

2.3.3 Link the particle centroids

The last part of the algorithm (Step 3) links the weighted centroid coordinates of each particle in a subsequent frame to construct particle trajectories. The algorithm was accomplished by identifying the same particle in the series frames using the nearest neighbor calculation, where, each particle was connected to the closest particle in the subsequent frame by calculating the inverse of square distance. Particles connected in the next frame were used in the next iteration while those particles which were not connected with any particle in the next frame were not used in further calculations, as shown in Fig. 2.5. Finally, the trajectory of Brownian motion of fluorescent particles in a polysaccharide solution were obtained and used to extract the information on the local physical property (micro-rheology) of the media, such as mean square displacement (MSD) (Geonzon, Bacabac, and Matsukawa, 2019b).

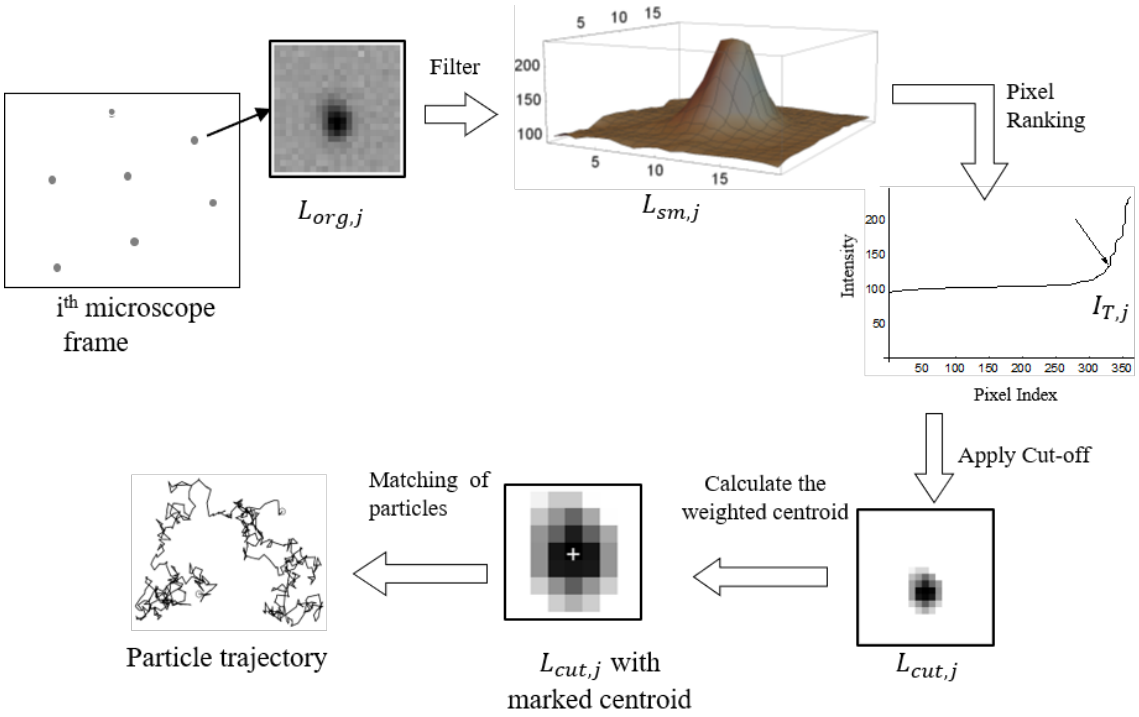

Fig. 2.5 Flow graph of the key steps in implementing the particle tracking algorithm.

2.4 Conclusion

In this chapter, we have demonstrated an improvement in the accuracy of particle tracking algorithm which identifies each probe particle with different threshold intensity in one source frame. The particle tracking algorithm facilitates to recognize, locate and track particles simultaneously from the first to the end for a series of frames. The algorithm was applied to systems with fluorescent probe particles in a variety of background intensities and considerable overlapping fluorescent signals of in-and-out-of-focus particles. The algorithm allows us to determine the centroid coordinates and track the movement of each particle with improved precision. With the proposed algorithm, the diffusive motion of fluorescent probe particle was determined and tracked with sub-pixel resolution. We believe that the algorithm presented here provides an improvement on the determination of the centroid coordinates

which provide great importance in studying the microrheological property of the different complex fluids.

Chapter 3

Network structure and gelation mechanism of kappa and iota carrageenan solutions elucidated by multiple particle tracking

In this chapter, the network structure and gelation mechanism of kappa carrageenan (KC) and iota carrageenan (IC) were investigated using multiple particle tracking. Based on bulk rheology measurements, KC gels exhibit characteristics of a hard and brittle gel, whereas IC gels form a soft and so-called "weak-gel". Particle tracking revealed the differences in the local physical properties of the two gel systems, which are not accessible with the macroscopic rheological measurements. The mean square displacement (MSD) of the probe particles were investigated to characterize changes in the gel network structure on cooling and storage. On cooling, the MSD of the probe particles in the KC solution decreased drastically at around the gelling temperature, demonstrating the trapping of particles within the network structures of KC gels. The MSD of the probe particles in the IC solution exhibited diffusive

behavior even far below the gelling temperature on cooling, although the MSD decreased on storage. These results suggest that KC solutions formed a permanent gel network structure of KC chain aggregates that restricted the motion of particles on cooling. For IC at low temperatures, in contrast, the results suggested two possible structures: 1. clusters of IC chain aggregates, or, 2. a loose network with large pores, which allow the diffusion of particles and lead to weak-gel behavior. The aggregates further aggregate to form a more permanent gel network structure during storage.

Based on: Lester C. Geonzon, Rommel G. Bacabac,Shingo Matsukawa. Network structure and gelation mechanism of kappa and iota carrageenan elucidated by multiple particle tracking. Food Hydrocolloids, 92, 173-180 (2019).

3.1 Introduction

Carrageenan is a family of linear sulfated polysaccharides extracted from red seaweeds (Necas and Bartosikova, 2013), composed of repeating units of 1,3 linked β-D-galactopyranose (G) and a 1,4 linked 3,6-anhydro-α-D-galactopyranose (AG). Carrageenans have been widely used in food industries because of their properties as gelling, thickening and stabilizing agents. The two industrially important gelling carrageenan are κ-carrageenan (KC) and ι-carrageenan (IC). The structural difference between KC and IC is determined by the number of sulfate groups: KC has one sulfate at O-4 of the G residue, whereas IC carries an additional sulfate group on O-2 of the AG residue. Despite the minute difference in molecular structure, their gels exhibit distinct physical properties.

A generally accepted model of the gelling process of carrageenan solutions involves the coil-to-helix transition, followed, in the presence of certain cations, by aggregation of double helices to form a spanning network (Du, Brenner, Xie, and Matsukawa, 2016; Rochas and

Rinaudo, 1980; Takemasa, Chiba, and Date, 2001). KC gelation is generally considered to involve extensive aggregation of double-helices that results in a stiff network (Hu, Du, and Matsukawa, 2016; Rees, Steele, and Williamson, 1969), making KC gels strong and brittle. Conversely, IC gels are soft and do not show thermal hysteresis (Piculell, Nilsson, and Muhrbeck, 1992; Zhang, Matsukawa, and Watanabe, 2004). The bulk rheological properties of the carrageenan gels have been extensively studied using dynamic rheology (Du, Brenner, Xie, and Matsukawa, 2016; Michel, Mestdagh, and Axelos, 1997; Takemasa, Chiba, and Date, 2001). Differential scanning calorimetry (DSC) revealed that KC formed aggregates, whereas IC formed fewer or no aggregates(Du, Brenner, Xie, and Matsukawa, 2016). However, these studies provided information on gel bulk properties, where the microscopic properties, such as micro-viscosity, are averaged. Some studies attempted to visualize the gel structure using various imaging techniques: scanning electron microscopy (SEM) (Thrimawithana, Young, Dunstan, and Alany, 2010), transmission electron microscopy (TEM) (Amici, Clark, Normand, and Johnson, 2002) , and confocal laser scanning microscopy (CLSM) (Heilig, Göggerle, and Hinrichs, 2009). While the methods provide direct information on the gel microstructure, it might lead to formation of artifacts (Aguilera and Stanley, 1999) caused by extensive drying (for SEM), staining (for TEM) or fluorophore labelling (for CSLM), thus obscuring the actual gel structure and gelation mechanism. In previous studies, diffusion measurements of pullulan (Zhao, Brenner, and Matsukawa, 2013; Zhao and Matsukawa, 2012) and poly(ethylene) oxide (PEO) (Hu, Du, and Matsukawa, 2016) by pulse-field gradient nuclear magnetic resonance (NMR) have been carried out for the elucidation of the network structure and gelation mechanism of KC and IC gels. These studies indicated coarse network structures were formed with thick aggregates in KC gels, while fine network structures were formed in IC gels. However, NMR diffusion measurements of probe polymers are not adequate to elucidate the network structure because of the short diffusion time (10 ms) and the size of the probe polymer (ca. 10 nm). In the current investigation, we studied

the network structure of carrageenan gels at larger length scales (>100 nm) using particle tracking.

Passive particle tracking is a noninvasive technique performed by monitoring the thermally driven random motion of the probe particle. It provides information on the microscopic viscoelasticity of fluids (Mason, Ganesan, van Zanten, Wirtz, and Kuo, 1997; Waigh, 2005). In this approach, probe particles are dispersed in the medium and are driven purely by Brownian forces, i.e., thermal energy. The Brownian motion of the individual probe particles can be used to extract the physical properties of the host sample, based on signatures of the corresponding mean square displacement (MSD) (Mason, Ganesan, van Zanten, Wirtz, and Kuo, 1997). Using particle tracking, the microscopic physical properties of the sample can be probed without affecting the developing network structure (Caggioni, Spicer, Blair, Lindberg, and Weitz, 2007; Moschakis, 2013). While bulk rheology provides information on the overall mechanical response of the material, it is important to understand the origin of this response. In this regard, probing the rheological properties over certain length scales provides valuable insights on the local physical properties.

In the present study, we used multiple particle tracking to elucidate the gelation mechanism and gel network formation of KC and IC solutions. The probe particles' MSD was measured on cooling of KC and IC solutions, as well as on further storage. Comparisons were made with the bulk Young's modulus of the gels, and the results were used to relate the microscopic rheological properties and the bulk rheology.

3.2 Materials and Methods

3.2.1 Materials

Sodium-type κ- and ι- carrageenan powders were purchased from Tokyo Chemical Industry Co., Ltd. (Tokyo, Japan). All samples were dialyzed against NaCl solution and subsequently against deionized water to obtain Na^+ type carrageenan solutions. The concentration of Na^+ and K^+ of the dialyzed carrageenans were analyzed by inductively coupled plasma atomic emission (ICP). For KC, Na^+ and K^+ contents were 0.4% and 0.11%, while for IC, they were 0.63% and 0.105%. No Mg^+ or Ca^+ ions were detected in either dialyzed sample.

3.2.2 Sample Preparation

Samples for the particle tracking experiments were prepared by diluting the dialyzed carrageenan solutions with deionized water, adding an appropriate amount of KCl solution, and heating at 70 °C for 30 min under vigorous stirring. The solutions were then further mixed and heated at 90 °C for 20 min. Subsequently, fluorescent labeled probe particles (0.1 μm, Green, ThermoScientific) were added to the solution (final concentrations: 1.5% w/w carrageenan, 10 mM KCl and $\sim$0.01% w/w probe particles), followed by heating at 90 °C for 5 min under vigorous stirring. Samples for the bulk rheology tests were prepared using the same procedure without the addition of probe particles.

3.2.3 Dynamic rheological measurements

Bulk shear moduli were measured using a HAAKE MARS II rheometer (Thermo Scientific, Waltham, MA, USA) equipped with a parallel-plate geometry (diameter = 35 mm, gap = 1 mm). Hot sample solutions were loaded on the preheated plate at 80 °C. Temperature dependence of the shear storage modulus (G') and loss modulus (G") was monitored on

cooling from 80 °C to 5 °C at a rate of 1 °C/min. After subsequent storage at 5 °C for 10 min, frequency sweep measurements (radial frequency ω = 0.1–100 rad/s) were performed.

3.2.4 Particle tracking measurements

Pre-heated sample solutions containing probe particles were placed in a custom-built sample chamber of a glass bottom dish (Matsunami Glass Inc. Ltd., Tokyo, Japan) equipped with a thermo sensor and sealed with a cover glass and silicone sealant. The sample was equilibrated at 50 °C for 10 min before the measurement. Particle tracking measurements of fluorescent particles embedded in carrageenan solutions were carried out using an inverted microscope, BZ-9000 (Keyence Corp., Osaka, Japan), equipped with a PlanFluor 100× NA 1.30 oil-immersion objective (Nikon Corp. Inc., Japan) and a temperature-controlled microscope stage (ALA Scientific Instruments Inc., New York). The sample temperature was controlled by the microscope stage and the sample temperature was monitored using a thermocouple temperature sensor (CENTER 309, Center Technology Corp., Japan) attached to the sample chamber.

Videos of the diffusing fluorescent labeled particles were recorded using a built-in 2/3-inch, 1.5 megapixel, 12-bit, monochrome cooled CCD camera (Keyence Corp., Osaka, Japan) at a rate of 7.5 frames per second for 110 seconds. The video recording of particle diffusion was deconstructed into a series of frames for analysis. In cooling experiments, the particle tracking was performed at different temperatures between 50 °C and 10 °C. For measurements at low temperatures (gel state), a total of 50–70 particles were tracked simultaneously. In the IC solution at high temperatures, the particles showed higher diffusivity and moved in-and-out of focus during the tracking and fewer particles (∼15–30 particles) were successfully tracked. Then, the reproducibility of the measurements was confirmed by carrying out the measurements at least three times for different areas of the sample. In

storage experiments, hot solutions of carrageenan were cooled down from 50 °C to 5 °C at a rate of 1 °C/min in a temperature-controlled incubator to form a gel. The gelled sample was stored at 5 °C prior to experiments and particle tracking was performed at 5 °C.

The position of each fluorescent labeled particles was determined using an algorithm which improves the accuracy of particle position using the image-intensity weighted centroid for each particle (Geonzon and Matsukawa, 2019), from which particle trajectories were formed and analyzed. In the particle tracking algorithm, the candidate particles were determined by template-matching where an ideal image of a single particle was selected as a template and was used to find particles in each frame which have similar images with the template (Geonzon and Matsukawa, 2019). Example image of a single particle and aggregated particles are shown in Appendix A Fig. 1. The aggregates of more than two particles were not included in the analysis. The time-averaged MSD for each particle, msd, was obtained from the trajectory of the particle as represented by the following equation (Lieleg, Vladescu, and Ribbeck, 2010; Wagner, Turner, Rubinstein, McKinley, and Ribbeck, 2017) :

$$msd(\tau) = \frac{1}{N - \frac{\tau}{\triangle t}} \sum_{i=1}^{N-\frac{\tau}{\triangle t}} [r(i \triangle t + \tau) - r(i \triangle t)]^2 \tag{3.1}$$

where the analysis is carried out on N images separated by the lag time τ, $\triangle$t is the time interval for each frame and $r(\triangle \mathrm{t})$ is the position of the centroid of each tracked particle. The exponent α in the relationship between *msd* and τ, $msd \sim \tau^{\alpha}$, was calculated for each particle at lag times τ between 1 and 20 s. The number of independent particle displacement at the longest lag time was 675 per particle. Because the number of displacements for the averaging ($(N - \frac{\tau}{\triangle t})$ in Eq.3.1) decreases, the *msd* points at longer lag times are less certain and have suffered from larger random errors (Michalet, 2010). The ensemble of *msd*, ($\langle msd \rangle$),

was obtained by taking the average of *msd* for the tracked particles. Particle tracking and *msd* calculations were performed using a custom-made program written in Mathematica 10 (Wolfram Research, Inc., Champaign, IL) (Geonzon and Matsukawa, 2019).

3.2.5 Youngs's Modulus measurement

The compression test was done on a RCT-2002D-D Fudoh Rheometer (Rheotech, Tokyo, Japan) with a spherical plunger (diameter = 15 mm). Hot sample solutions (1.5% w/w carrageenan, 10 mM KCl) were poured into cylindrical containers (height = 13 mm, diameter = 30 mm) and allowed to gel at a cooling rate of 1 °C/min in a temperature-controlled incubator. Samples were stored at 5 °C for different storage times prior to experiments. In compression test measurements, gelled samples were compressed at a rate of 1 mm/s. The Young's modulus, E, was obtained by fitting the Hertz equation to the experimental stress-strain curve Hertz equation (Hanaor, Gan, and Einav, 2015; Wu, Lin, and Juang, 2016). Measurements were repeated at least 3 times and the results represent mean values. All measurement was performed at room temperature ($\sim$25 °C).

3.3 Results and Discussion

3.3.1 Rheological properties and critical temperatures

Rheological measurements and the determination of critical transition temperature on cooling were carried out on a 1.5% w/w KC and IC solution with 10 mM KCl. The critical temperatures were determined from the sharp increase in G' as shown in Fig. 3.1. Note that the results above the critical temperature are unreliable, because the moduli of the solutions were too low to be determined under the experimental conditions employed. The critical temperatures of IC ($T_{c,IC}$) and KC ($T_{c,KC}$) obtained in the rheological measurements were $\sim$35 °C and $\sim$23 °C, respectively.

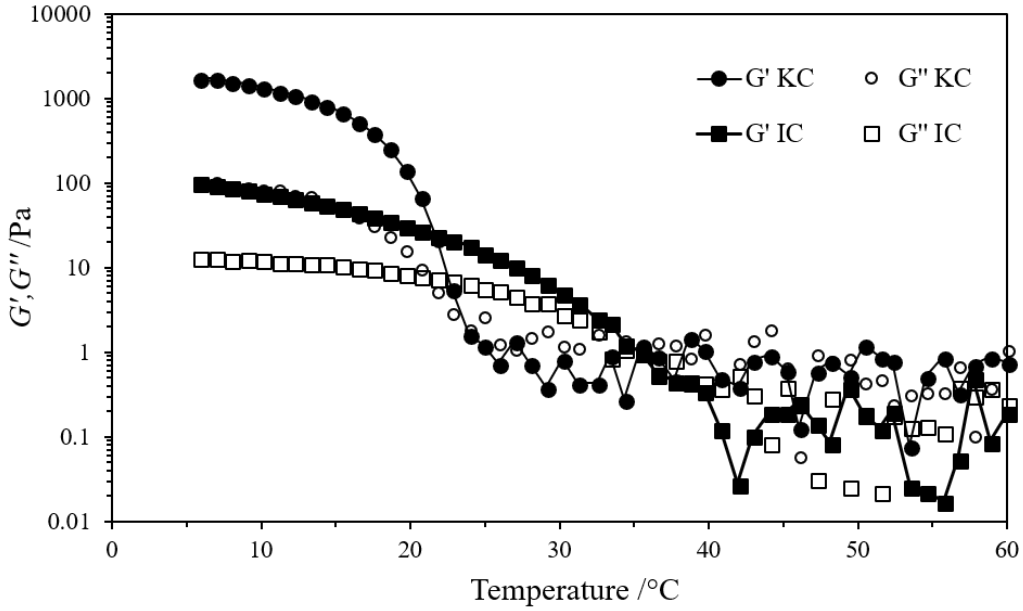

Fig. 3.1 Temperature dependence of G' (solid) and G" (open) of 1.5% solution of KC (circle) and IC (square) with 10 mM KCl on cooling.

The frequency dependence of G' and G" for KC and IC indicated a gel-like response, i.e., G'>G", with frequency-independent moduli in the range from 0.1 to 100 rad/s, as seen in Fig. 3.2. Rheological measurements showed that KC gels have higher moduli than IC gels. Conversely, for IC gels, the relatively low G' and the substantial viscous component (G" often > G'/10) is a typical feature of so-called weak gels (Chronakis, Piculell, and Borgström, 1996; Ikeda and Nishinari, 2001).

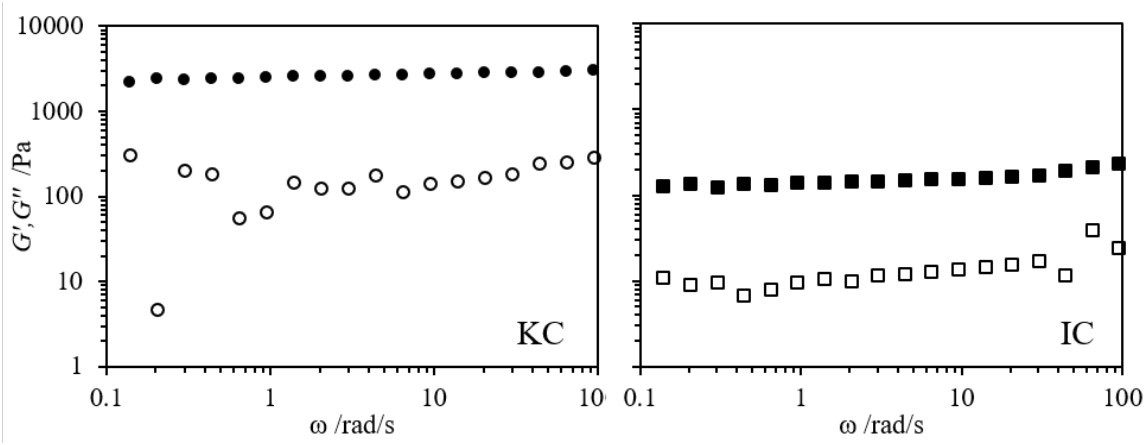

Fig. 3.2 Frequency dependence of G' (solid) and G" (open) of 1.5% solution of KC (circle) and IC (square) with 10 mM KCl at 5 °C.

3.3.2 Temperature dependence of particle movement

The movement of probe particles in the evolving network structures of KC and IC gels was tracked and quantified through the msd, cf. Eq. 3.1. The exponent α in the relationship between $msd \sim \tau^{\alpha}$, which corresponds to the slope in the double logarithmic plot of *msd* vs. the lag time τ, describes the type of particle diffusion (Gardel, Valentine, and Weitz, 2005; Mason and Weitz, 1995; Price, 2009). Particle diffusion with α=1 implies unrestricted diffusion. Meanwhile, if α lies between zero and one, the sample is considered to restrict the diffusion space within the developed network structure (Waigh, 2005). Furthermore, when the *msd* becomes independent of the lag time, α = 0, the probe particles are trapped by the gel network.

Fig. 3.3 shows the *msd* of particles embedded as a function of lag time τ at various temperatures. The dashed lines are drawn as a reference for the slope = 1, indicating free diffusion. Different behaviors in KC and IC solutions were observed, reflecting the difference in the gelation mechanism. At temperatures above the gelation temperatures, all the particles in both KC (Fig. 3.3A-B) and IC (Fig. 3.3D) solutions showed an almost linear increase of *msd* with the lag time. The magnitude and distribution of *msd* curves of the particles in KC solution changed significantly below $T_{c,KC}$ (Fig. 3.3C), while the *msd* curves of those particles in IC solution did not markedly change, with particles exhibiting free diffusion even below $T_{c,IC}$ (Fig. 3.3E-F). It is also worth mentioning that the *msd* in KC showed a broad distribution as compared to IC. This result indicates that particles were present in different microenvironments and exhibited different diffusion behaviors even for the longest (110 s) observation time, and even at temperatures above $T_{c,KC}$.

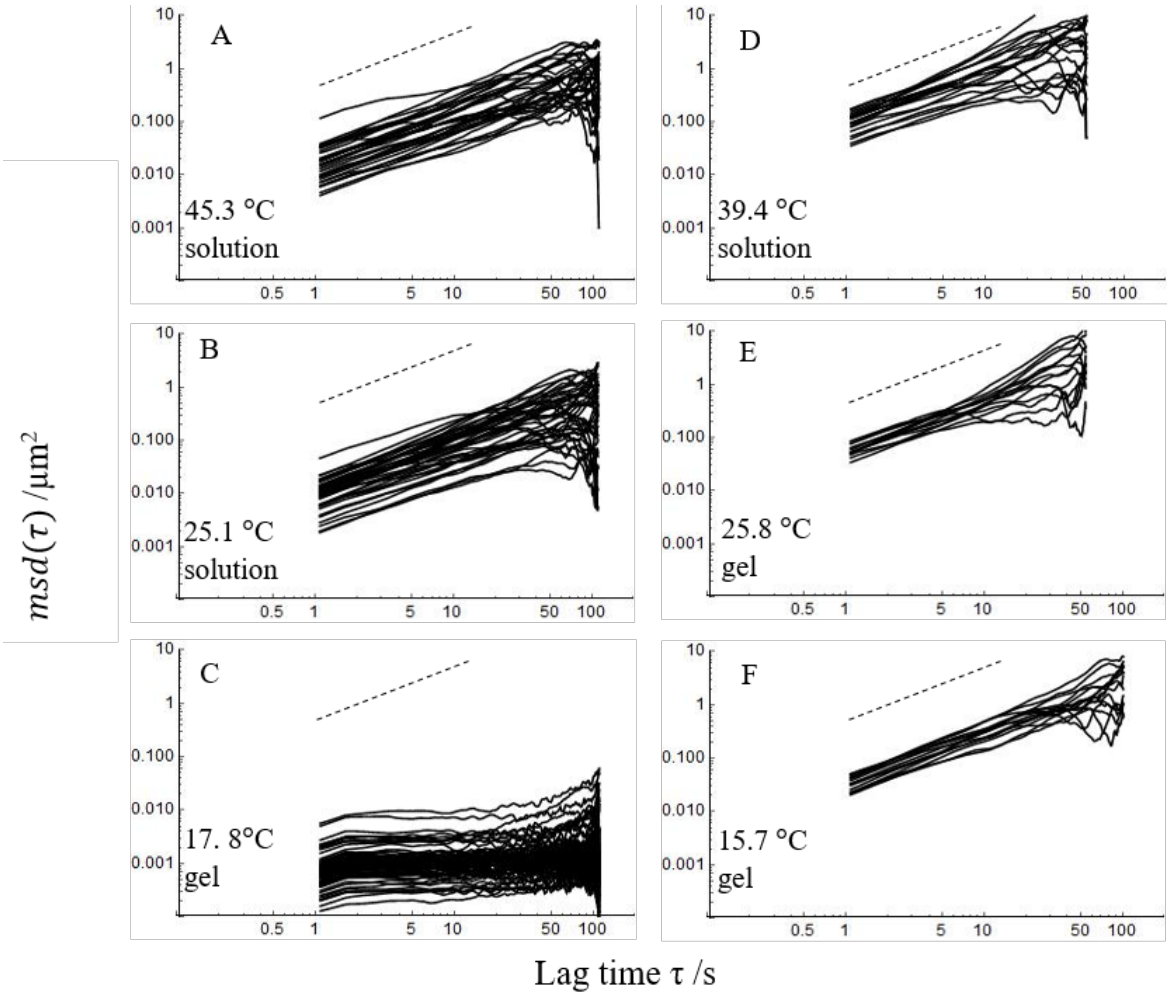

Fig. 3.3 Individual mean square displacement (*msd*) plot against lag time of 0.1 μm probe particles embedded in 1.5% w/w carrageenan solutions with 10 mM KCl at different temperature on cooling for KC at A) 45.3 °C, B) 25.1 °C, C) 17.8 °C and IC at D) 39.4 °C, E) 25.8 °C, F) 15.7 °C.

An underlying assumption in particle tracking experiments is that the embedded particles do not affect the structure of the host material (Moschakis, 2013). Several experiments have been performed to investigate the structure of gel networks, where probe particles with diameters of 0.5-0.75 μm were utilized with no inherent effects (Caggioni, Spicer, Blair, Lindberg, and Weitz, 2007; Moschakis, Lazaridou, and Biliaderis, 2014; Papagiannopoulos, Sotiropoulos, and Pispas, 2016). It is therefore expected that introduction of particles of this size does not affect the bulk rheology. Equilibrium condition is also expected to be

hold even with the addition of particles and the variation in the msd is then more attributed to the local differences in the gel network structure as single particles probe the rheology locally (Michalet, 2010). In our previous studies, we utilized poly(ethylene) oxide (PEO) probes with a hydrodynamic radius of around 10 nm to carry out diffusion measurements by pulse-field gradient NMR where the length scales probed do not exceed several hundreds nm (Hu, Du, and Matsukawa, 2016). The particles used in this study (diameter = 100 nm) can probe the gels at larger length scales.

The *msd* at short τ is considered to reflect local motion affected only by the local viscosity. Fig. 3.4 shows the temperature dependence of $\langle msd \rangle$ at τ =10 s in the KC and IC solutions. The $\langle msd \rangle$ in the KC sample was multiplied by 3 to facilitate the comparison with IC. At temperatures above $T_{c,KC}$, the $\langle msd \rangle$ in the KC solution remained almost constant, indicating a small effect of the temperature. At around $T_{c,KC}$, namely, the macroscopic gelation temperature, the $\langle msd \rangle$ decreased steeply, showing that the motion of the particles was restricted by the network formation of KC chain aggregates (Gardel, Valentine, and Weitz, 2005). On the other hand, the $\langle msd \rangle$ in IC solutions showed high values at temperatures higher than $T_{c,IC}$ indicating that the particles are in a microenvironment with low microviscosity. The $\langle msd \rangle$ decreased at around $T_{c,IC}$ due to the gradual network formation of IC chain aggregates (Hu, Du, and Matsukawa, 2016).

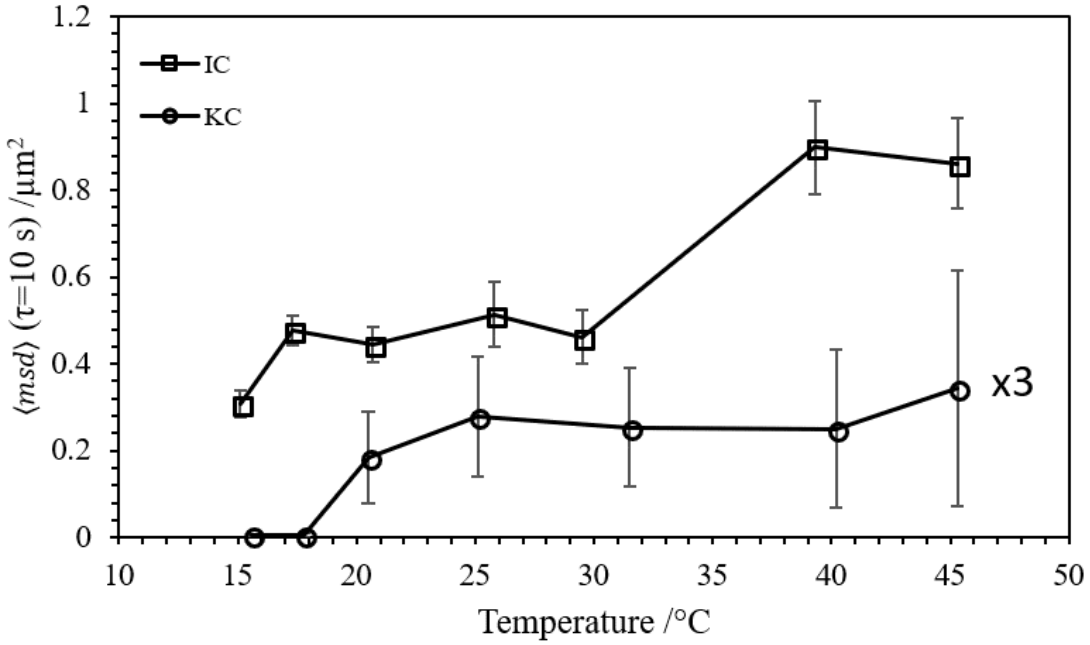

Fig. 3.4 Temperature dependence of $\langle msd \rangle$ at τ=10s of 0.1 μm probe particles embedded in KC (circles), and IC (square). $\langle msd \rangle$ for KC was expanded 3 times for clarity. Error bars were corresponding to the standard deviation in the distribution of *msd* at τ=10s.

To understand the evolution of the network structure, the $msd(\tau = 10s)$ against exponent α at different temperatures on cooling are plotted in Fig. 3.5. At the temperatures above $T_{c,KC}$, the particles in KC solution showed diffusive behavior with $\alpha \sim 1$, suggesting a viscous response of the sample (Fig. 3.5A-B). At this temperature range, the KC chains exist as random coils, allowing the particles to diffuse in a viscous solution microenvironment. With decreasing temperature around $T_{c,KC}$, both the $msd(\tau = 10s)$ and exponent α decreased drastically (Fig. 3.5 C), indicating trapping of the particles within the network structures of KC aggregates due to the formation of a stiff and permanent gel network (Du, Brenner, Xie, and Matsukawa, 2016).

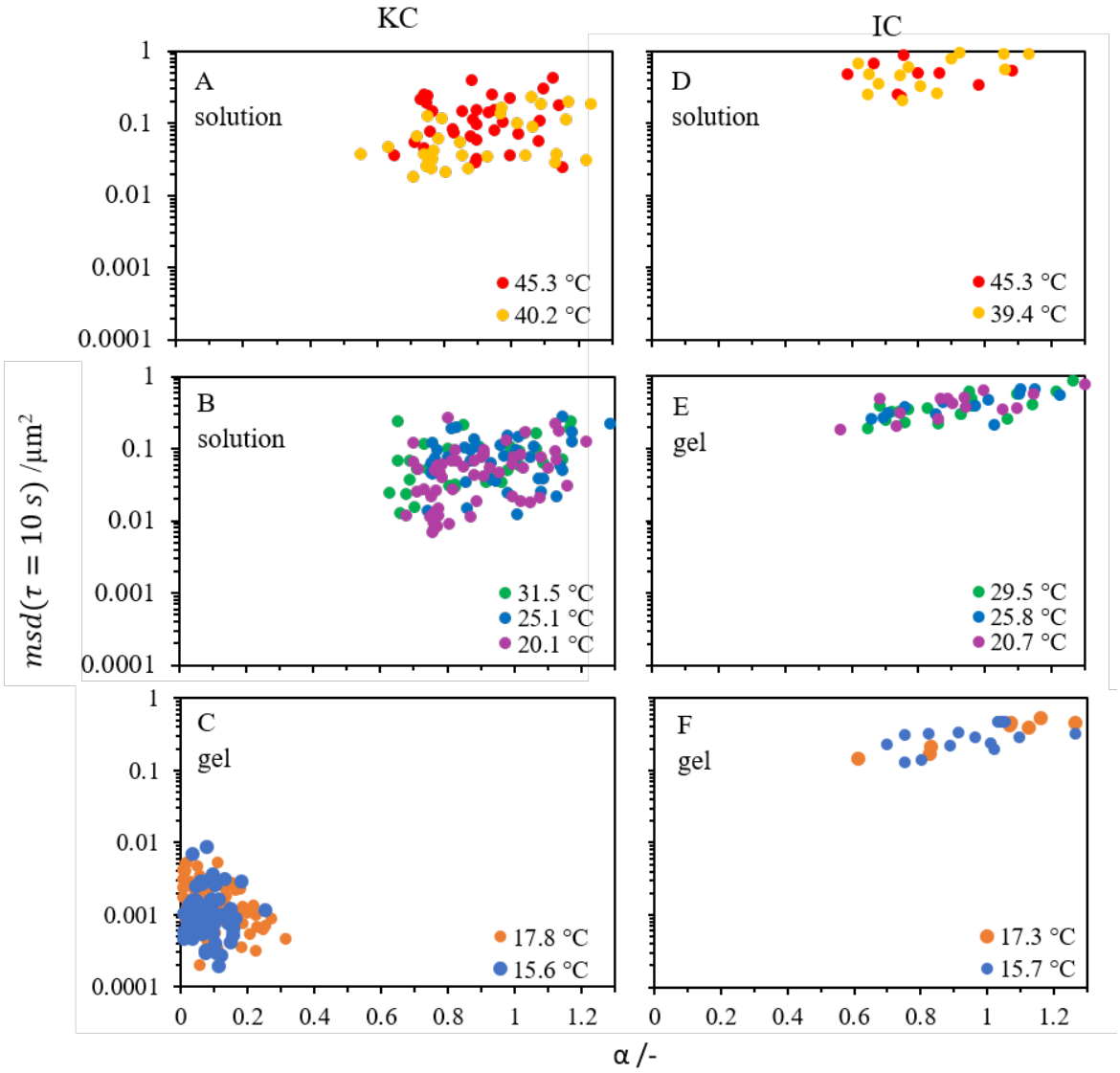

Fig. 3.5 Distribution of *msd* at τ=10s plotted against the exponent α fitted at lag time 1s<τ<20s during cooling for KC (A-C) and IC (D-F).

The *msd* of particles in IC solutions clearly showed diffusive behavior over the entire temperature range observed (Fig. 3.5 D-F). The exponent α was in the range 0.8–1 and did not show a significant decrease even far below $T_{c,IC}$ (Fig. 3.5 D-F). Similar diffusive behavior has been reported for 0.75 μm particles in β-glucan solutions, even though bulk rheological measurements showed an elastic behavior indicating formation of gel (Moschakis, Lazaridou, and Biliaderis, 2014). In that study, CLSM images of fluorescence showed unconnected

clusters of chain aggregates, which would allow particle diffusion. Our results suggest that heterogeneous clusters of IC chain aggregates are formed, but macroscopic gelation does not involve irreversible percolation of these clusters. Furthermore, the existence of the clusters restricts particle movement leading to the decrease in $\langle msd \rangle$ around $T_{c,IC}$, see Fig. 3.4. The cluster formation is also responsible for the macroscopic behavior (G' and G", see Fig. 3.1), i.e., the formation of the so-called "weak gel". There is another possibility for the network structure, namely, that a permanent but loose network structure is formed, with pore size strongly exceeding 100 nm, thus still allowing free diffusive motion of the particle used in this study. The difference between these two possibilities would be observed in the frequency dependency under large strain.

3.3.3 Change of network structure during storage

The msd measurements were carried out as a function of storage time. Fig. 3.6 shows the msd of particles embedded in 1.5% w/w carrageenan gels following storage at 5 °C. As shown in Fig. 3.6 a-d, the particles in KC gels did not show a significant change with storage time. As shown in Fig. 3.7a, the exponent α was ~0 for all the particles in KC gels at all storage times, indicating trapping of the particles within the gel network. This result demonstrates that KC chains formed a permanent gel, immobile network due to extensive aggregation.

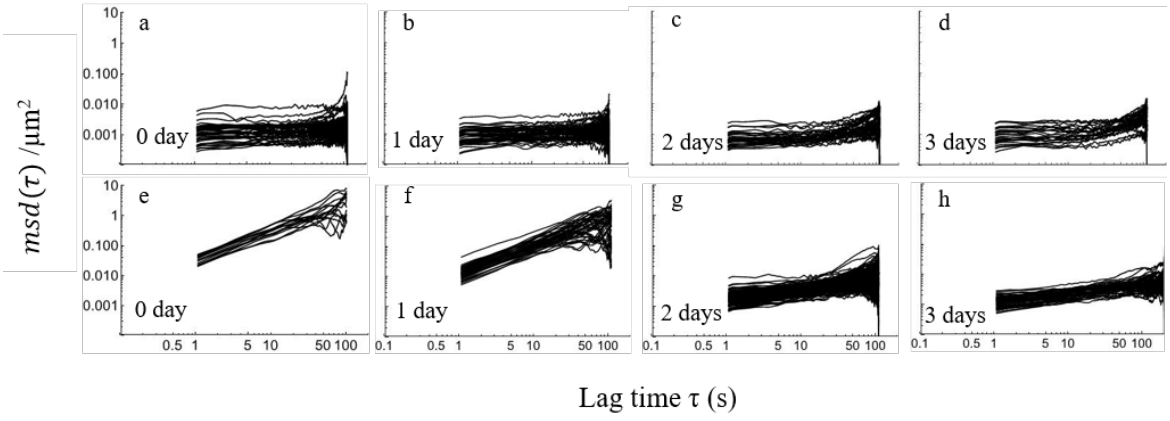

Fig. 3.6 Individual mean square displacement (*msd*) plot against lag time of 0.1 μm probe particles embedded in 1.5% w/w solutions with 10 mM KCl at different storage kept at 5°C for KC (a-d) and IC (e-h).

The *msd* of particles in IC solution depended on storage time as shown in Fig. 3.6 e-h. Free diffusion ($\alpha \sim 1$) was observed at both days 0 and 1, although *msd* decreased during this period. At day 2, a strong decrease in both *msd* and α ($\sim$0.3) was observed. The continuous decrease in msd shown in Fig 3.7b indicates continuous structural changes of IC gels. The decrease in the magnitude of the msd from 0 to 1 day storage implies an increasing resistance on the particle motion. This finding probably indicates an increase in size of IC clusters. The drastic decrease in *msd* after 2 days of storage, however, corresponds to the formation of a permanent network structure, which obstructs particle movement and leads to the decrease in α. This finding implies that the clusters continue to grow and eventually bind to each and from a permanent gel network. It is also possible that the particles stuck to the gel network, but it was denied by the observation of particle movement in the solution with chopped minute gels, which showed a diffusive behavior indicating that the particles did not stick on the chopped gel and that the change in the *msd* with storage was due to the change of network structure.

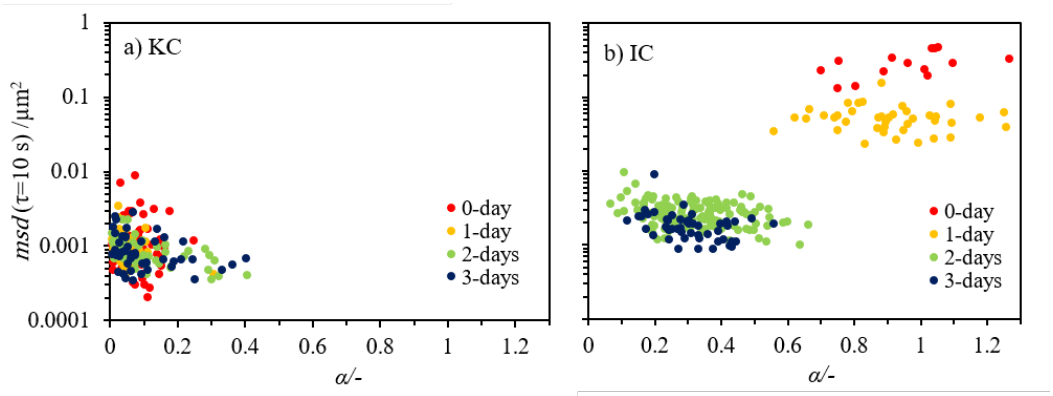

Fig. 3.7 Distribution of *msd*(τ=10s) plotted against exponent α at different storage time for a) KC and b) IC.

Fig. 3.8 shows the Young's modulus, *E*, for IC and KC gels, as obtained from compression tests, as a function of storage time at 5 °C. Error bars represent the standard deviation obtained from at least three independent measurements. The E values of KC gels clearly indicate that KC formed a hard and brittle gel compared to IC. As shown in Fig. 3.8, *E*of the KC gels remained nearly constant, indicating that KC formed a permanent gel network upon cooling that did not change on further storage. Conversely, IC gels showed soft gel behavior with a low modulus. However, the *E* of IC gels increased during storage, which reflects the continuous growth of the clusters of IC chain aggregates, which eventually yield a permanent gel. This result is consistent with the microscopic behavior observed in particle tracking measurements.

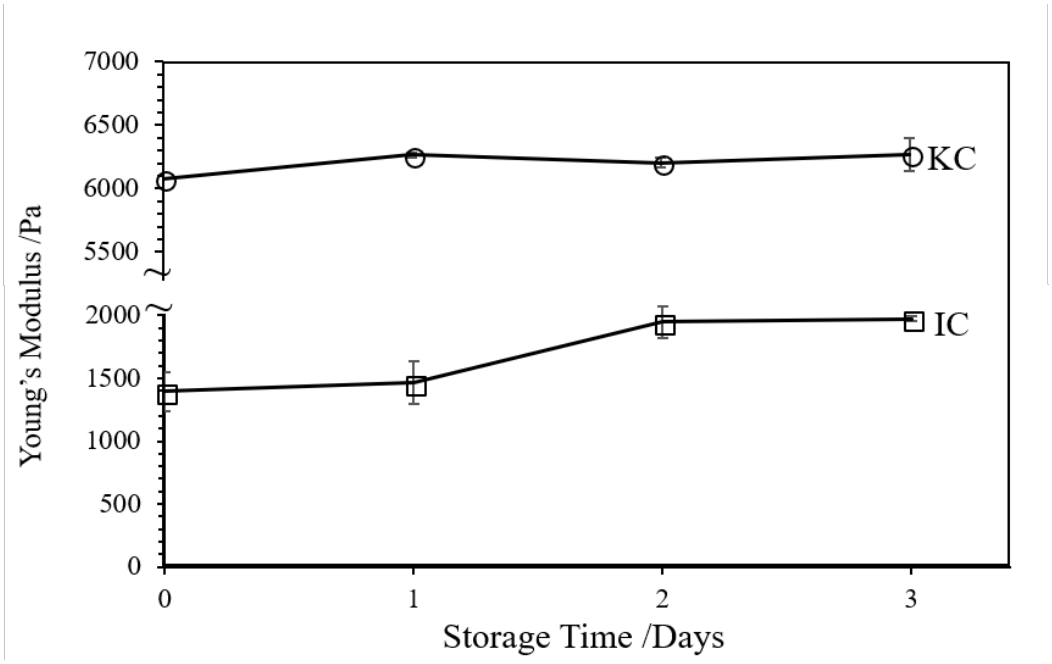

Fig. 3.8 Storage dependence of the Young's modulus *E* in 1.5% w/w carrageenan solutions with 10 mM KCl stored at 5 °C for KC (circle) and IC (square). Error bars were corresponding to the standard deviation in the distribution of *E*.

NMR measurements affirmed that KC gels formed thick aggregates of KC chains while IC gels formed fine and loose aggregates (Hu, Du, and Matsukawa, 2016). This molecular level observation checks with the bulk rheological response shown by KC (hard and brittle)

gels and IC (soft) gels (see Fig. 3.1). We postulate that clusters of carrageenan aggregates are formed and percolate to eventually yield a permanent gel network. For KC gels, the formation of thick aggregates of interconnected clusters proceeds rapidly and yields a permanent gel network, and the process was completed within the cooling time using the cooling rate employed in this study (1 °C/min). On the other hand, for IC gels there are two possibilities: 1. Heterogeneous clusters of IC chain aggregates were formed but did not percolate, and, 2. IC chains formed a loose network structure with pores larger than 100 nm. Either way, cluster rearrangement or network coarsening on storage led to an eventual permanent gel network. This process is depicted in Fig. 3.9.

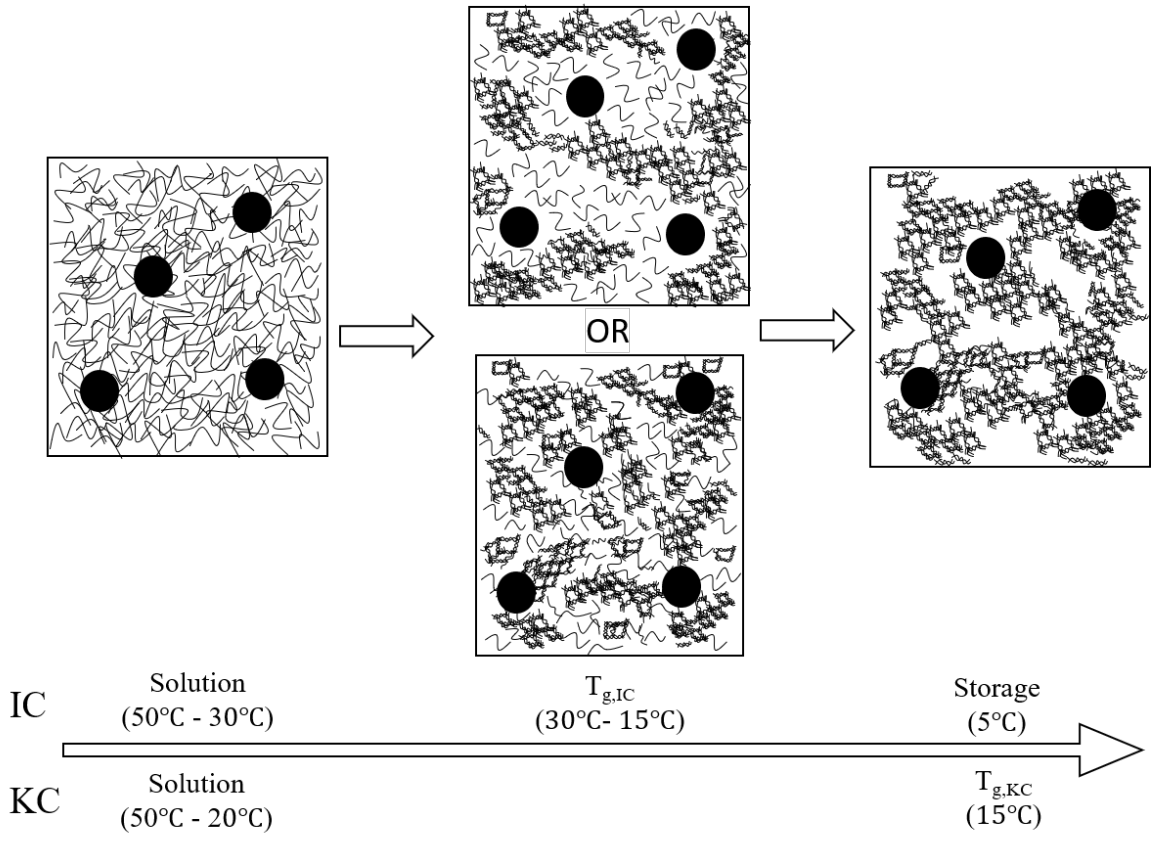

Fig. 3.9 Graphical representation on the proposed interpretation of gelation mechanism for carrageenan isoforms on cooling and storage.

3.4 Conclusion

Particle tracking measurements have been performed to investigate the network structure and gelation mechanism in KC and IC solutions. For KC, the particle $\langle msd \rangle$ steeply decreased around$T_{c,KC}$ and $\alpha \sim 0$ was found in the gel state, indicating formation of a permanent gel network structure. While the particle $\langle msd \rangle$ in IC solution decreased at $T_{c,IC}$, α remained ~ 1, indicating formation of clusters of IC chain aggregates that are not permanently connected, and still allow free particle diffusion. The longtime diffusion of probe particles in the IC gel provides information on the network structure of this so-called weak gel. The storage time dependence of *msd* and *E* revealed that KC formed a permanent gel network structure upon cooling and did not show significant changes with storage. Conversely, *msd* of the particles in IC showed a continuous decrease with storage. In addition, the Young's modulus *E* of IC gels continuously increased with storage time. These results suggest that the clusters of IC chains are continuously growing, and eventually bind and form a permanent gel network.

Chapter 4

Microscopic characterization of phase separation in mixed carrageenan gels using particle tracking

In this chapter, the gelation mechanism and phase-separated network structure of mixed κ-carrageenan (KC) and ι-carrageenan (IC) were investigated using particle tracking. The thermally driven random motion of fluorescent particles (diameter = 100 nm) was utilized to probe the local circumstances of the gelling carrageenan at the sub-micron scale. The mean square displacement (MSD) was used to characterize the changes in the network structure on cooling and storage for 1 day. The temperature dependence of ensemble-averaged MSD for the particles in the mixture of KC and IC gels showed a two-step decrease on cooling, consistent with the two-step increase in viscoelasticity observed in macroscopic rheological measurements. This result revealed the independent formation of KC and IC chain aggregates in the mixture. The individual MSD of particles in the mixture showed a large distribution after 1-day storage, indicating the emergence of microstructural heterogeneity in the gel. We consider that this heterogeneity came from the frozen structure on the way to phase-separated network structure. The van Hove correlation plots suggested the presence of two groups

of particles with fast and slow mobilities in the mixture. Plotting the MSD of individual particles vs α with the MSD scaled as t^{α} and t the lag time suggested a bimodal distribution made up of fast and slow particles. The presence of two groups of particles with different mobilities suggested that mixtures of KC and IC was frozen on the way to a phase-separated network structures made of KC-rich and IC-rich domains with a size of $>$100 nm due to the network formation of KC and IC chains.

Based on: Lester C. Geonzon, Rommel G. Bacabac, Shingo Matsukawa. Microscopic characterization of phase separation in mixed carrageenan gels using particle tracking. Journal of the Electrochemical Society, 166(9) B3228-B3234 (2019).

4.1 Introduction

The gelation mechanism of solutions of KC, IC and their mixtures have been extensively studied (Du, Brenner, Xie, and Matsukawa, 2016; Du, Lu, Geonzon, Xie, and Matsukawa, 2016; Hu, Du, and Matsukawa, 2016). Macroscopic rheological measurements showed that the mixtures of KC and IC undergo a two-step gelation process (Bui, Nguyen, Renou, and Nicolai, 2019; Du, Brenner, Xie, and Matsukawa, 2016). Differential scanning calorimetry (DSC) revealed that KC and IC chains formed aggregates in the mixture independently (Du et al., 2016). These results suggested a formation of a phase-separated network structure in the mixed gels. Nevertheless, there is no direct microscopic evidence of this phase separation. Several studies utilized various imaging techniques in an attempt to visualize the actual gel structure, namely, scanning electron microscopy (SEM) (Thrimawithana et al., 2010), transmission electron microscopy (TEM) (Amici et al., 2002), and confocal laser scanning microscopy (CLSM) (Bui et al., 2019; Heilig et al., 2009). While the methods provide direct information on the gel microstructure, sample treatment could lead to formation of artifacts and change the gelation mechanisms of KC and IC (Aguilera and Stanley, 1999). These

artifacts could arise from extensive drying (for SEM), staining (for TEM) or fluorophore labeling (for CSLM). In previous studies carried out by our group, probe polymer diffusion measurements done by pulse-field gradient nuclear magnetic resonance (NMR) have been carried to study the network structure and gelation mechanism of pure (Zhao, Brenner, and Matsukawa, 2013) and mixed carrageenan gels (Hu, Du, and Matsukawa, 2016) at the nanometer scale. However, these studies could not resolve the network structure of the mixed gels due to the short diffusion time (10 ms) and the size (usually several tens of nanometer) of the probe polymer chosen, and concluded two possibilities existed for mixed carrageenan gels: either an interpenetrating network of IC and KC, or a micro-phase separated network structure with a domain size of $\sim$ 450 nm (Hu, Du, and Matsukawa, 2016). While diffusion NMR measurements provide detailed information on structure at the nanometer scale, their inability to provide information on the micrometer scale serves as an incentive to the current work, in which we aimed to study carrageenan gel structure on larger scales.

Passive particle tracking is a popular tool used to investigate microscopic physical properties, e.g. micro-rheology, based on the thermally driven random motion of probe particles. It provides access to important information on the local viscoelastic properties of fluids (Mason, Ganesan, van Zanten, Wirtz, and Kuo, 1997; Waigh, 2005). The diffusion of particles, driven by Brownian forces (i.e., thermal energy) can be used to probe these properties non-invasively, as long as appropriate particles are chosen that do not alter the host materials into which they are introduced (Moschakis, Lazaridou, and Biliaderis, 2012; Shabaniverki and Juárez, 2017). In particle tracking, the Brownian motion of individual probe particles is used to calculate the mean square displacement (MSD). The MSD can be used to deduce local physical properties of the host material. Using particle tracking, spatial differences in the local physical properties and structural heterogeneity of the host material can be probed without affecting the developing network structure. An important factor in particle tracking

experiments is the size of the probe particles in relation to the characteristics structural length scale of the medium probed (Valentine, Kaplan, Thota, Crocker, Gisler, Prud'homme, Beck, and Weitz, 2001). In particular, particle tracking experiments are expected to provide information on the network structure of the mixed gels, whether they phase-separated or interpenetrating in nature, as long as probe particles of an appropriate size are chosen.

In this chapter, we employed particle tracking to elucidate the gelation mechanism and network structure of mixed KC/IC gels at different mixing ratios. The temperature dependence of particle MSD in mixed gels was studies on cooling and compared to results from macroscopic rheological measurements. Further measurements were carried out to elucidate any further changes in the network structure of the mixed gels on storage.

4.2 Materials and Methods

4.2.1 Materials

Please refer to Section 3.2.1

4.2.2 Sample Preparation

The mixture solutions of KC and IC were prepared at a total carrageenan concentration of 1.5% with 10 mM KCl by mixing pure KC and IC solutions at different mixing ratios. Samples were designated KC80IC20, KC70IC30, KC60IC40, KC50IC50, KC40IC60 and KC30IC70, where x and y in the code KCxICy indicate the percentage of KC and IC, respectively (x + y = 100). Samples for the rheological measurements were prepared using the same procedure except for the addition of probe particles

4.2.3 Dynamic rheological measurement

Rheological properties were measured using HAAKE MARS II rheometer (Thermo Scientific, Waltham, MA, USA) equipped with blasted parallel-plates (diameter 35 mm) with 1 mm gap. Hot sample solutions were loaded on preheated plates at 80 °C and covered with oil to avoid water evaporation. The storage modulus (G') and loss modulus (G") were monitored on cooling from 80 °C to 5 °C at a rate of 1 °C/min.

4.2.4 Particle tracking measurements

Pre-heated sample solutions containing probe particles were placed in a custom-built sample chamber of a glass bottom dish (Matsunami Glass Inc. Ltd., Tokyo, Japan) equipped with a thermosensor (CENTER 309, Center Technology Corp., Tokyo) for temperature monitoring and sealed with a cover glass using a silicone sealant (Geonzon, Bacabac, and Matsukawa, 2019b). The thermosensor was set at a position within 10 mm from the view area between the glass plates. The sample was kept at 50°C for 10 min to equilibrate prior to measurement. Particle tracking measurements of fluorescent particles added to carrageenan solutions were carried out using an inverted microscope, BZ-9000 (Keyence Corp., Osaka, Japan), equipped with a PlanFluor 100× NA 1.30 oil-immersion objective (Nikon Corp. Inc., Japan) and a temperature-controlled microscope stage (ALA Scientific Instruments Inc., New York). The sample temperature was controlled by the microscope stage and monitored using the thermosensor.

Movies of the diffusing fluorescent-labeled particles were recorded using a built-in 2/3-inch, 1.5 megapixels, 12-bit, monochrome cooled CCD camera (Keyence Corp., Osaka, Japan) at a rate of 7.5 frames per second for 110 seconds. The video recording of particle movement was then deconstructed into a series of frames for analysis. In cooling experiments, the particle tracking was performed at different temperatures from 50 °C to 10 °C.

For measurement at low temperatures (gel state), a total of 50–70 particles were tracked simultaneously. For measurement at high temperatures, particles were observed to have high mobility and occasionally moved in-and-out of focus during the tracking and fewer particles ($\sim$15-30 particles) were successfully tracked throughout the measurement. The repeatability of the measurements was confirmed by carrying out the measurements at least four times for different areas of the sample. In storage experiments, hot solutions of carrageenan were cooled down from 50 °C to 5 °C at a rate of 1 °C/min in a temperature-controlled incubator to form a gel and stored at 5 °C prior to experiments of the particle tracking, also done at 5 °C.

The position of each fluorescent labeled particles was determined using an algorithm which improves the accuracy of particle position using the image-intensity weighted centroid for each particle (Geonzon and Matsukawa, 2019), from which particle trajectories were calculated and analyzed. The time-averaged MSD for each particle (*msd*) obtained from N images representing a total diffusion time τ was calculated with the following equation(Lieleg, Vladescu, and Ribbeck, 2010; Wagner, Turner, Rubinstein, McKinley, and Ribbeck, 2017) :

$$msd(\tau) = \frac{1}{N - \frac{\tau}{\triangle t}} \sum_{i=1}^{N-\frac{\tau}{\triangle t}} [r(i\triangle t + \tau) - r(i\triangle t)]^2 \tag{4.1}$$

where $\triangle$t is the interval time for each frame, that is the inverse of the frame rate, and r($\triangle$t) is the position of the centroids of each tracked particle. The exponent α in the relationship between *msd* and *tau*, $msd \sim \tau^{\alpha}$, was calculated for each particle at lag times in the range 1–20 s. Because the number of displacements for the averaging $(N - \frac{\tau}{\triangle t})$ decreases, the *msd* points at longer lag times tend to have larger statistical fluctuations (Michalet, 2010). The ensemble-averaged MSD, $\langle msd \rangle$, was obtained by averaging the msd of all tracked particles. Particle tracking and MSD calculations were performed using a custom-made

program written in Mathematica 10 (Wolfram Research, Inc., Champaign, IL) (Geonzon and Matsukawa, 2019).

4.3 Results and Discussion

4.3.1 Rheological properties and critical temperatures

The viscoelastic measurements of KC, IC, and mixed KC/IC were carried out at a total carrageenan concentration of 1.5% and 10 mM KCl. The G' values of these solutions are plotted against the temperature on cooling, as shown in Fig. 4.1. The critical gelling temperature, T_c, was defined as the temperature at which G' showed a sharp increase (Fernandes, Gonçalves, and Doublier, 1991). G' above the critical temperatures showed large noise because the moduli of the solutions were low.

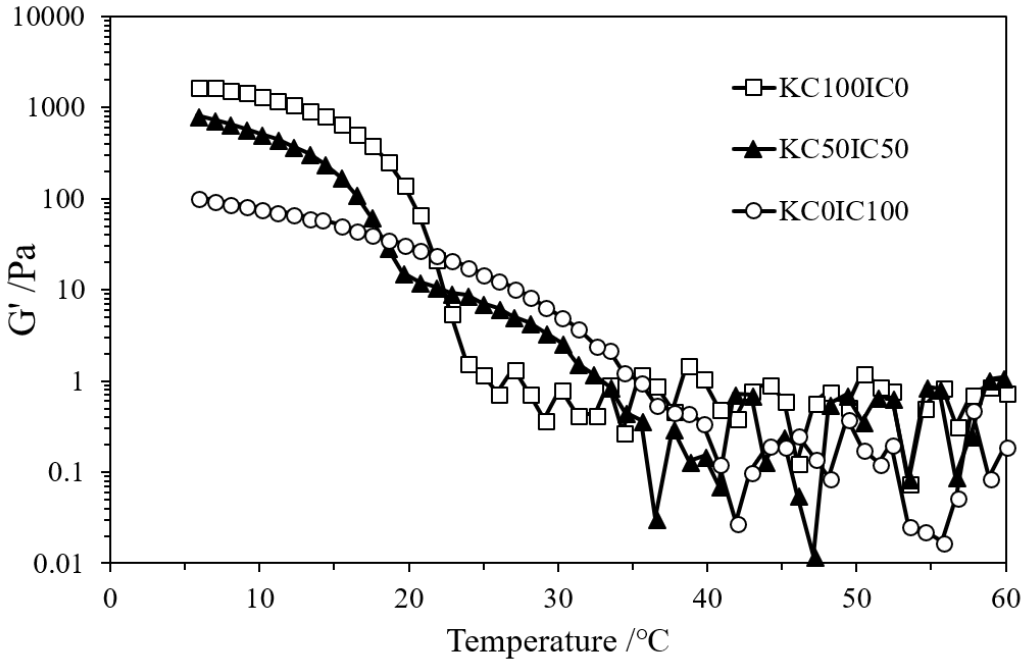

Fig. 4.1 Temperature dependence of storage modulus of 1.5% solutions of pure KC (open square), IC (open circle) and mixture of KC:IC (filled triangle) in 10 mM KC on cooling.

A two-step increase in G' was observed in KC50IC50 at temperatures closed to those observed in the pure KC and IC solutions. This result is consistent with previous studies (Du, Brenner, Xie, and Matsukawa, 2016; Hu, Du, and Matsukawa, 2016). The T_c of pure IC ($T_{(c,IC)}$) and KC ($T_{c,KC}$) were $\sim$35 °C and $\sim$23 °C, respectively. These temperatures were used to categorize the stages of gelation for the mixed KC and IC: we refer to the sample as "Solution" above $T_{c,IC}$, "Gel I" between $T_{c,IC}$ and $T_{c,KC}$ and "Gel II" below $T_{c,KC}$.

4.3.2 Temperature dependence of particle mobility

The dynamic rheological measurements of the mixed KC/IC system showed a two step increase in G' that suggests independent aggregation steps of KC and IC chains. This two-step process presents the possibility of a phase-separated network structure with KC- and IC-rich domains (Du, Brenner, Xie, and Matsukawa, 2016). In our previous studies, poly(ethylene) oxide (PEO) was used as a probe with a hydrodynamic size around 10 nm to carry out pulse-field gradient NMR diffusion measurements. These measurements could not extract structural information on length scales exceeding about 100 nm (Hu, Du, and Matsukawa, 2016). In this study, particles with a diameter of 100 nm were used to obtain information on larger length scales. The mobility of probe particles added to the mixture solution of KC and IC was measured to gain insight into the microstructure and the microrheology. We note that in particle tracking experiments, the structure of the host medium is expected to be unchanged by particle addition (Michalet, 2010; Moschakis et al., 2012; Shabaniverki and Juárez, 2017; Waigh, 2005)

The *msd* of particles measured on cooling are shown in Fig. 4.2. The different stages of gelation, as determined from critical temperatures obtained in the bulk rheological measurements, are indicated in the figure. Results for pure KC and IC solutions taken from (Geonzon,

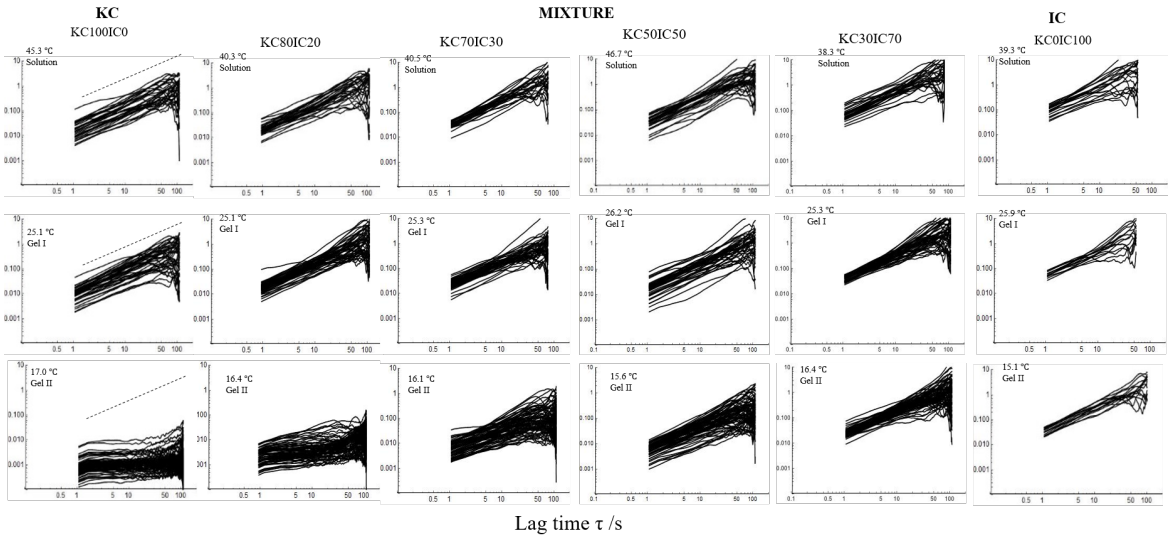

Fig. 4.2 Individual *msd* of particles at different mixing ratio of KC and IC on cooling. Data on the pure KC and IC are also shown in reference (Geonzon, Bacabac, and Matsukawa, 2019b).

Bacabac, and Matsukawa, 2019b) are also indicated for comparison.

Different particle dynamics were observed for the mixtures in each stage of gelation. In the Solution stage above $T_{c,IC}$, all particles exhibited an α exponent of 1 at all mixing ratios of the carrageenans. This exponent indicates normal diffusion. Such normal diffusion behavior was also observed below $T_{c,IC}$ in the Gel I stage. With decreasing temperature below $T_{c,KC}$ to the Gel II stage, different particle mobilities were observed at different mixing ratio. For KC80IC20, the magnitude and distribution of msd curves changed significantly, in a way similar to that observed in pure KC. However, some of the probe particles still showed diffusive behavior. At intermediate mixing ratios (50–70% KC), almost all the particles showed normal diffusive behavior with a broad distribution of *msd*. For KC40IC60 and KC30IC70, all particles showed normal diffusive behavior similar to that observed in pure IC(Du et al., 2016).

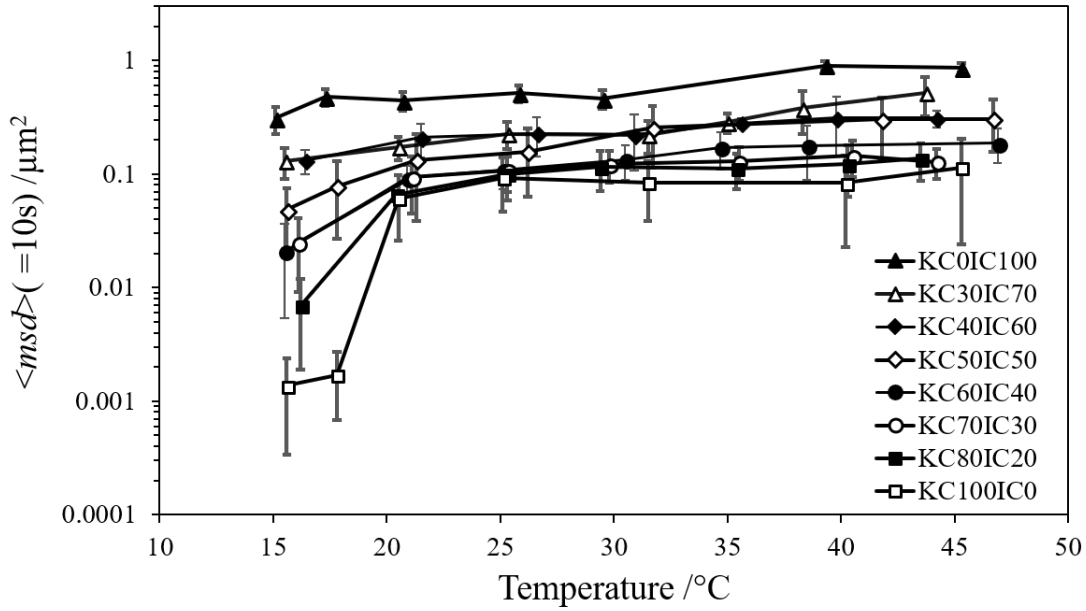

Fig. 4.3 Temperature dependence of $\langle msd \rangle$ at lag time τ= 10s of probe particles in mixed KC and IC at different mixing ratio on cooling. Error bars indicate the standard deviation of *msd* at lag time τ= 10s

The microscopic viscosity of the solutions was considered by calculating$\langle msd \rangle$ at short τ. Fig. 4.3 shows the temperature dependencies of $\langle msd \rangle$ at τ = 10 s. Error bars are corresponding to the standard deviation of the distribution of *msd* at τ = 10 s for individual particles. The $\langle msd \rangle$ in the mixtures showed intermediate behavior between the $\langle msd \rangle$ of the two pure carrageenan solutions at all temperature range. A two-step decrease in the $\langle msd \rangle$ was observed for KC40IC60, KC50IC50 and KC60IC40 while other mixtures showed a more monotonous decrease. Obvious changes were observed close to those observed for the pure carrageenan solutions. This finding is consistent with the two-step increase in G' in the macroscopic rheological measurements. The first decrease in the $\langle msd \rangle$ at around $T_{c,IC}$ was attributed to the formation of IC chain aggregates, which hinder particle mobility. The second decrease at around $T_{c,KC}$ suggests network formation by KC chain aggregates. Increasing the volume fraction of IC or KC from KC50IC50, the weak distinct changes morphed into a single-step decrease in the $\langle msd \rangle$. This single step decrease was generally observed at

the critical temperature of the major constituent carrageenan. This finding suggests that the $\langle msd \rangle$ of the particles were unaffected by the aggregation of the minor constituent.

To further clarify the diffusive behavior of individual particles, the exponent α was plotted against the *msd* (τ = 10 s) as shown in Fig. 4.4. As explained earlier, α is the slope in the double logarithmic plot of *msd* against τ, which describes the type of particle diffusion (Gardel et al., 2005; Moschakis et al., 2006; Price, 2009). Particle diffusion with α=1 implies that the sample has free space for normal diffusion. Meanwhile, the sample is considered to have a restricted diffusion space when α lies between zero and one (Gardel, Valentine, and Weitz, 2005). In materials where such sub-diffusive behavior is observed, the particle movement is hindered by some network structure (Waigh, 2005). When the *msd* becomes independent of the lag time, α= 0, the probe particles are considered to be fully constrained, i.e., trapped. In the Solution stage (Fig. 4.4, top row), almost all the particles showed diffusive behavior with $\alpha \sim 0.8$–1. Both KC and IC chains exist as random coils at this stage, allowing the particles to diffuse in a viscous solution.In the Gel I stage (Fig. 4, middle row), diffusive behavior was still observed, suggesting formation of disconnected or weakly connected IC clusters of aggregates, still allowing normal particle diffusion. Furthermore, the formation of these clusters of aggregates restricts the particle mobility, thus leading to decrease in $\langle msd \rangle$ (Fig. 4.3) that is concomitant with the increase of G' (Fig. 4.1) in (Geonzon, Bacabac, and Matsukawa, 2019b).

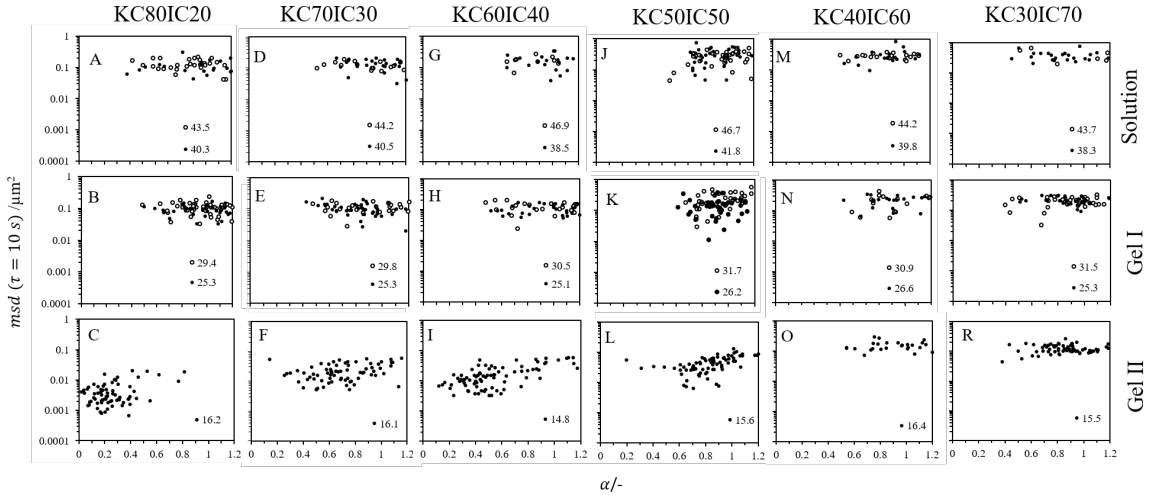

Fig. 4.4 Distribution of individual *msd* at τ=10 s plotted against exponent α fitted at lag time 1 s$<\tau<$20s during cooling at different mixing ratio of KC:IC.

In the Gel II stage (Fig. 4.4, bottom row), different particle mobilities were observed. In KC80IC20, most of the particles showed low *msd* values with α ~0-0.5, indicating trapping of particles in a strong and stiff network structure, while few particles showed sub-diffusive behavior with $\alpha > 0.5$. At intermediate mixing ratios (50–70% KC) broad distributions of α were observed with α in the range 0.2–1, indicating the presence of vastly different microenvironments. We considered particles with $\alpha <$0.5 and $\alpha > 0.5$ to be in KC-rich and IC-rich domains, respectively. In mixtures with a lower concentration of KC (KC40IC60 and KC30IC70), almost all the particles showed diffusive behavior with α ~0.8–1, suggesting that the aggregation of KC chains has little influence on the particle mobility. One possibility is that KC chains could only form small aggregates due to obstruction by IC clusters, and could not reach a size that could affect particle diffusivity.

4.3.3 Particle tracking in stored gels

Fig. 4.5 shows the *msd* of particles in mixed of KC/IC gels after cooling and after 1-day storage at 5 °C. For KC70IC30, KC60IC40, KC50IC50 and KC40IC60, the distribution of *msd* was clearly broader than for other gels, suggesting different particle dynamics within

the sample due to structural heterogeneity.

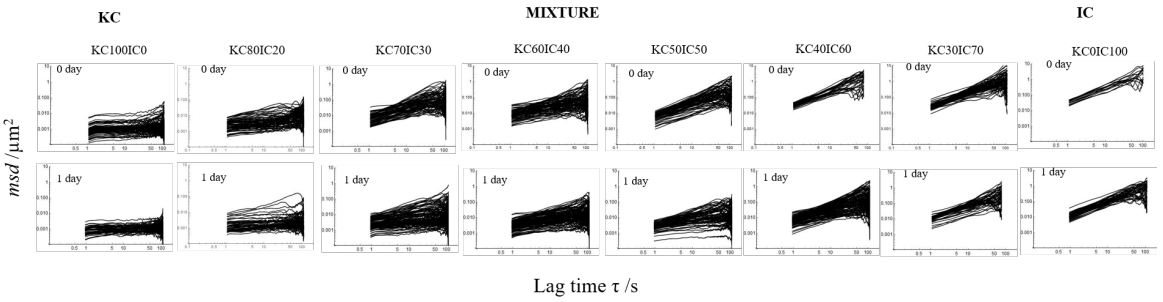

Fig. 4.5 Individual *msd* of particles in mixed KC and IC at different mixing ratio after 1 day storage. Data on pure KC and IC are also shown for reference.

The tracking of 100 nm particles suggests a large distribution of micro-rheology and microstructure in the mixed KC/IC gels. We propose that the observed structural heterogeneity was frozen on the way to the phase-separated structure due to the network formation of KC and IC chains at the cooling rate (1 °C/min) employed in this experiment. The information to support this consideration will be described in the later section.

The structural heterogeneity is reflected in the distribution of particle displacement ($\triangle$r) at a lag time τ, (P($\triangle$r,τ)), known as the van Hove correlation function (Valentine et al., 2001). The distribution P($\triangle$r,τ) of a homogenous medium is described by a Gaussian function, where the deviation, σ, is proportional to $\langle msd \rangle$. A non-Gaussian distribution indicates a inhomogeneous medium, implying that the particles experience different microenvironments (Moschakis et al., 2006; Valentine et al., 2001). Fig. 4.6a shows P($\triangle$r,10s) for pure KC, IC and KC50IC50. The solid line indicates a Gaussian fit to the distribution of in KC50IC50, while the dashed lines indicate fits employing a combination of two Gaussian functions (Gao and Kilfoil, 2007),

$$P(\triangle r,\tau) = \frac{f_1}{\sqrt{2\pi\sigma_1^2}} \exp^{-\frac{1}{2}(\frac{\triangle r}{\sigma_1})^2} + \frac{f_2}{\sqrt{2\pi\sigma_2^2}} \exp^{-\frac{1}{2}(\frac{\triangle r}{\sigma_2})^2} \tag{4.2}$$

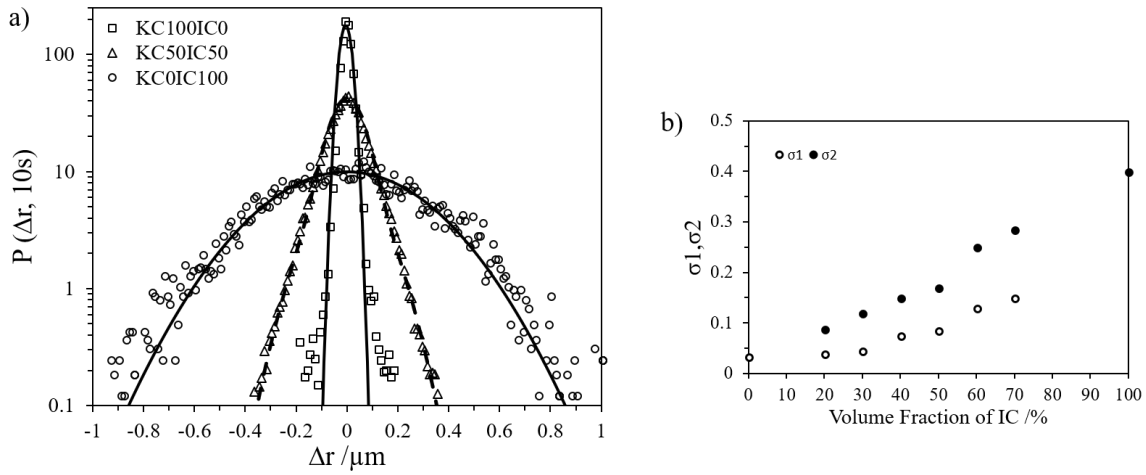

Fig. 4.6 a) van Hove correlation plots for particles in KC, IC and mixture at KC50IC50. The solid lines indicates the single Gaussian fits while the broken line indicates the mixture of broad and narrow Gaussian form. b) Dependence of σ as a function of volume fraction of IC

where f_1 and f_2 are component fraction (f_1+f_2=1), and σ_1 and σ_2 are small and large σ, respectively. As seen in Fig. 4.6a, P($\triangle$r,10s) in pure KC and IC fit well with a single Gaussian function although the discrepancy at low probability looks large in the logarithmic plot. On the other hand, the distribution P($\triangle$r,10s) in KC50IC50 showed a non-Gaussian behavior and a single Gaussian could not fit well on the experimental data but rather a combination of two Gaussian functions could fit. We adopted a mixture of two Gaussian function based on the consideration that the heterogeneity of the mixture was frozen on the way to the phase-separated network structure. Fig. 4.6b shows the dependence of σ_1 and σ_2 on the IC content. The two σ terms in P($\triangle$r,10s) of the mixtures implies the presence of particles with different mobility, i.e., slow particles and fast particles. This suggests that different particle probe different microenvironments owing to phase separation into KC-rich and IC-rich domains.

The van Hove distribution suggested the presence of two populations of particles with different mobilities. Further information can be obtained if particles are classified according

to their characteristic α exponents. Fig. 4.7 presents the distribution of *msd* at τ = 10 s as a function of α at different mixing ratios. The solid lines indicate the contour lines of the 2D Gaussian probability distribution. Fig. 4.7a and 4.7h present the distributions in pure KC and IC gels, wherein unimodal 2D Gaussian distributions could be used to fit to the results. A clear difference in the distributions was observed where the *msd* of particles in the IC gel showed $\alpha \sim 1$ with higher *msd*, while those in the KC gel showed $\alpha \sim 0$. This implies a distinct difference in the microrheology of pure KC and IC gels. Figs. 4.7 b–g show the distributions of the particles in different KC/IC mixtures. The distribution of $msd(\tau$=10s) and α for the mixture showed a broad distribution. Because $msd(\tau$=10s) and α have no correlation therefore fitting the distribution with a unimodal Gaussian function showed large error while the bimodal Gaussian function showed minimal error. The red dashed line corresponds to the bimodal 2D Gaussian distribution with the weight of each 2D Gaussian equal to the ratio of KC and IC in the mixture.

The 2D Gaussian distributions for pure KC and IC are also drawn in each figure for reference. Broad distributions of $msd(\tau$=10s) and α were observed for all gels, and could be fitted with 2D bimodal Gaussian distributions. The presence of a bimodal distribution is consistent with the observation in the van Hove correlation function, implying the presence of two groups of particles with fast and slow mobilities. The fast mode is clearly close to that of particles in pure IC gels, while the slow mode is close to that observed in pure KC gels. Thus, we consider the fast particles to be present in IC-rich domains, while the slow**fast** particles should experiencing a microenvironment rich in KC.

In KC50IC50, broad distributions of *msd* and α are observed (Fig. 7d). It is shown that the particles in the IC-rich domain showed slower mobility than in pure IC while the particles in the KC-rich domain showed higher mobility compared to that of the pure KC. The differ-

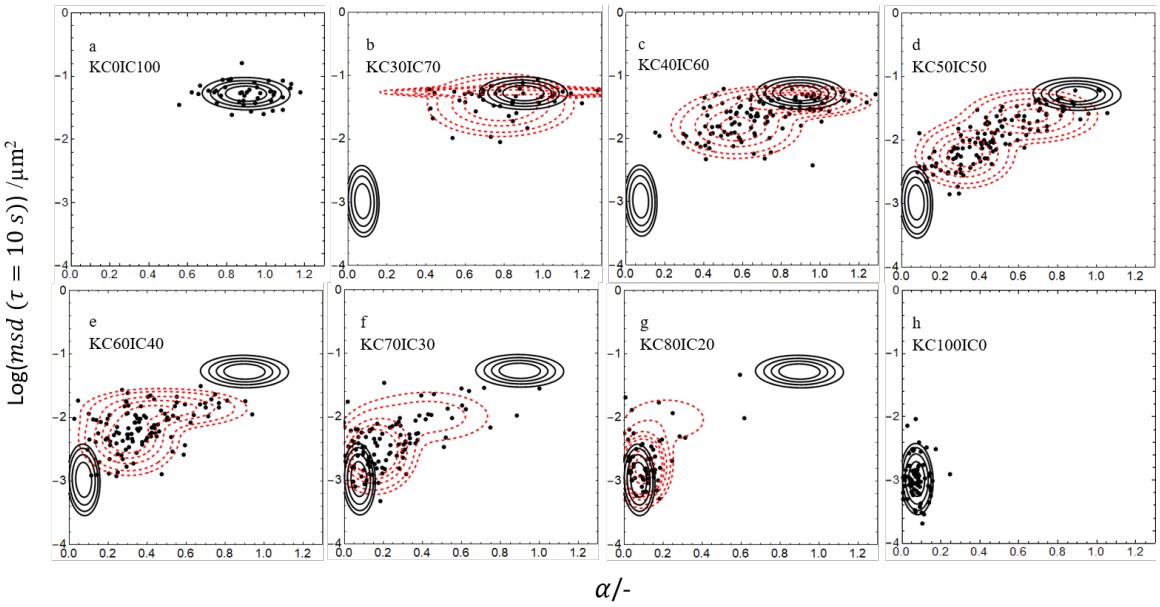

Fig. 4.7 Distribution of *msd* at τ= 10s and α. Figures a and h indicates the distribution for pure IC an KC respectively. The solid lines were corresponding to the contour lines of the Gaussian probability distribution of KC and IC. In figures b to g, the red dashed lines correspond to the bimodal Gaussian distribution.

ence of particle mobility between the pure solutions and each domain in the KC50IC50 is considered to be affected by the presence of non-negligible amounts of both carrageenans in both KC-rich and IC-rich domains. The presence of KC chains in IC-rich domains increases the local viscosity while the presence of IC chains in KC-rich domains decreases the local obstruction. These changes were reflected in shifts of the distributions of both *msd* and α to either lower (in the IC domains) or higher (in the KC domains) values. In the extreme mixing ratios (Fig. 4.7b and Fig. 4.7g), the distributions were almost identical to those observed in pure carrageenan gels, as discussed in Section 4.3.2. The distribution of $msd(\tau$=10s) and α in the mixture suggests two groups of particles. The *msd* of particles in each group were clustered using a non-hierarchal clustering method in Mathematica 10 with a criterion based on the distribution of $msd(\tau$=10s) and α as shown in Fig. 4.8a. The dependence of f_1 and f_2 on the concentration of IC is plotted in Fig. 4.8b. The clear dependence of these fractions on IC is clearly related to the volume fractions of IC-rich and KC-rich domains in

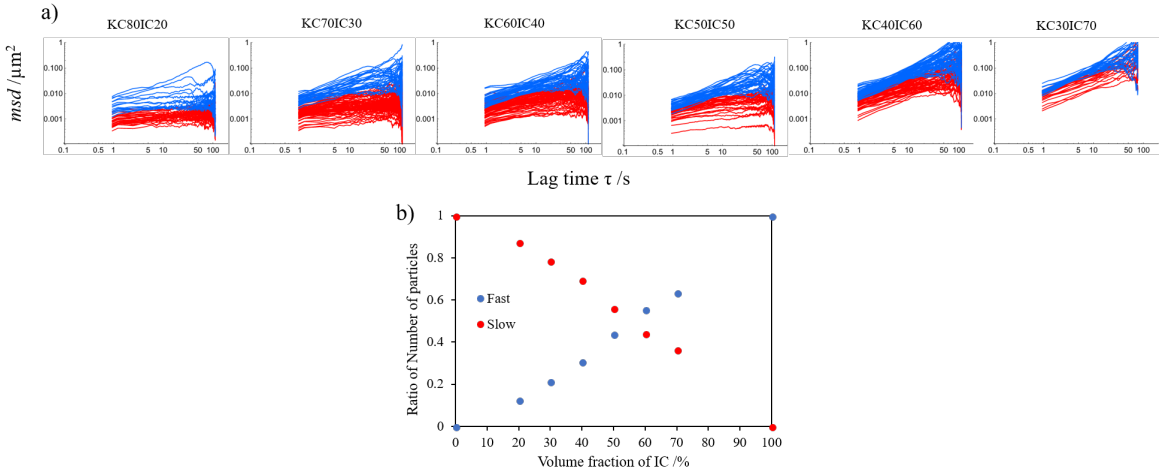

Fig. 4.8 a) Individual *msd* of particles in mixed KC and IC at different mixing ratio after 1 day storage clustered into fast (blue) and slow (red) population of particles. b) The changes in the number of slow and fast particles with volume fraction of IC.

the phase-separated gel.

For the mixed carrageenan gels, macroscopic rheological measurements showed a possible phase separation of KC and IC chain aggregates, while NMR measurements suggested two possibilities: either interpenetration of the two networks, or micro-phase separation with a domain size of ∼450 nm (Hu, Du, and Matsukawa, 2016). No decisive evidence has been reported to date. In the present study, particle tracking revealed inhomogeneity of microscopic structure in the mixed gels, demonstrating phase separated structure with KC-rich and IC-rich domains. On cooling, particle tracking suggested that both KC and IC formed relatively small clusters that still allowed particle diffusion (Fig. 4.4). These clusters of aggregates caused the two-step decrease in the $\langle msd \rangle$ (Fig. 4.3) and the two-step increase in G' observed in the bulk rheological measurements (Fig. 4.1). These results suggest that phase separation was induced by two exclusive aggregation steps. Upon aging at 5°C the clusters of KC and IC chain aggregates continue grow but remain free of each other; this further grow of both types of aggregates leads to formation of a permanent gel network. Based on this discussion, the mobility of particles in the mixture of KC and IC

suggests a high degree of structural heterogeneity and micro-rheology. We proposed that the structural heterogeneity was frozen on the way to the formation of a phase-separated network structure, with KC-rich and IC-rich domains both of which having a domain size larger than the particle size (100 nm) due to the network formation of KC and IC chains using the cooling rate (1°C/min) employed in this experiment. In a separate experiment on KC50IC50 at a cooling rate of 0.055°C/min, considerable splitting in the distribution of msd was observed (see Appendix B). This suggest an enhanced phase-separated network structure made of KC and IC rich domains, however it requires further investigation to ensure the consideration of the phase separated structure. In addition, the characteristic domain size increased with storage time as shown in the graphical representation in Fig. 4.9.

4.4 Conclusion

Particle tracking measurements on cooling and storage were conducted to elucidate the phase separation of mixed KC and IC gels. The temperature dependence of $\langle msd \rangle$ on cooling showed a two-step decrease consistent with the two-step increase in macroscopic rheological measurements. This result indicates independent formations of KC clusters and IC chain aggregates, which lead to phase-separation. However, the aggregates did not evolve to length-scales exceeding the probe particle size as seen in Fig. 4.4. Upon storage, however, broad distributions of *msd* were observed in the mixtures, indicating the formation of inhomogeneous structures. We consider that this heterogeneity came from the frozen structure on the way to phase-separated network structure. The degree of heterogeneity was characterized using the van Hove correlation function, indicating the presence of two groups of particles. The distributions of $msd(\tau$=10s) and α were bimodal in mixtures of KC and IC, revealing slow and fast particles present in KC-rich and IC-rich domains. These results lead us to suggest a view that the mixture was frozen on the way to phase-separated gel network

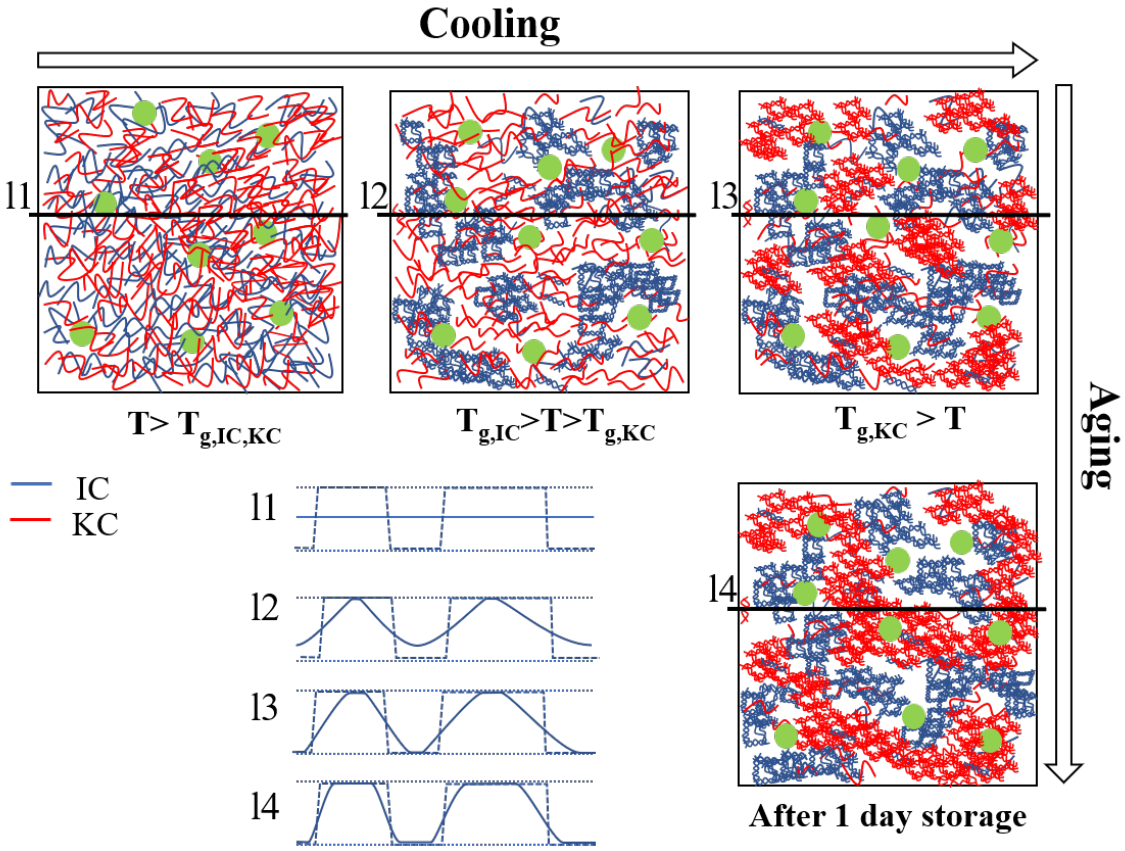

Fig. 4.9 Graphical representation on the proposed gelation mechanism of mixed KC and IC solutions.

with the size of the KC-rich and IC-rich domains is in excess of 100 nm, at least following 1 day of storage. The volume fractions and sizes of KC-rich and IC-rich domains depend on the KC/IC mixing ratio.

Chapter 5

Gelation mechanism and network structure of mixed kappa carrageenan/lambda carrageenan gels studied by macroscopic and microscopic observation methods

Dynamic rheology and particle tracking experiments were carried out to investigate the gelation mechanism and network structure of mixed κ-carrageenan (KC) and λ-carrageenan (LC) gels on the macroscopic and microscopic levels. Mixtures of KC and LC (total carrageenan concentration = 1.5%, K^+ concentration = 15 mM) were prepared at different mixing ratios. The storage modulus (G') was highest for pure KC and decreased monotonously with decreasing KC content. The mean square displacement (MSD) of probe particles was used to characterize the network on cooling and after one day of storage. On cooling, a single step decrease in the ensemble-averaged MSD was observed, in agreement with the rheological

measurements. Time-averaged MSD values of individual particles showed a large distribution after one day in storage, especially for gels with low content of KC. This heterogeneity reflects microstructural heterogeneity, suggesting phase separation into KC-rich and LC-rich domains. Individual particle MSD values showed a bimodal distribution. The MSD could be described as a power-law, MSD$\sim t^{\alpha}$, with τ the lag time. The exponent α also showed a bimodal distribution. These findings suggest that two groups of probe particles with distinctly different mobilities are present in the mixed gels where particles in KC-rich domains exhibit inhibited mobilities while in LC-rich domains exhibit diffusive mobilities. Based on the rheological results, interpreted within the frame of the Takayanagi laws of mixtures, as well as the particle tracking experiments, we propose that mixtures of KC and LC separate into a continuous phase and a non-continuous filler phase, with the continuous phase being made up of the more concentrated carrageenan. When the concentrations of the two carrageenans are roughly equal, we suggest that a bicontinuous phase-separated network is formed.

Based on: Lester C. Geonzon, Xinye Zhuang, Amos M. Santoya, Rommel G. Bacabac, Jingli Xie, Shingo Matsukawa. Gelation mechanism and network structure of mixed kappa carrageenan/lambda carrageenan gels studied by macroscopic and microscopic observation methods. In preparation.

5.1 Introduction

The most industrially utilized carrageenans are the $\kappa-$ (KC), $\iota-$ (IC) and $\lambda-$ (LC) carrageenan which differs in the amount of sulfate groups: one (G4S-DA) for KC, two (G4S-DA2S) for IC, and three (G2S-D2S,6S) for LC (Usov, 1992). Among the three types, KC and IC exhibited gelling properties influenced by temperature and presence of cations (K^{+}, Ca^{2+}), while LC is a non-gelling type carrageenan.

The functionality of carrageenan in various applications depends largely on their rheological properties. Polysaccharide mixtures or blends have gained widespread applications in foods due to greater controllability of the physical property and texture enhancement of the final product (Zheng, 2018). Among the aforementioned carrageenans, KC have been mostly used owing to its different conformations depending on the temperature, cations and polysaccharide concentration. Given low concentration of polysaccharide and salt at higher temperature, KC behaves as a solution and can be used as thickening and stabilizing agent while at lower temperature with high polysaccharide and salt concentration it is an effective gelling agent (Tecante and del Carmen Núñez Santiago, 2012). Mixtures of KC with other gelling ingredients (alginates (Fan et al., 2013), iota carrageenan (Brenner, Tuvikene, Parker, Matsukawa, and Nishinari, 2014; Du, Brenner, Xie, and Matsukawa, 2016), agar (Norziah et al., 2006), and gelatin (Derkach et al., 2015) and non-gelling ingredients (locust bean gum, guar gum and starch (Huc et al., 2014) have been studied resulting in different physical behaviors that are used in wide range of applications (Zia et al., 2017).

In our previous study, binary mixtures of KC and IC have been thoroughly investigated to understand the underlying network structure of the mixed carrageenan gels at different length scale of observations ranging from macroscopic level (Brenner, Tuvikene, Parker, Matsukawa, and Nishinari, 2014; Du, Brenner, Xie, and Matsukawa, 2016) and molecular level using NMR (Hu, Du, and Matsukawa, 2016). Possible structures in mixed KC and IC gels have been reported to have phase-separated (Brenner, Tuvikene, Parker, Matsukawa, and Nishinari, 2014; Du, Brenner, Xie, and Matsukawa, 2016) or interpenetrating (Bui, Nguyen, Renou, and Nicolai, 2019) network structures. Recently, observation at microscopic level using particle tracking of 100 nm particles suggests a high degree of heterogeneity for the mixed gels which was attributed to the possible formation of phase separated structure made of KC-rich and IC-rich domains. However, the ability of both carrageenans (KC and IC) to

form aggregates freezes the phase separated structure due to the network formation of KC and IC chain aggregates (Geonzon, Bacabac, and Matsukawa, 2019a). Hence, understanding the interaction between KC to a non-gelling carrageenan (LC) will provide more information on the phase separated structure of the carrageenan mixtures. This serves as our motivation to investigate the interaction between KC and LC using rheology and particle tracking.

In this light, we aimed to investigate the gelation mechanism and network structure of KC and LC blends at different mixing ratio in macro- and microscopic level. The temperature dependent viscoelasticity was measured by dynamic rheological measurements using small amplitude oscillatory shear on cooling. Results of rheological measurements was compared with the particle tracking using sub-micron particles. Furthermore, particle tracking measurements following 1-day storage was also performed to clarify the network structure of the formed gels.

5.2 Materials and Methods

5.2.1 Materials

Please refer to Section 3.2.1

5.2.2 Sample Preparation

Sodium-type $\kappa-$ carrageenan powder (Tokyo Chemical Industry Co., Ltd. Tokyo, Japan) was dialyzed against NaCl solution and subsequently against deionized water to obtain Na+ type carrageenan solution. The concentrations of Na^+ and K^+ of the dialyzed carrageenan were analyzed by inductively coupled plasma (ICP) atomic emission and were 0.4% and 0.11% while no Mg^+ or Ca^+ were detected in the sample. $\lambda-$ carrageenan was purchased from Sigma Chemical Co. (St. Louis, MO, USA) and used without further purification.

The content elements of LC were Na, 4.71% K, 4.72% and Ca, 0.65%. Samples for the particle tracking experiments and rheological measurements were prepared using the same procedure as described in reference (Geonzon, Bacabac, and Matsukawa, 2019a,b) except that the K^+ concentration was set at 15 mM. Since 1.5% of pure LC solution contained 18 mM K^+, the addition of KCl in the mixture was varied to obtain a fixed K^+ concentration to 15 mM. For pure LC solution, a small amount of LC solution was dialyzed and mixed to the solution of LC without dialysis to obtain a solution of 1.5% with 15 mM K^+. The mixture solutions of KC and LC were prepared by mixing pure KC and LC solutions at different mixing ratio. Samples were designated using a code KC*x*LC*y* (e.g. KC50LC50), where *x* and *y* indicate the percentage of KC and LC ($x + y = 100$), respectively. Samples for the rheological measurements were prepared using the same procedure except for the addition of probe particles.

5.2.3 Dynamic rheological measurement

Rheological properties were measured using HAAKE MARS II rheometer (Thermo Scientific, Waltham, MA, USA) equipped with blasted parallel-plates (diameter 35 mm) with 1 mm gap. Hot sample solutions were loaded on preheated plates at 80 °C and covered with oil to avoid water evaporation. The storage modulus (G') and loss modulus (G") were monitored on cooling from 80 °C to 5 °C at a rate of 1 °C/min with a frequency of 1 Hz and at strain of 1%.

5.2.4 Particle tracking measurements

Particle tracking measurements of fluorescent particles (0.1 μm, Green, ThermoScientific) embedded to the carrageenan solutions were carried out using an inverted microscope, BZ-9000 (Keyence Corp., Osaka, Japan), equipped with a PlanFluor 100× NA 1.30 oil-immersion objective (Nikon Corp. Inc., Japan) and a temperature-controlled microscope stage (ALA

Scientific Instruments Inc., New York). Hot sample solutions were placed in a custom-made sample chamber equipped with temperature sensor for actual sample temperature monitoring as described in reference (Geonzon, Bacabac, and Matsukawa, 2019a,b). Particle diffusion were recorded using a built-in 2/3-inch, 1.5 megapixels, 12-bit, monochrome cooled CCD camera (Keyence Corp., Osaka, Japan) at a rate of 7.5 frames per second for 110 seconds. In cooling experiments, the particle tracking was performed at different temperatures from 50°C to 10°C. For measurement at low temperatures (gel state), a total of 60–80 particles were tracked simultaneously. For measurement at high temperatures, particles were observed to have high mobility and occasionally moved in-and-out of focus during the tracking and fewer particles (∼20-40 particles) were successfully tracked throughout the measurement. In storage experiments, hot solutions of carrageenan were cooled down from 50°C to 5°C at a rate of 1°C/min in a temperature-controlled incubator to form a gel and stored at 5°C prior to experiments of the particle tracking, also done at 5°C.

The position of each fluorescent labeled particles was determined using an algorithm which improves the accuracy of particle position using the image-intensity weighted centroid for each particle (Geonzon and Matsukawa, 2019), from which particle trajectories were calculated and analyzed. The time-averaged MSD for each particle (*msd*) obtained from *N* images representing a total diffusion time τ was calculated with the following equation (Lieleg, Vladescu, and Ribbeck, 2010; Wagner, Turner, Rubinstein, McKinley, and Ribbeck, 2017):

$$msd(\tau) = \frac{1}{N - \frac{\tau}{\triangle t}} \sum_{i=1}^{N-\frac{\tau}{\triangle t}} [r(i \triangle t + \tau) - r(i \triangle t)]^2 \tag{5.1}$$

where $\triangle$t is the interval time for each frame, that is the inverse of the frame rate, and r($\triangle$t) is the position of the centroids of each tracked particle. The exponent α in the relationship

between *msd* and τ, $msd \sim \tau^{\alpha}$, was calculated for each particle at lag times in the range 1–10 s. Because the number of displacements for the averaging $(N - \frac{\tau}{\triangle t})$ decreases, the *msd* points at longer lag times tend to have larger statistical fluctuations (Michalet, 2010). The ensemble-averaged MSD $\langle msd \rangle$ was obtained by averaging the *msd* of all tracked particles. Particle tracking and MSD calculations were performed using a custom-made program written in Mathematica 10 (Wolfram Research, Inc., Champaign, IL) (Geonzon and Matsukawa, 2019).

5.3 Results and Discussion

5.3.1 Temperature-dependent viscoelastic properties

The temperature dependence of dynamic viscoelasticity were measured for the mixture solutions of KC and LC at a total carrageenan concentration of 1.5% with 15 mM K^+. Fig. 5.1 shows the G' and G" as a function of temperature for the mixture solutions of KC and LC on cooling. The point with a sharp increase in G' was defined as the critical temperature, T_c, at which polysaccharide chain start to aggregate and form the three-dimensional network to increase elasticities (Fernandes, Gonçalves, and Doublier, 1991). Pure KC solution showed the largest G' with T_c at around 29.1°C, indicating the network formation of helix aggregates conforming a hard and brittle gel. On the other hand, pure LC solution showed no distinct increase in G' or G". In addition, G" is always higher than G' at all temperature range implying that LC exists as a solution and unable to form gel under the experimental conditions employed. Mixture solutions of KC and LC showed similar tendency with the pure KC at relatively high proportion of KC while a decrease in moduli and a slight shift in Tc to lower temperature were observed as the proportion of KC in the mixture was decreased. It is notable that, a single step increase in viscoelasticity was observed in the mixture implying that gelation of mixture solutions of KC and LC was only influenced by the aggregation of KC helices (Du, Brenner, Xie, and Matsukawa, 2016; Du, Lu, Geonzon, Xie, and Matsukawa,

2016) (Du et.al, 2016). For mixtures with low proportion of KC, G" was always higher than G' over the entire temperature range similar to pure LC, however a slight increase in G' and G" was observed at around 15-10°C.

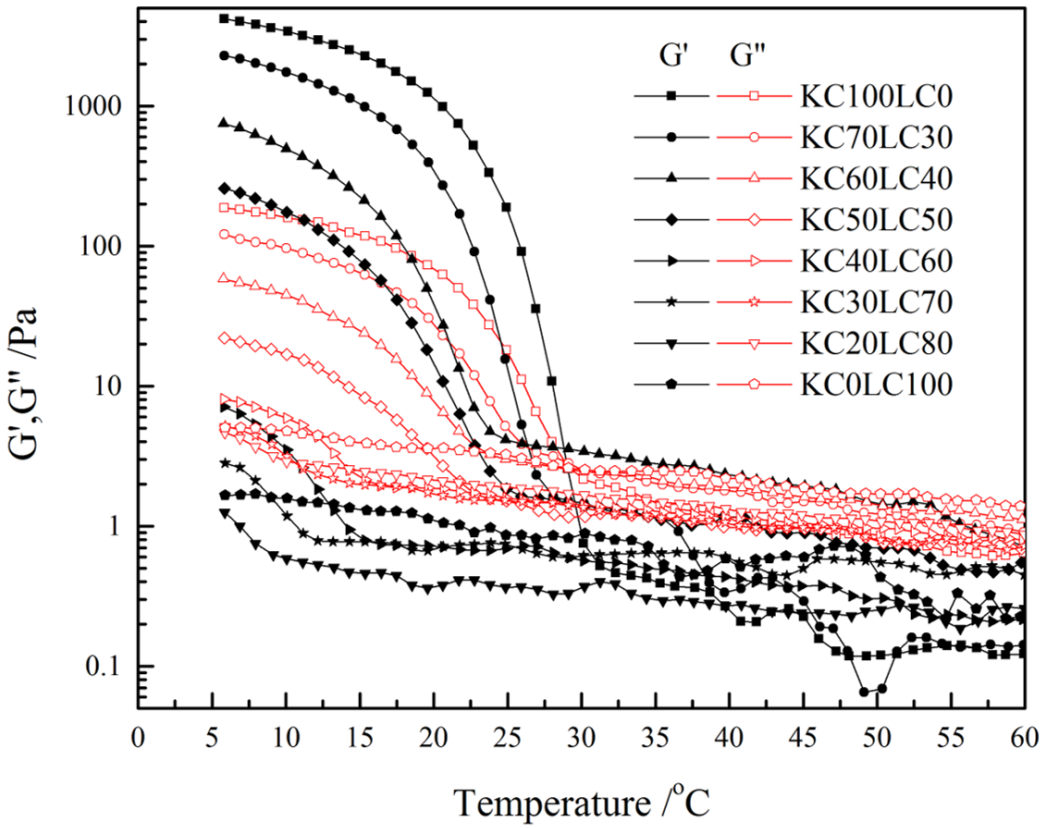

Fig. 5.1 Temperature dependence of viscoelastic moduli at 1 °C/min for 1.5% mixture solutions of KC and LC with 15 mM K^+ at different mixing ratios on cooling.

In our previous work, studies on mixture solutions of KC and IC by rheology measurements and particle tracking proposed the formation of a phase separated network structure due to the network formation of KC and IC chains (Geonzon, Bacabac, and Matsukawa, 2019a,b). In addition, it was suggested that each chain of KC and IC in the mixtures rarely interact with each other (Brenner, Tuvikene, Parker, Matsukawa, and Nishinari, 2014; Du, Brenner, Xie, and Matsukawa, 2016; Du, Lu, Geonzon, Xie, and Matsukawa, 2016). Therefore, it is also considered that mixture solutions of KC and LC formed a phase separated structure due to the stronger immiscibility of KC and LC chains owed to the larger difference

in the chemical structure of KC from LC than that of IC.

In general, for polymer blends with two phases, the Takayanagi model provide means for estimating the upper (isostrain) and lower (isostress) bounds of the moduli values of the composite gel, G_c, from the moduli G_k and volume fraction ϕ_k of the individual component k (Takayanagi, Harima, and Iwata, 1963). The theoretical bound (isostrain and isostress) estimates were calculated using the following equation (Kasapis, 2008; Ross-Murphy, 1995):

$$G_C = (\phi_1 G_1^x + \phi_2 G_2^x)^{\frac{1}{x}} \tag{5.2}$$

where the exponent x determines the behavior of the composite gels. For x=1 corresponds to isostrain where the continuous phase is stronger than the filler phase while for x=-1 corresponds to isostress which describes the inverse situation wherein the filler phase is stronger than the continuous phase (Kasapis, 2008; Richardson and Kasapis, 1998). Meanwhile, the phase separated structure with bi-continuous networks shows ϕ dependence with x=0.2 (Davies, 1971). Fig. 5.2 presents the complex modulus, G*, for mixture solutions KC and LC gels against the proportion of LC with the boundary lines (isostrain, bi-continuous and isostress) calculated using Eq. 5.2. The experimental data in Fig. 5.2 showed an obvious decrease in G* and a gradual transition from isostrain to bi-continuous to isostress boundary limits as the proportion of LC was increased. The G* value of KC70LC30 was close to the isostrain boundary limit suggesting that the network structure of KC chain aggregates formed the continuous phase while LC solution serves as a filler. The probability of KC forming the continuous phase in KC70LC30 is high due to the larger ϕ of KC indicating a stronger continuous phase than filler phase. At intermediate mixing ratio (KC60LC40 and KC50LC50), the data showed a satisfactory fit with the bi-continuous model (x=0.2) suggesting the formation of bi-continuous structure. Meanwhile, at high ϕ of LC (KC40LC60, KC30LC70, KC20LC80), the isostress boundary limit fit well to the data implying the

formation of a stronger filler phase than continuous phase. This is attributed to the formation of weak network of LC in the continuous phase and the formation of filler of solid network by the extensive aggregation of KC.

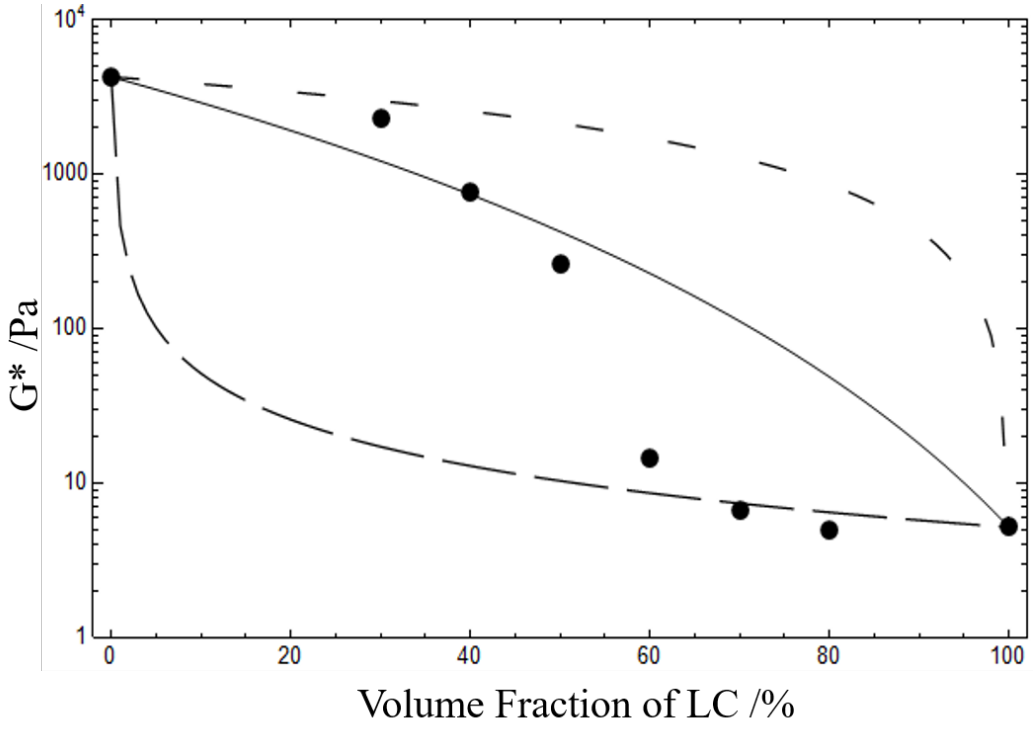

Fig. 5.2 Experimental complex modulus (G*) as a function of volume fraction of LC for a total carrageenan content of 1.5% with 15 mM K^+. The lines are the boundary lines using the Takayanagi blending laws: short dashed (upper, isostrain, x=1, solid (bi-continuous, x=0.2), long dashed (lower, isostress, x=-1).

5.3.2 Particle mobility during cooling

The theoretical models based on phase separated structure could explain the rheological measurements based on the phase transition among sea-island, bi-continuous and island-sea structures. However, the explanation was based on the macroscopic observation and does not have enough reliability to describe the microscopic structure. The particle tracking for Brownian motion is a useful method to investigate the local physical property in the media to add the microscopic information to the macroscopic rheological measurements (Moschakis,

Lazaridou, and Biliaderis, 2012; Shabaniverki and Juárez, 2017), indicating the usefulness to verify the micro-phase separation. Fig. 5.3 shows the *msd* of particles in mixture solutions of KC and LC at different temperatures on cooling. For pure KC, a linear increase with τ and a broad distribution of *msd* was observed at temperatures above T_c but showed a clear decrease and change in the slope below T_c indicating the formation of solid network structure of KC helix aggregates. For pure LC, the *msd* of the particles showed a linear increase with τ and did not show any significant change with temperature. Meanwhile, the *msd* of particles in the mixture solutions of KC and LC showed a high diffusivity at high temperatures but a pronounced broad distribution below T_c especially for KC70LC30.

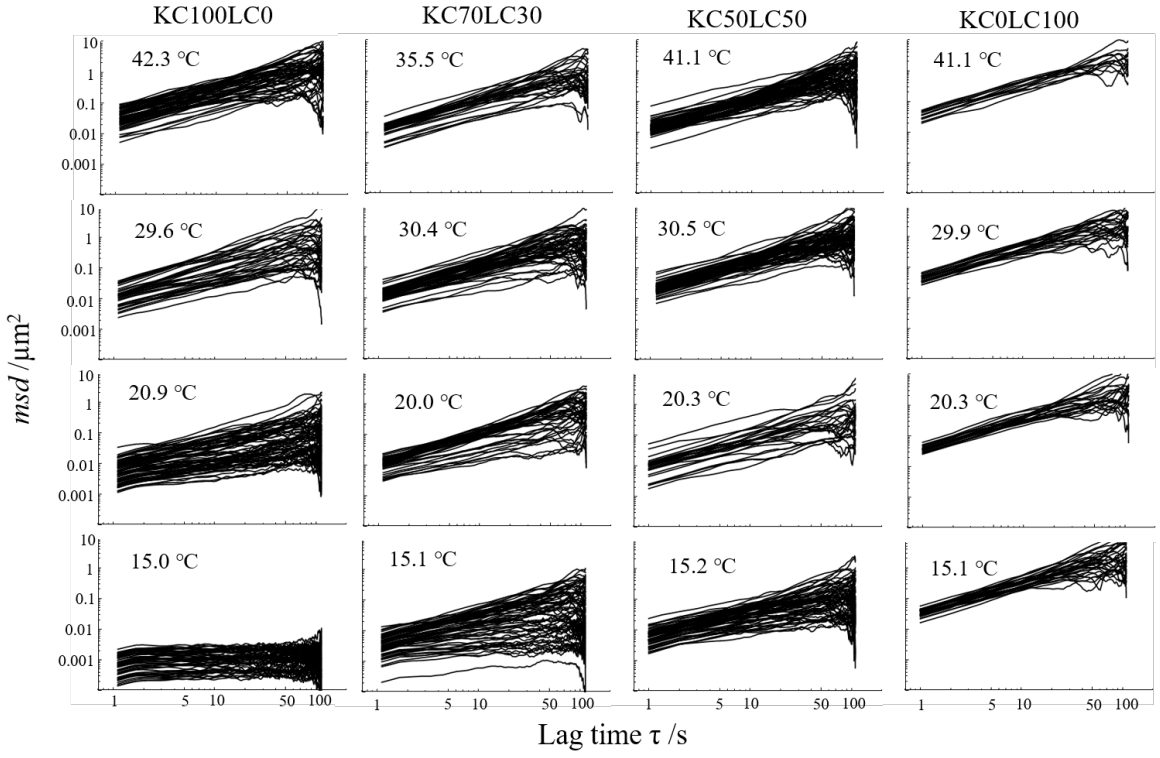

Fig. 5.3 Individual msd of particles in 1.5% total carrageenan concentration with 15 mM K^+ at different mixing ratio of KC and LC at different temperatures on cooling.

The change in the local viscosity with temperature was examined by calculating the $\langle msd \rangle$ at τ=10s ($\langle msd(10s) \rangle$). Fig. 5.4 shows the temperature dependence of $\langle msd(10s) \rangle$ of particles in mixture solutions of KC and LC on cooling. The error bars are corresponding to

the standard deviation of the distribution of *msd* at τ=10s for each particle. The $\langle msd(10s)\rangle$ for pure KC showed a drastic decrease at around T_c demonstrating the rapid formation of KC network structures that yields to a stable gel (Geonzon, Bacabac, and Matsukawa, 2019a). For pure LC, the $\langle msd(10s)\rangle$ did not show any significant decrease implying that LC chains were unable to form aggregates to restricts the particle movement with the temperature decrease, in agreement with the macroscopic rheological measurements. Meanwhile, for mixture solutions, the $\langle msd(10s)\rangle$ exhibited an intermediate behavior between pure KC and LC solutions at all temperature range and showed a clear decrease at around T_c indicating an inhibited mobility due to the formation of KC aggregates as described in Section 5.3.1.

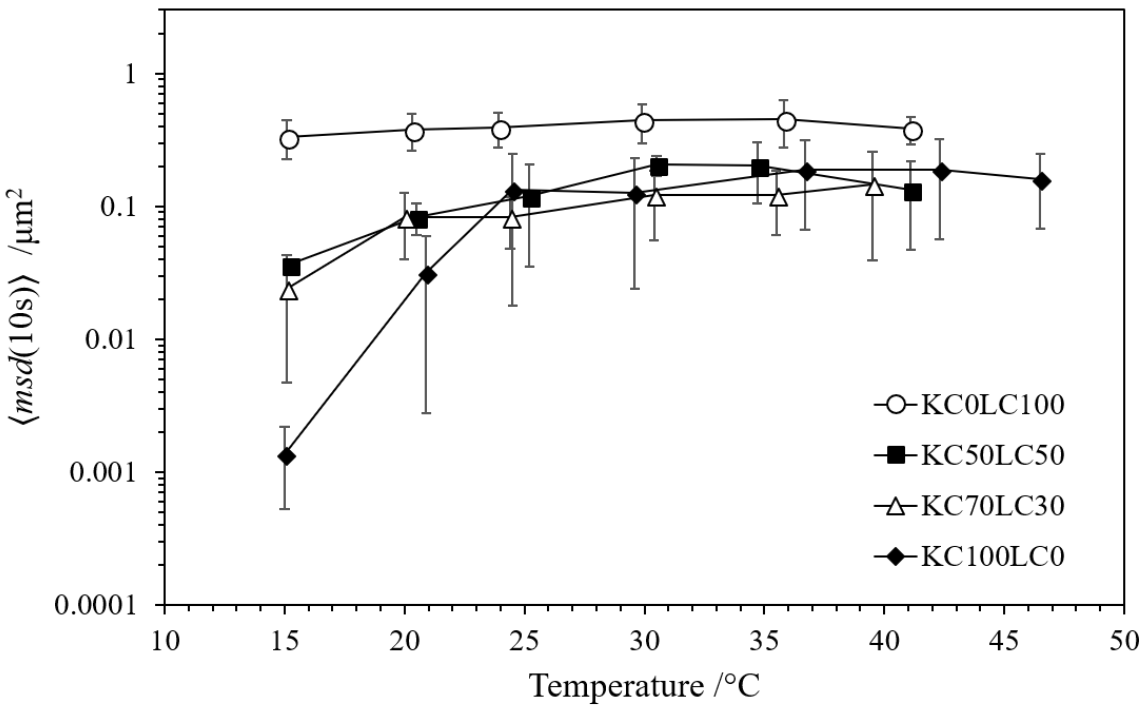

Fig. 5.4 Temperature dependence of $\langle msd(10s)\rangle$ at lag time 10s of particle in different mixing ratio of KC and LC. Error bars are corresponding to the standard deviation of the distribution of *msd* at τ=10s for each particle.

The behavior of individual particles for different mixing ratio at around 15°C was further clarified by indicating plots of *msd* at 10s (*msd*(10s) and α on the plot with axes of *msd*(10s)

and α where α describes the type of particle diffusion and *msd*(10s) corresponds to the local viscosity at τ=10s (Geonzon, Bacabac, and Matsukawa, 2019a,b). Particle diffusion with α=1 implies that the sample has free space for normal diffusion while α=0 implies that the probe particles are fully constrained, i.e., trapped in the network structure. Furthermore, the sample is considered to have a restricted diffusion space when α lies between zero and one indicating the relationship between observation time and timescale of diffusion in the media (Gardel, Valentine, and Weitz, 2005; Mason, Ganesan, van Zanten, Wirtz, and Kuo, 1997; Price, 2009). In materials where such sub-diffusive behavior is observed, the particle movement is considered to be inhibited by some network structure (Waigh, 2005). Fig. 5.5 presents the distribution of *msd*(10s) and α for pure and mixture solutions of KC and LC at around 15°C on cooling. Distribution of *msd*(10s) and α the particles in pure gels showed a clear difference between KC (with $\alpha \sim$0 and lower *msd*(10s)) and LC (with $\alpha \sim$1 and higher *msd*(10s)) implying a distinct difference in the microrheology between the two solutions. Meanwhile, the mixture solutions of KC and LC showed a broad distribution that spread between the pure carrageenan solutions suggesting the presence of different microenvironments due to the developed structural heterogeneity. In the mixture, the heterogeneous structure with different microenvironment may come from the formation of phase-separated structure made of KC-rich and LC-rich domains due to the extensive aggregation of KC chains.

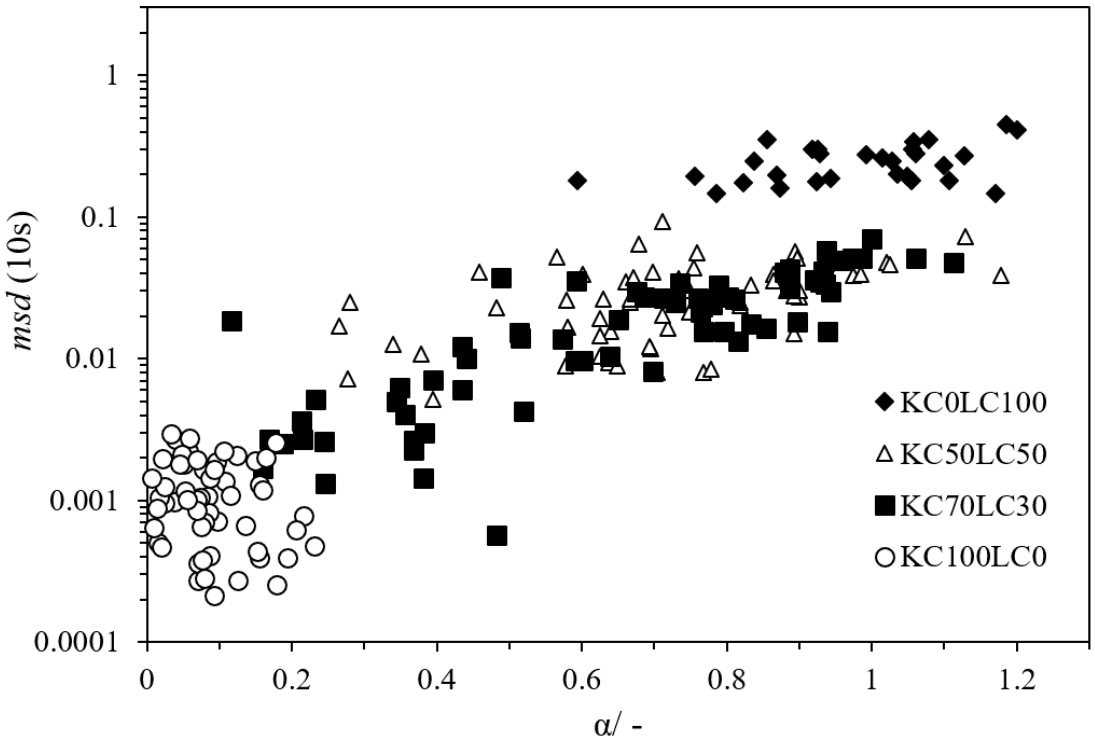

Fig. 5.5 The distribution of *msd*(10s) against slope α for mixture of KC and LC at around 15°C on cooling.

5.3.3 Particle mobility in stored gels

The change in the network structure of the mixed gels were investigated by the particle tracking following 1 day storage at 5°C. Fig. 5.6 presents the *msd* of particles in mixture of KC and LC gels measured at around 5°C after 1 day storage . Measurements for the first day (Fig.5.3) showed a distribution in msd especially for KC70LC30 suggesting the possible formation of phase separated structures but was not so clear. The *msd* after 1 day storage showed a larger distribution with different behaviors of *msd* observed for solutions with various mixing ratio of KC and LC showing a distinct enhanced behavior of structural changes in the mixture. For samples with low proportion of LC (KC70LC30, KC60LC40, KC50LC50), a narrow distribution of *msd* was observed with few particles which showed dif-

fusivity. On the other hand, for samples with high proportion of LC (KC20LC80, KC30LC70, KC40LC60), a broad distribution of *msd* was observed associated with the heterogeneity in the local physical properties of the mixture gels.

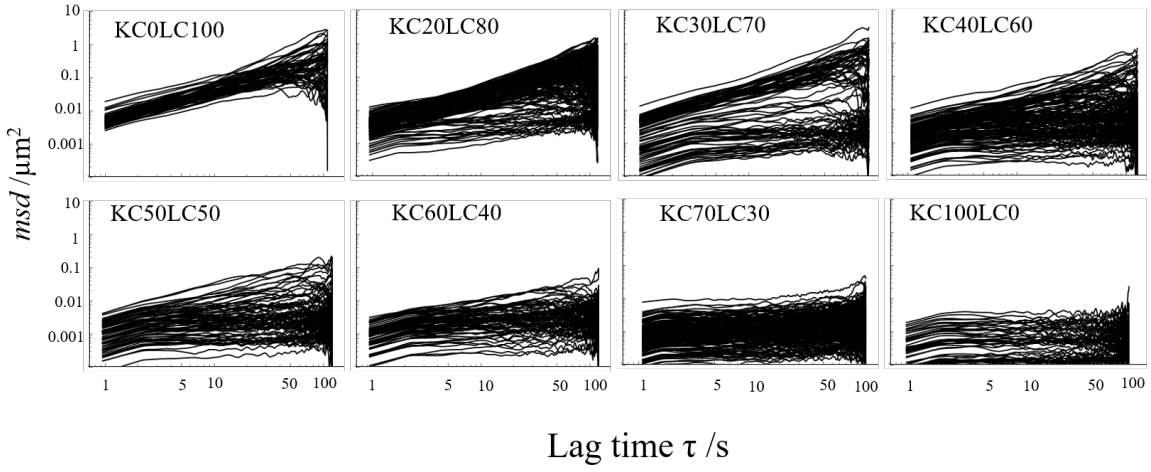

Fig. 5.6 Individual mean square displacement of particles in 1.5% total carrageenan concentration with 15 mM K^+ after 1 day storage at different mixing ratio of KC and LC at around 5 °C.

The *msd* of particles in the mixture especially at high proportion of LC revealed a comparatively high degree of heterogeneity. The rheological measurements were explained by the theoretical model based on the phase separated structure (Section 5.3.1). Therefore, the structural heterogeneity in the mixture was considered to be attributed to the formation of phase separated structure made of KC-rich and LC-rich domain. To understand the degree of heterogeneity in the gels, the plot of *msd*(10s) and α for each particle were used which provides insights on the distribution of microenvironment surrounding the probe particles (Geonzon, Bacabac, and Matsukawa, 2019a). Fig. 5.7 presents the plot of *msd*(10s) and α for each particle in the mixture of KC and LC after 1 day storage at 5°C. Particles in pure KC and LC gels showed a unimodal 2D distribution of *msd*(10s) and α as shown in Figs. 5.7a and 5.7h indicating the probe particles in pure gels experiences the same microenvironment *i.e*. homogenous media. In addition, as explained earlier, there is a clear difference in the distribution between pure KC and pure LC implying a distinct difference in

micro-rheology. The plot of *msd*(10s) and α for particles in the mixture of KC and LC at all mixing ratio showed a broad distribution that spread in between the pure KC and LC. Based on the consideration that the mixtures formed a phase-separated structure and *msd*(10s) and α are independent with each other, we adopted a bimodal 2D Gaussian functions with no correlation parameter between *msd*(10s) and α to fit the data. The red dashed lines in Figs. 5.7 b-g are the contour lines of the bimodal 2D Gaussian functions with no correlation parameter where the fraction of two components in the function was set to be the mixing ratio for each mixture. The observed bimodal 2D distribution suggested that the particles in the mixture solutions probes different microenvironment due to the formation of phase separated structure made of KC-rich and LC-rich domains. Correspondingly, the KC-rich and LC-rich domains depress and allow particle diffusion that results to the presence of particles with small α implying inhibited mobility and large α implying diffusive mobility, respectively. For low proportion of LC, the distribution was observed closed to pure KC suggesting the extensive aggregation of KC chains yields to a more stable gel primarily made of KC network structure while few particles showed diffusivity. For gels with high proportion of LC, a broad distribution indicates the presence of particles with vastly different diffusivity due to the phase-separated structure. This suggests that for gels with low proportion of KC, the extensive aggregation of KC chains resulted the formation of filler of KC chains aggregates that inhibits particle mobility. In addition, it was considered that the filler of KC chains yields to the slight increase in G' and G" in the rheological measurements and reflects the predictions obtained from the isostress blending law in Fig. 5.2.

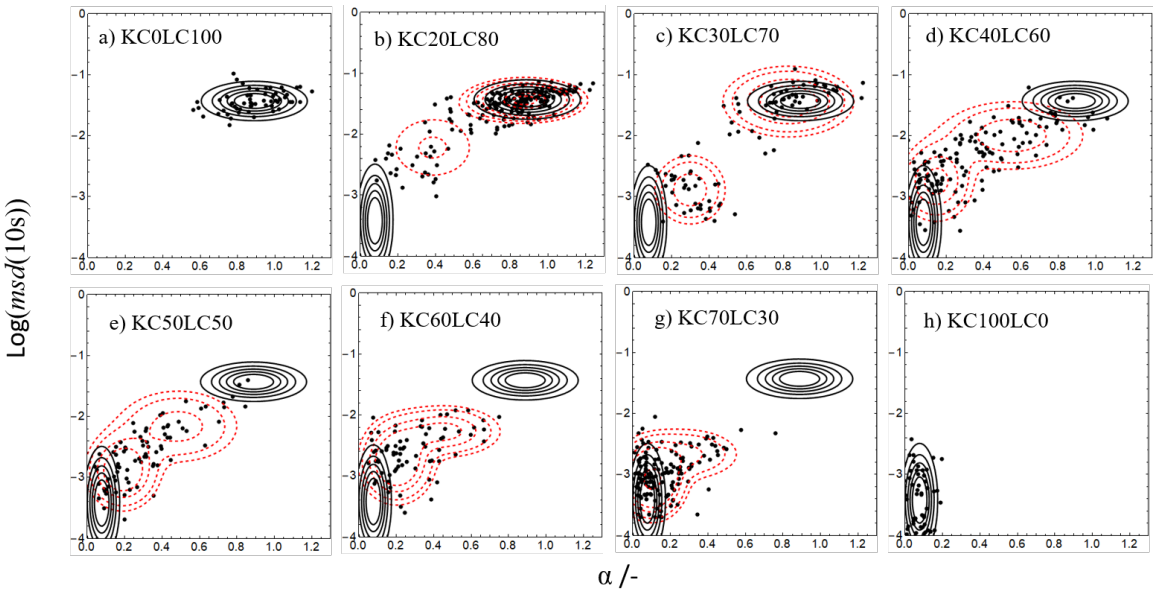

Fig. 5.7 Distribution of *msd* and α of particles in different ratio of KC and LC at 5°C after 1 day storage. The black solid lines in Figs. a-h indicates the unimodal 2D Gaussian distribution of particles in pure KC and LC, while the red-dashed lines in Figs. b-g indicates the bimodal 2D Gaussian distribution.

The effect of K^+ concentration on the *msd* of mixture solutions of KC and LC after 1 day storage at 5°C was also investigated as shown in Fig. 5.8a. The increase of K^+ concentration caused the depression of *msd* for both KC30LC70 and KC50LC50. A clear shift of distribution in plot *msd*(10s) and α was observed from 10 mM to 19 mM K^+ (see Fig. 5.8b). For KC50LC50, at low concentration of K^+ (10 mM), the distribution was skewed towards high *msd*(10s) and α implying that most of the particles showed diffusivity suggesting that KC chains were unable to form a stable network structure. With increasing K^+ concentration to 19 mM, the distribution shifted towards lower *msd*(10s) and α indicating that most of the particles are confined in the network due to the formation of KC chain aggregates resulting to the formation of stable KC gels that could possibly affect the phase separated structure.

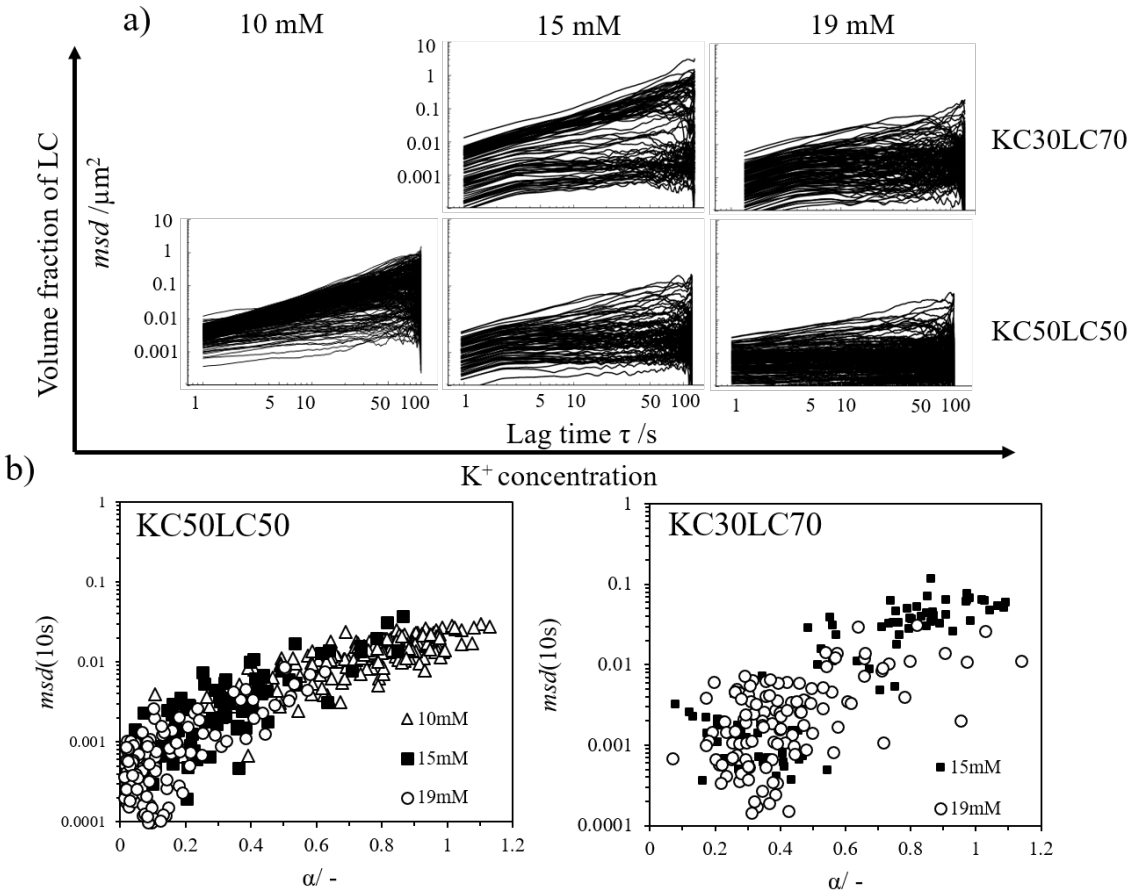

Fig. 5.8 a) *msd* of particles in mixture solutios of KC and LC with different K^+ concentration. b) Distribution of *msd*(10s) and α on the dependence of K^+ in mixture solutions of KC and LC.

5.3.4 Consideration for the phase separated structure

On the basis of the rheological measurements and particle tracking measurements, we postulate that mixture solutions of KC and LC formed a phase-separated structure. In addition, the phase transition from sea-island to bi-continuous to island-sea network structure were suggested as the ratio of KC and LC in the mixture was varied. Particle tracking revealed a high degree of heterogeneity in the mixture of KC and LC gels which was attributed to the possible phase separated structure of KC-rich and LC-rich domains. The broad msd of particles in mixture solutions of KC and LC were grouped into two populations based

on distribution in the plot of *msd*(10s) and α using a clustering method in Mathematica 10. Fig. 5.9 presents the trajectories of individual particles in the mixture of KC30LC70 after grouping. The red particles (inhibited) and blue particles (diffusive) were attributed to be in the KC-rich phase and in the LC-rich phase revealing a clear phase separated structure. The diffusive particles and inhibited particles observed in Fig. 5.9 showed a non-localized distribution suggesting that the particles were not migrated. In addition, the distribution of msd in Fig. 5.6 indicated that the domain size is larger than the particle size. Finally, depending on the mixing ratio of KC and LC, the phase separated structure and the phase transition from sea-island to bi-continuous to island-sea structure were suggested as shown in the graphical representation in Fig. 5.10.

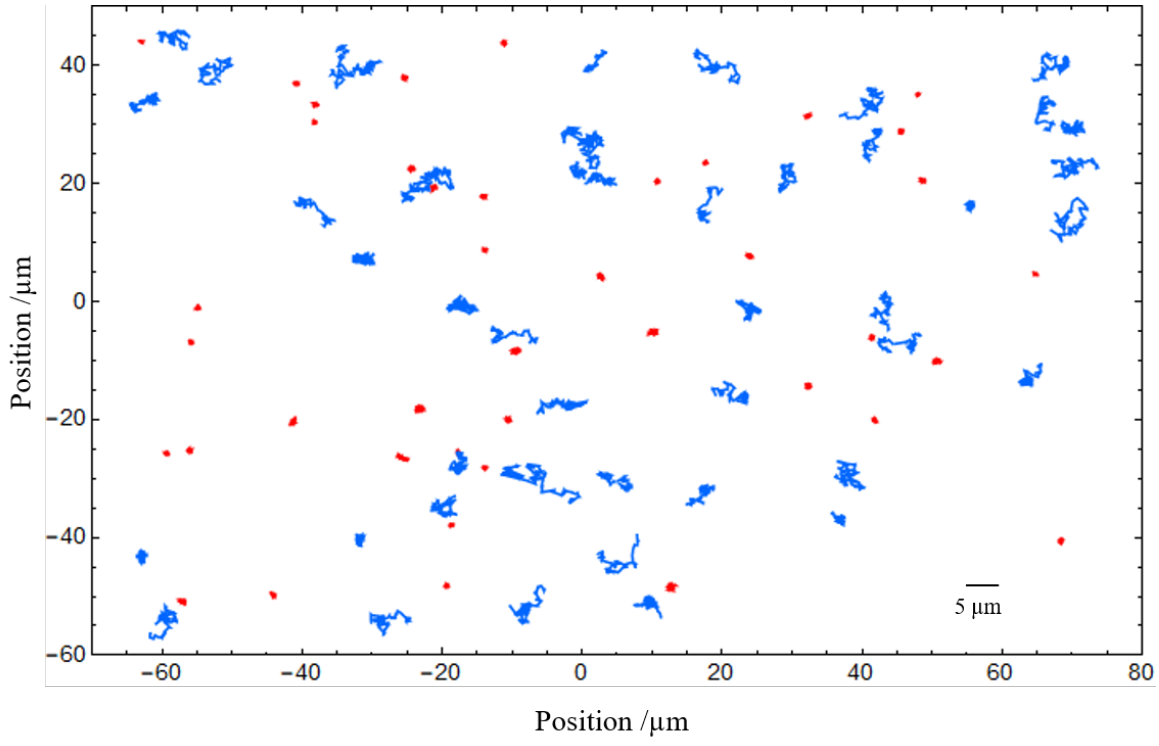

Fig. 5.9 Trajectory of individual particles in KC30LC70 having a concentration of 1.5% with 15 mM KCl after 1 day storage at 5°C. The red and blue trajectories are corresponding to inhibited and diffusive particles, respectively. The trajectory of each particle was magnified 5 times for clarity.

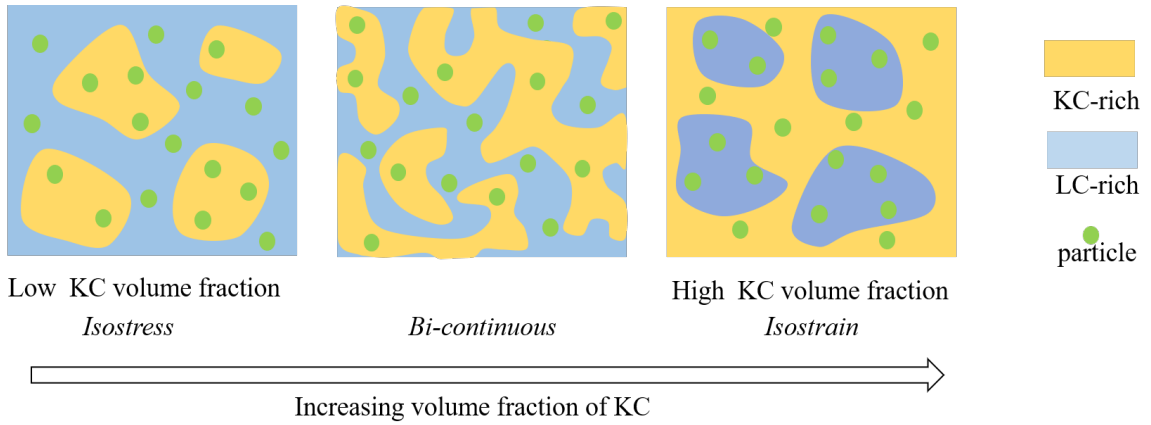

Fig. 5.10 Schematic representation of the proposed structure of mixed KC and LC gels at different volume fraction of KC.

5.4 Conclusion

The present study investigated the gelation mechanism and network structures of mixed KC/LC gels. The rheological results could be interpreted by invoking the Takayanagi laws of mixtures, implying phase separation between KC and LC. The dependence of the elastic modulus on the mixing ratio suggested the formation of a continuous phases formed by the more concentrated carrageenan, with the other carrageenan forming finite filler domains. At intermediate mixing ratios, a phase inversion suggested to take place, where both carrageenans may percolate and form a bicontinuous structure.

Particle tracking measurements showed a single step decrease of $\langle msd(10s) \rangle$ at temperatures that were close for pure KC and mixed KC/LC gels. This finding is consistent with the macroscopic rheological measurements, implying the inhibition of probe particle mobility once KC aggregates begin to form. Following one-day storage, probe particle msd in mixed gels showed a wide distribution, especially at low proportion of KC contents, underlining the enhanced microscopic heterogeneity, as reflected in the microviscosity. The distributions of

msd(10s) and α in these gels could be described using bimodal 2D distributions, indicating particle diffusion in distinct KC-rich and LC-rich domains.

Chapter 6

General Summary

The gelation mechanism and network structure of carrageenan gels as well as its mixtures were studied in the macro- and microscopic points of view using the particle tracking technique. The local physical property obtained in the particle tracking were related to the overall mechanical property of gels. The primary results of this thesis can be summarized as follows:

Particle tracking algorithm was developed for the microrheological studies, to probe the local physical properties of gels. The algorithm allowed us to track 100 nm particles with improved accuracy of centroid coordinates and particle identification. In the particle tracking algorithm, new technique was introduced by deciding a cut-off threshold for each particle based on the pixel intensity distribution for each image of local area around the particles. This algorithm will be significantly useful in particle tracking technique for biological systems or gels, especially for fluorescence microscopy observations with considerable obstructive stray fluorescent signals.

Using the particle tracking algorithm, thermal fluctuations of probe particles embedded in the pure kappa and iota carrageenan gels were investigated. The results provide information on the microscopic scale the physical property of a strong and hard gel and for a soft and a

so-called “weak gel”. In particular, the results allowed us to propose the network structure and gelation mechanism of the weak gel. This development is helpful and provides additional definition of what is a weak gel in the microscopic level.

In addition to pure gels, the gelation mechanism and phase separated network structures of mixed carrageenan gels of kappa-iota and kappa-lambda were investigated using particle tracking. The results showed greater degree of heterogeneity in the local physical property for the mixed gels following 1-day storage as compared to the pure carrageenan gels. For the kappa and iota mixtures, the formation of heterogenous network was attributed on the way to phase separation of kappa-rich and iota-rich domains but was frozen due to the network formation of kappa and iota chains. These results allowed us to contribute on the existing issue on the gelation mechanism of mix kappa and iota carrageenan gels whether it forms a phase-separated or interpenetrated network structure. In a separate experiment on the mixture of kappa-lambda, the phase separated network was clearly observed due to the inability of lambda to form network. In addition, a phase transition from sea-island, bicontinuous and island-sea network structure was suggested.

Overall, this research is focused on the microrheological investigation for the mixed polysaccharide gels with an aim of understanding the interaction of different ingredient in food product. Since, interactions between ingredients greatly influenced the quality of foods thus, understanding this will provide useful information in a way of improving and developing the food product with desired texture and physical properties.

References

Aguilera, J. M. and D. W. Stanley (1999). *Microstructural Principles of Food Processing and Engineering*.

Ahmed, E. S. A., R. E. A. Elatif, and Z. T. Alser (2015). Median filter performance based on different window sizes for salt and pepper noise removal in gray and rgb images.

Amici, E., A. H. Clark, V. Normand, and N. B. Johnson (2002). Interpenetrating network formation in agarose kappa carrageenan gel composites. *Biomacromolecules 3*(3), 466–474. PMID: 12005516.

Apgar, J., Y. Tseng, E. Fedorov, M. B. Herwig, S. C. Almo, and D. Wirtz (2000). Multiple-particle tracking measurements of heterogeneities in solutions of actin filaments and actin bundles. *Biophysical Journal 117*(2), 1095–1106.

Ashkin, A., J. M. Dziedzic, J. E. Bjorkholm, and S. Chu (1986, May). Observation of a single-beam gradient force optical trap for dielectric particles. *Opt. Lett. 11*(5), 288–290.

Brenner, T., R. Tuvikene, A. Parker, S. Matsukawa, and K. Nishinari (2014). Rheology and structure of mixed kappa-carrageenan/iota-carrageenan gels. *Food Hydrocolloids 39*, 272 – 279.

Bui, V. T., B. T. Nguyen, F. Renou, and T. Nicolai (2019). Rheology and microstructure of mixtures of iota and kappa-carrageenan. *Food Hydrocolloids 89*, 180 – 187.

Caggioni, M., P. T. Spicer, D. L. Blair, S. E. Lindberg, and D. A. Weitz (2007). Rheology and microrheology of a microstructured fluid: The gellan gum case. *Journal of Rheology 51*(5), 851–865.

Cheezum, M. K., W. F. Walker, and W. H. Guilford (2001). Quantitative comparison of algorithms for tracking single fluorescent particles. *Biophysical Journal 81*(4), 2378 – 2388.

Cheng, L.-C., L. C. Hsiao, and P. S. Doyle (2017). Multiple particle tracking study of thermally-gelling nanoemulsions. *Soft Matter 13*, 6606–6619.

Chronakis, I. S., L. Piculell, and J. Borgström (1996). Rheology of kappa-carrageenan in mixtures of sodium and cesium iodide: two types of gels. *Carbohydrate Polymers 31*(4), 215 – 225.

Crocker, J. C. and D. G. Grier (1996). Methods of digital video microscopy for colloidal studies. *Journal of Colloid and Interface Science 179*(1), 298 – 310.

Davies, W. E. A. (1971, sep). The theory of elastic composite materials. *Journal of Physics D: Applied Physics 4*(9), 1325–1339.

Derkach, S. R., S. O. Ilyin, A. A. Maklakova, V. G. Kulichikhin, and A. Y. Malkin (2015). The rheology of gelatin hydrogels modified by κ-carrageenan. *LWT - Food Science and Technology 63*(1), 612 – 619.

Du, L., T. Brenner, J. Xie, Z. Liu, S. Wang, and S. Matsukawa (2016). Gelation of iota/kappa carrageenan mixtures. In *Gums and Stabilisers for the Food Industry 18: Hydrocolloid Functionality for Affordable and Sustainable Global Food Solutions*, pp. 47–55. The Royal Society of Chemistry.

Du, L., T. Brenner, J. Xie, and S. Matsukawa (2016). A study on phase separation behavior in kappa/iota carrageenan mixtures by micro dsc, rheological measurements and simulating water and cations migration between phases. *Food Hydrocolloids 55*, 81 – 88.

Du, L., Y. Lu, L. Geonzon, J. Xie, and S. Matsukawa (2016). Rheological properties and interactions between polysaccharides in mixed carrageenan solutions. *Journal of Biorheology 30*(1), 13–18.

Fan, L., K. Peng, M. Li, L. Wang, and T. Wang (2013). Preparation and properties of carboxymethyl κ-carrageenan/alginate blend fibers. *Journal of Biomaterials Science, Polymer Edition 24*(9), 1099–1111. PMID: 23651117.

Fernandes, P., M. Gonçalves, and J. Doublier (1991). A rheological characterization of kappa-carrageenan/galactomannan mixed gels: A comparison of locust bean gum samples. *Carbohydrate Polymers 16*(3), 253 – 274.

Fish, J. and J. Scrimgeour (2015, Jul). Fast weighted centroid algorithm for single particle localization near the information limit. *Appl. Opt. 54*(20), 6360–6366.

Furst, E. M. and T. M. Squires (2017). *Microrheology*.

Gao, Y. and M. L. Kilfoil (2007, Aug). Direct imaging of dynamical heterogeneities near the colloid-gel transition. *Phys. Rev. Lett. 99*, 078301.

Gardel, M., M. Valentine, and D. Weitz (2005). *Microrheology*, pp. 1–49. Berlin, Heidelberg: Springer Berlin Heidelberg.

Geonzon, L. C., R. G. Bacabac, and S. Matsukawa (2019a). Microscopic characterization of phase separation in mixed carrageenan gels using particle tracking. *Journal of The Electrochemical Society 166*(9), B3228–B3234.

Geonzon, L. C., R. G. Bacabac, and S. Matsukawa (2019b). Network structure and gelation mechanism of kappa and iota carrageenan elucidated by multiple particle tracking. *Food Hydrocolloids 92*, 173 – 180.

Geonzon, L. C., S. L. Flores, R. G. Bacabac, and S. Matsukawa (2018). (invited) phase separation in mixed polysaccharide gels. *ECS Transactions 88*(1), 9–13.

Geonzon, L. C. and S. Matsukawa (2019). Accuracy improvement of centroid coordinates and particle identification in particle tracking technique. *Journal of Biorheology 33*(1), 2–7.

Hanaor, D. A., Y. Gan, and I. Einav (2015). Contact mechanics of fractal surfaces by spline assisted discretisation. *International Journal of Solids and Structures 59*, 121 – 131.

Heilig, A., A. Göggerle, and J. Hinrichs (2009). Multiphase visualisation of fat containing β-lactoglobulin–κ-carrageenan gels by confocal scanning laser microscopy, using a novel dye, v03-01136, for fat staining. *LWT - Food Science and Technology 42*(2), 646 – 653.

Hu, B., L. Du, and S. Matsukawa (2016). Nmr study on the network structure of a mixed gel of kappa and iota carrageenans. *Carbohydrate Polymers 150*, 57 – 64.

Huc, D., A. Matignon, P. Barey, M. Desprairies, S. Mauduit, J. Sieffermann, and C. Michon (2014). Interactions between modified starch and carrageenan during pasting. *Food Hydrocolloids 36*, 355 – 361.

Ikeda, S. and K. Nishinari (2001). "weak gel"-type rheological properties of aqueous dispersions of nonaggregated κ-carrageenan helices. *Journal of Agricultural and Food Chemistry 49*(9), 4436–4441. PMID: 11559151.

Kasapis, S. (2008). Phase separation in biopolymer gels: A low- to high-solid exploration of structural morphology and functionality. *Critical Reviews in Food Science and Nutrition 48*(4), 341–359. PMID: 18409116.

Khan, M. and T. G. Mason (2014). Trajectories of probe spheres in generalized linear viscoelastic complex fluids. *Soft Matter 10*, 9073–9081.

Knutsen, S., D. Myslabodski, and B. Larsen (2009). A modified system of nomenclature for red algal galactans. *Botanica Marina 37(2)*, 163–170.

Kreizer, M., D. Ratner, and A. Liberzon (2010, Jan). Real-time image processing for particle tracking velocimetry. *Experiments in Fluids 48*(1), 105–110.

Lewis, J. P. (1995). Fast normalized cross-correlation.

Lieleg, O., I. Vladescu, and K. Ribbeck (2010). Characterization of particle translocation through mucin hydrogels. *Biophysical Journal 98*(9), 1782 – 1789.

Liu, J., X. Zhan, J. Wan, Y. Wang, and C. Wang (2015). Review for carrageenan-based pharmaceutical biomaterials: Favourable physical features versus adverse biological effects. *Carbohydrate Polymers 121*, 27 – 36.

Mason, T. G., K. Ganesan, J. H. van Zanten, D. Wirtz, and S. C. Kuo (1997, Oct). Particle tracking microrheology of complex fluids. *Phys. Rev. Lett. 79*, 3282–3285.

Mason, T. G. and D. A. Weitz (1995, Feb). Optical measurements of frequency-dependent linear viscoelastic moduli of complex fluids. *Phys. Rev. Lett. 74*, 1250–1253.

Michalet, X. (2010, Oct). Mean square displacement analysis of single-particle trajectories with localization error: Brownian motion in an isotropic medium. *Phys. Rev. E 82*, 041914.

Michel, A.-S., M. Mestdagh, and M. Axelos (1997). Physico-chemical properties of carrageenan gels in presence of various cations. *International Journal of Biological Macromolecules 21*(1), 195 – 200.

Moschakis, T. (2013). Microrheology and particle tracking in food gels and emulsions. *Current Opinion in Colloid and Interface Science 18*(4), 311 – 323.

Moschakis, T., A. Lazaridou, and C. G. Biliaderis (2012). Using particle tracking to probe the local dynamics of barley β-glucan solutions upon gelation. *Journal of Colloid and Interface Science 375*(1), 50 – 59.

Moschakis, T., A. Lazaridou, and C. G. Biliaderis (2014). A micro- and macro-scale approach to probe the dynamics of sol–gel transition in cereal β-glucan solutions varying in molecular characteristics. *Food Hydrocolloids 42*, 81 – 91. Special Issue: A Festschrift in honour of Professor Eric Dickinson.

Moschakis, T., B. S. Murray, and E. Dickinson (2006). Particle tracking using confocal microscopy to probe the microrheology in a phase-separating emulsion containing nonadsorbing polysaccharide. *Langmuir 22*(10), 4710–4719. PMID: 16649786.

Necas, J. and L. Bartosikova (2013, may). Carrageenan: a review. *Veterinární Medicína 58*(No. 4), 187–205.

Norziah, M., S. Foo, and A. Karim (2006). Rheological studies on mixtures of agar (gracilaria changii) and κ-carrageenan. *Food Hydrocolloids 20*(2), 204 – 217. 7th International Hydrocolloids Conference.

Oppong, F. K., L. Rubatat, B. J. Frisken, A. E. Bailey, and J. R. de Bruyn (2006, Apr). Microrheology and structure of a yield-stress polymer gel. *Phys. Rev. E 73*, 041405.

Papagiannopoulos, A., K. Sotiropoulos, and S. Pispas (2016). Particle tracking microrheology of the power-law viscoelasticity of xanthan solutions. *Food Hydrocolloids 61*, 201 – 210.

Parker, A., G. Brigand, C. Miniou, A. Trespoey, and P. Vallée (1993). Rheology and fracture of mixed ι- and κ-carrageenan gels: Two-step gelation. *Carbohydrate Polymers 20*(4), 253 – 262.

Piculell, L., S. Nilsson, and P. Muhrbeck (1992). Effects of small amounts of kappa-carrageenan on the rheology of aqueous iota-carrageenan. *Carbohydrate Polymers 18*(3), 199 – 208.

Price, W. S. (2009). *Chapter (1) NMR studies of translational motion: Principles and Applications*.

Rees, D. A., I. W. Steele, and F. B. Williamson (1969). Conformational analysis of polysaccharides. iii. the relation between stereochemistry and properties of some natural polysaccharide sulfates (1). *Journal of Polymer Science Part C: Polymer Symposia 28*(1), 261–276.

Richardson, R. K. and S. Kasapis (1998). Rheological methods in the characterisation of food biopolymers. In D. L. B. Wetzel and G. Charalambous (Eds.), *Instrumental Methods in Food and Beverage Analysis*, Volume 39 of *Developments in Food Science*, pp. 1 – 48. Elsevier.

Rochas, C. and M. Rinaudo (1980). Activity coefficients of counterions and conformation in kappa-carrageenan systems. *Biopolymers 19*(9), 1675–1687.

Ross-Murphy, S. B. (1995). Rheological characterisation of gels1. *Journal of Texture Studies 26*(4), 391–400.

Shabaniverki, S. and J. J. Juárez (2017). Characterizing gelatin hydrogel viscoelasticity with diffusing colloidal probe microscopy. *Journal of Colloid and Interface Science 497*, 73 – 82.

Takayanagi, M., H. Harima, and Y. Iwata (1963). Viscoelastic behavior of polymer blends and its comparison with model experiments. *Journal of the Society of Materials Science, Japan 12*(116), 389–394.

Takemasa, M., A. Chiba, and M. Date (2001). Gelation mechanism of κ and ι carrageenan investigated by correlation between the strain optical coefficient and the dynamic shear modulus. *Macromolecules 34*(21), 7427–7434.

Tecante, A. and M. del Carmen Núñez Santiago (2012). Solution properties of κ-carrageenan and its interaction with other polysaccharides in aqueous media. In J. D. Vicente (Ed.), *Rheology*, Chapter 10. Rijeka: IntechOpen.

Thrimawithana, T., S. Young, D. Dunstan, and R. Alany (2010). Texture and rheological characterization of kappa and iota carrageenan in the presence of counter ions. *Carbohydrate Polymers 82*(1), 69 – 77.

Tseng, Y., T. P. Kole, and D. Wirtz (2002). Micromechanical mapping of live cells by multiple-particle-tracking microrheology. *Biophysical Journal 83*(6), 3162 – 3176.

Tseng, Y., J. S. H. Lee, T. P. Kole, I. Jiang, and D. Wirtz (2004). Micro-organization and visco-elasticity of the interphase nucleus revealed by particle nanotracking. *Journal of Cell Science 117*(10), 2159–2167.

Tuvikene, R., K. Truus, A. Kollist, O. Volobujeva, E. Mellikov, and T. Pehk (2007, Aug). Gel-forming structures and stages of red algal galactans of different sulfation levels. *Journal of Applied Phycology 20*(5), 527.

Usov, A. (1992). Sulfated polysaccharides of the red seaweeds. *Food Hydrocolloids 6*(1), 9 – 23.

Valentine, M. T., P. D. Kaplan, D. Thota, J. C. Crocker, T. Gisler, R. K. Prud'homme, M. Beck, and D. A. Weitz (2001, Nov). Investigating the microenvironments of inhomogeneous soft materials with multiple particle tracking. *Phys. Rev. E 64*, 061506.

van de Velde, F. (2008). Structure and function of hybrid carrageenans. *Food Hydrocolloids 22*(5), 727 – 734.

Wagner, C. E., B. S. Turner, M. Rubinstein, G. H. McKinley, and K. Ribbeck (2017). A rheological study of the association and dynamics of muc5ac gels. *Biomacromolecules 18*(11), 3654–3664. PMID: 28903557.

Waigh, T. A. (2005, feb). Microrheology of complex fluids. *Reports on Progress in Physics 68*(3), 685–742.

Wu, C.-E., K.-H. Lin, and J.-Y. Juang (2016). Hertzian load–displacement relation holds for spherical indentation on soft elastic solids undergoing large deformations. *Tribology International 97*, 71 – 76.

Zhang, Q., S. Matsukawa, and T. Watanabe (2004). Theoretical analysis of water ht_2 based on chemical exchange and polysaccharide mobility during gelation. *Food Hydrocolloids 18*(3), 441 – 449.

Zhao, Q., T. Brenner, and S. Matsukawa (2013). Molecular mobility and microscopic structure changes in κ-carrageenan solutions studied by gradient nmr. *Carbohydrate Polymers 95*(1), 458 – 464.

Zhao, Q. and S. Matsukawa (2012). Estimation of the hydrodynamic screening length in κ-carrageenan solutions using nmr diffusion measurements. *Polymer Journal 44*(8), 901 – 906.

Zheng, H. (2018). *Polymers for Structure Design of Dairy Foods*, pp. 509–528. Cham: Springer International Publishing.

Zia, K. M., S. Tabasum, M. Nasif, N. Sultan, N. Aslam, A. Noreen, and M. Zuber (2017). A review on synthesis, properties and applications of natural polymer based carrageenan blends and composites. *International Journal of Biological Macromolecules 96*, 282 – 301.

Appendix A

Supplementary Figure

A.1 Supplementary Figure 1 of Chapter 4

A.2 Supplementary Figure 1 of Chapter 5

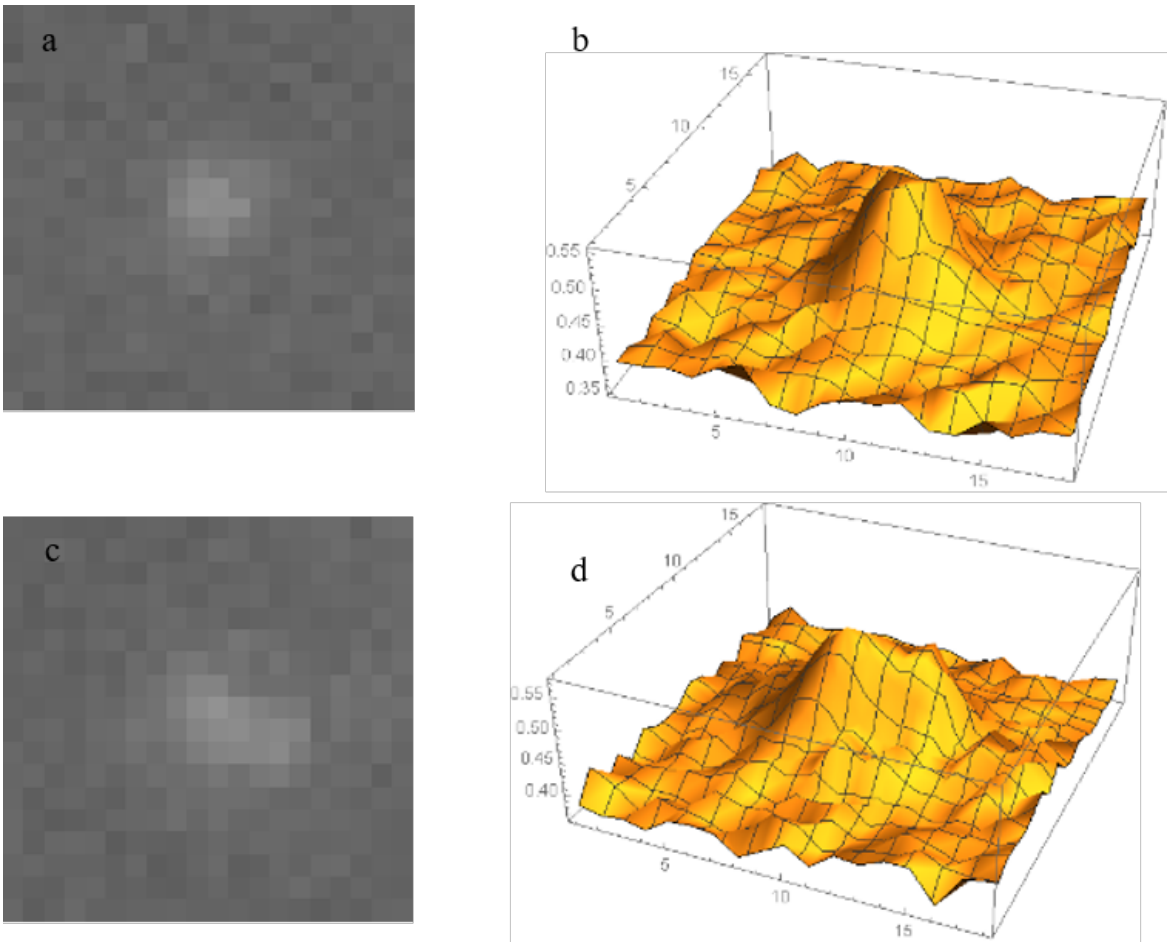

Fig. A.1 a) Image of a single particle. b) Intensity profile of a single particle. c) Image of an aggregated two particles. d) Intensity profile of an aggregated particles.

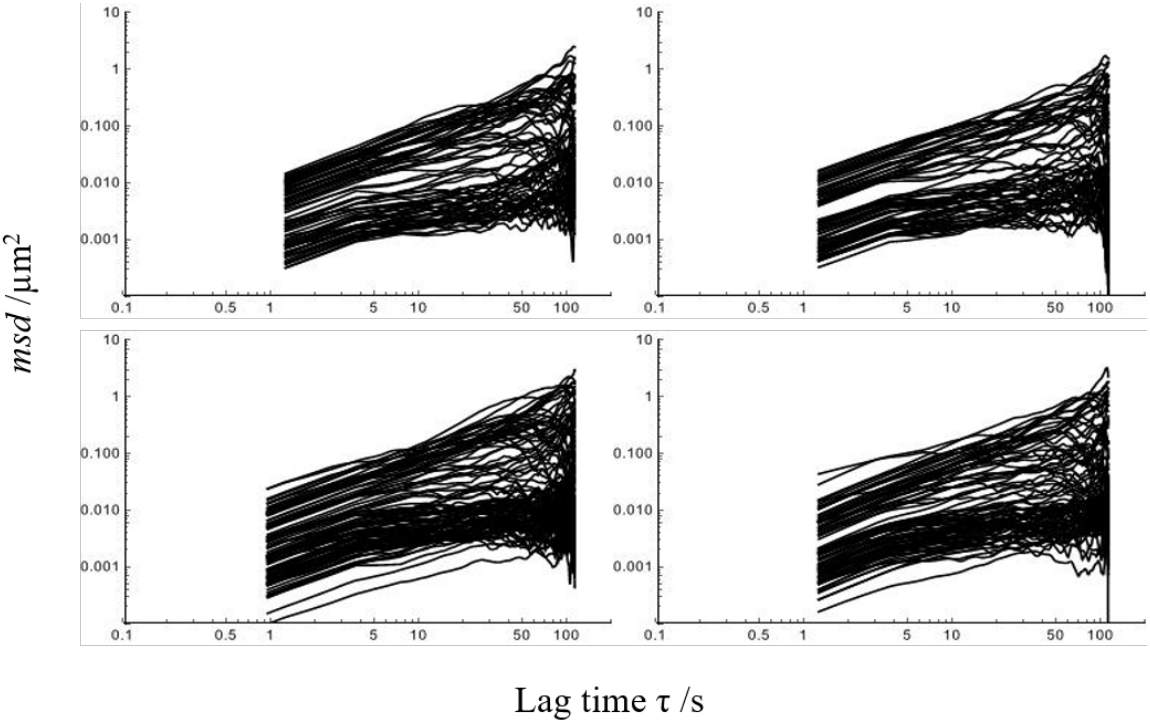

Fig. A.2 Individual *msd* of particles in KC50IC50 using a cooling rate of 0.055°C/min for four different areas in the KC50IC50 sample.